UC Santa Cruz

UC Santa Cruz Electronic Theses and Dissertations

Title

Synthesis, Design, and Applications of Lanthanide-based Metal-Organic Structures

Permalink

https://escholarship.org/uc/item/424151n5

Author

Chatenever, Ana Rosa Kareh

Publication Date

2019

Peer reviewed|Thesis/dissertation

eScholarship.org Powered by the California Digital Library
University of California

UNIVERSITY OF CALIFORNIA
SANTA CRUZ

SYNTHESIS, DESIGN, AND APPLICATIONS OF LANTHANIDE-BASED METAL-ORGANIC STRUCTURES

A dissertation submitted in partial satisfaction of the requirements for the degree of

DOCTOR OF PHILOSOPHY

in

CHEMISTRY

by

Ana Rosa Kareh Chatenever

June 2019

The Dissertation of Ana Rosa Kareh Chatenever is approved:

_____
Professor Scott R. J. Oliver

_____
Professor Pradip Mascharak

_____
Professor Yat Li

_____
Lori Kletzer
Vice Provost and Dean of Graduate Studies

Copyright © by

Ana Rosa Kareh Chatenever

2019

Table of Contents

Chapter 2. Experimental Methods of Lanthanide Metal-Organic Structures

Chapter 5. Summary and Future Work

Appendix

List of Figures

List of Tables

Abstract

Synthesis, Design, and Applications of Lanthanide-based Metal-Organic Structures

by

Ana Rosa Kareh Chatenever

This work focuses on lanthanide-based inorganic-organic structures. The properties of lanthanide-based metal organic frameworks (Ln-MOFs) and layered rare earth hydroxides (LREHs) are reviewed and compared. Three distinct projects are presented herein: 1) the solvothermal syntheses of a series of Ln-MOFs with the ligand biphenyl-4,4-dicarboxylate (BPDC), 2) the solvothermal syntheses of a series of Ln-MOFs with the ligand 2,6-naphthalenedicarboxylate (NDC), and 3) the hydrothermal syntheses of a series of neodymium-based LREHs with increasing α,ω-alkanedisulfonate (ADS) carbon chain lengths.

The first project, which we refer to as Ln-BPDC (structures SLUG-43–48), is an isomorphous series of six anionic frameworks with the general structure $[Ln(BPDC)_2^-][NH_2(CH_3)_2^+]$ (Ln = La, Ce, Nd, Eu, Gd, Er). The Ln(III) metal centers exhibit eight-coordinate binding to six different $BPDC^{2-}$ ligands. The anionic

framework is charge-balanced by a dimethylammonium cation. The materials all possess the same 3-D structure and crystallize in the orthorhombic space group *Pbcn*. All exhibit thermal stability up to 300 °C and decompose to Ln_2O_3 after 800 °C. The Eu-BPDC structure exhibits strong fluorescence in the 612-620 nm range and a quantum yield of 2.11%.

The second project, we refer to as Ln-NDC (structures SLUG-49–52). This project consists of four neutrally charged structures that each crystallize in distinct space groups. Their formulas are $[La_6(NDC)_9(DMF)_3 \cdot 6\ DMF]$, $[Nd_2(NDC)_3(DMF)_2]$, $[Eu_2(NDC)_3(DMF)_2 \cdot DMF]$, and $[Gd_4(NDC)_6(DMF)_4]$. The Ln(III) centers exhibit different coordination numbers (ranging from seven to nine), the NDC ligand exhibits multiple binding modes, and DMF solvent molecules are found either coordinated or floating within the structures. Despite these differences, the NDC-based structures exhibit similar thermal decomposition profiles and infrared spectra. The Eu-NDC structure exhibits a sharp red-orange luminescence at 613 nm and a quantum yield of 3.56%.

Lastly, the Nd-ADS project (structures SLUG-28–30) consists of three LREHs made of $[Nd_2(OH)_4(OH_2)_2^{2+}]$ layers with interlamellar α,ω-$[^{-}O_3S(CH_2)_nSO_3^{-}]$ anions (n = 2 to 4). These LREHs show an increase in thermal stability with increasing alkanedisulfonate chain length. As an initial example of anion exchange, all three materials show exchange for adipate, $^{-}O_2C(CH_2)_4CO_2^{-}$.

Several insights on the structural differences between Ln-MOFs and LREHs are proposed. In comparing the mentioned projects, we suggest the differences between the isomorphous Ln-BPDC series and the diversity of structures in the Ln-NDC series are due to the rigidity of the NDC ligand and the synthesis temperatures. The dimensionality of lanthanide-based materials (3-D or 2-D) are affected by reaction pH. This work expands the chemistry of lanthanide MOFs and LREHs.

Dedication

To my husband

Simon Chatenever

without your love, humor, and support

none of this would be possible

Acknowledgements

There are countless people I would like to thank for their help and support during my time at UCSC. Throughout my undergraduate and graduate studies, I have spent nearly ten years (over a third of my life!) in Santa Cruz. It has become a second home and I am so lucky to have been able to spend so much time here and have met many influential people.

I would first like to thank my advisor Professor Scott R. J. Oliver for guiding me in my projects and for giving me the freedom to pursue the chemistry I found interesting. To my committee members Distinguished Professor Pradip Mascharak and Professor Yat Li: thank you for being encouraging, giving advice, and helping me grow as a chemist. I would also like to thank the faculty that became mentors to me throughout this journey: Professor Bakthan Singaram, Professor Emeritus Eugene Switkes, and Professor Alegra Eroy-Reveles.

I would like to thank my two graduate mentors who gave me the confidence as an undergraduate that I too could complete a PhD in chemistry – Dr. Rachel Snelling and Dr. Jessica Palomino. I cannot thank my labmates enough for making the lab a place of support, collaboration, and laughter: Dr. Eaindar Soe, Dr. Susan Citrak, Dr.

Ian Colinas, Dr. Jesse Hauser, Dr. Yashar Abdollahian, Beatriz Ehlke, and Jerah Barnett. Thank you to the crystallographers Dr. Eric Reinheimer, Dr. Pierre Le Magueres, and Dr. Allen Oliver – without your work, this thesis would not be complete. Thank you to my undergraduates who helped with research and were a joy to mentor: Louis Warne, Joe Matsuoka, and Stanley Wang. Thank you also to my graduate cohort who supported each other throughout these past five years.

Lastly, I would like to thank my family for their undying support: my dad for always offering financial help because he couldn't help with the academics; my mom for always listening and keeping me company during my commutes; my brothers for supporting me and being proud of my work; my mother-in-law and sister-in-law for always asking the right questions and providing encouragement and emotional help. Last but certainly not least: thank you to my husband for being with me along this journey, bearing the brunt of my stresses, and never doubting my abilities for a second.

…We're a team. We win together; we lose together. We celebrate and we mourn together. And defeats are softened and victories sweetened because we did them together…

Chapter 1

Introduction to Lanthanide Metal-Organic Frameworks

Abstract

Metal-organic frameworks (MOFs) are three-dimensional, crystalline materials. The choice of metal and organic linker can be carefully tailored to produce desired applications such as ion exchange/adsorption, sensing, catalysis, or gas storage. Lanthanide-based structures such as MOFs and layered rare earth hydroxides (LREHs) are relatively new classes of materials that have the advantage of high coordination numbers and potential luminescent applications for optical sensing. The luminescent properties of lanthanide-based MOFs and layered metal hydroxides are described and reviewed herein.

1.1. Metal-Organic Frameworks (MOFs)

1.1.1. Structural Properties

Metal-organic frameworks (MOFs) are a growing class of robust, crystalline, three-dimensional porous materials.[1,2] They are constructed by metal nodes, or M_xO_y clusters referred to as secondary building units (SBUs), connected by organic linkers which give rise to extended frameworks (Figure 1.1.1).[3,4] The first MOFs were reported in the early 1990s by various groups, and were based on transition metals (e.g. Zn, Cd, Cu) and the organic linker 4,4'-bipyridine.[5–7] Currently there are over

20,000 articles and reviews on the topic of MOFs and thousands of new structures have been reported.[8,9] The seemingly endless combinations of metal and linker allow for high surface areas and tunable pore sizes, as demonstrated in the isoreticular MOF (IRMOF) series (Figure 1.1.2).[10] Isoreticular refers to structures having the same framework topology while varying the organic component. In the IRMOF series, SBUs of Zn_4O tetrahedra remain constant while the organic linkers are modified to increase the pore volume of the framework.

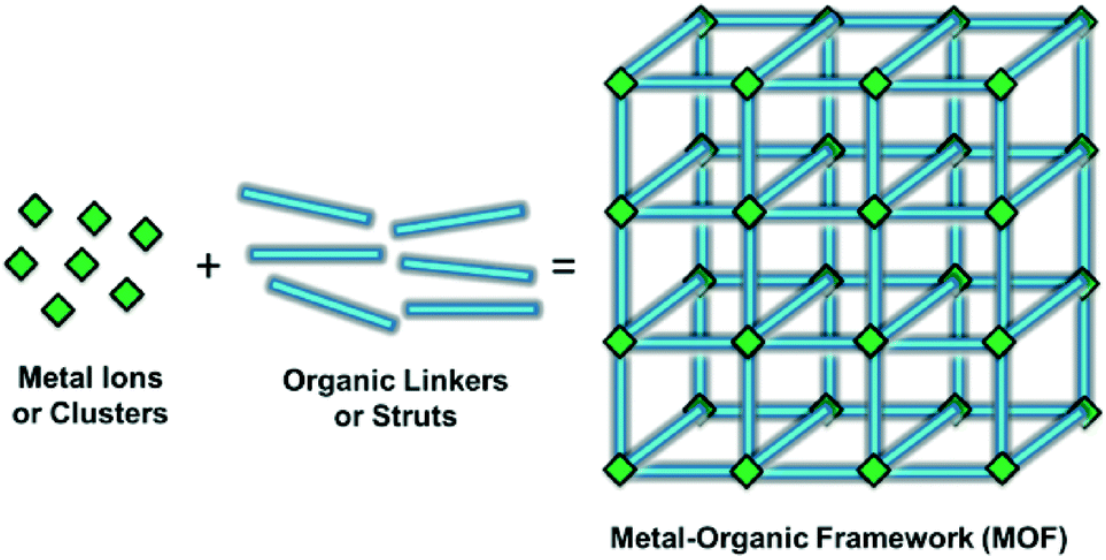

Figure 1.1.1. Simplified schematic of a three-dimensional MOF, constructed from metal nodes and organic linkers.[3]

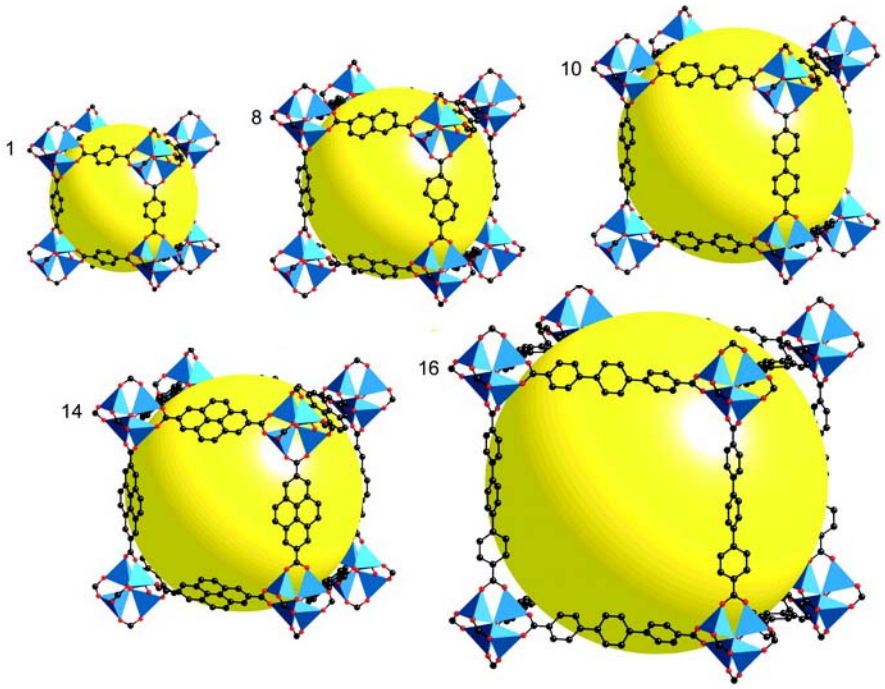

Figure 1.1.2. Crystallographic images of IRMOF-n (n = 1, 8, 10, 14, 16), showing the tunable pore sizes (represented by yellow spheres) of MOFs by varying the organic linker and retaining the same Zn_4O SBU (Zn = blue, O = red, C = black, H omitted for clarity).[10]

The oxidation state of the metal used as well as the charge of the organic linker/ligand will lead to anionic, neutral, or cationic structures.[11] Anionic and cationic frameworks have potential applications in ion exchange, which will be discussed in section 1.1.3. The Oliver group has reported a variety of anionic, neutral, and cationic lanthanide-based structures (Table 1.1.1, Figure 1.1.3).[11–13] SLUG-7 is a two-dimensional anionic material composed of nine-coordinate gadolinium(III) aquacarbonate layers which are charge-balanced by ammonium. SLUG-8 is a three-dimensional neutral

structure, closely related to SLUG-7, but is more condensed and is coordinated by ammonia and water. SLUG-27 is a cationic two-dimensional material consisting of seven- and eight-coordinate erbium(III) aquahydroxide layers with α,ω-ethanedisulfonate in the interlamellar space, either doubly-bound, singly-bound, or floating. Extra-framework species in MOFs include charge-balancing ions or solvent molecules that help template the pores during synthesis. These species are also referred to as 'guest' species, while the metal-organic framework is referred to as the 'host' structure. As has hopefully been demonstrated by this section, MOFs have the possibility to be carefully designed for their desired structural properties.

Table 1.1.1. Examples of anionic, neutral, and cationic rare earth structures published by the Oliver group[11–13]

Name	Formula	Charge on Frame-work	Extra-Framework Species
SLUG-7	$[Gd(CO_3)_2H_2O^-][NH_4^+]$	Anionic	NH_4^+
SLUG-8	$Gd_2(CO_3)_3(NH_3)(H_2O)$	Neutral	N/A
SLUG-27	$[Er_{12}(OH)_{29}(H_2O)_5^{7+}][^-O_3SCH_2CH_2SO_3^-]_{3.5} \cdot 5H_2O$	Cationic	$^-O_3SCH_2CH_2SO_3^-$

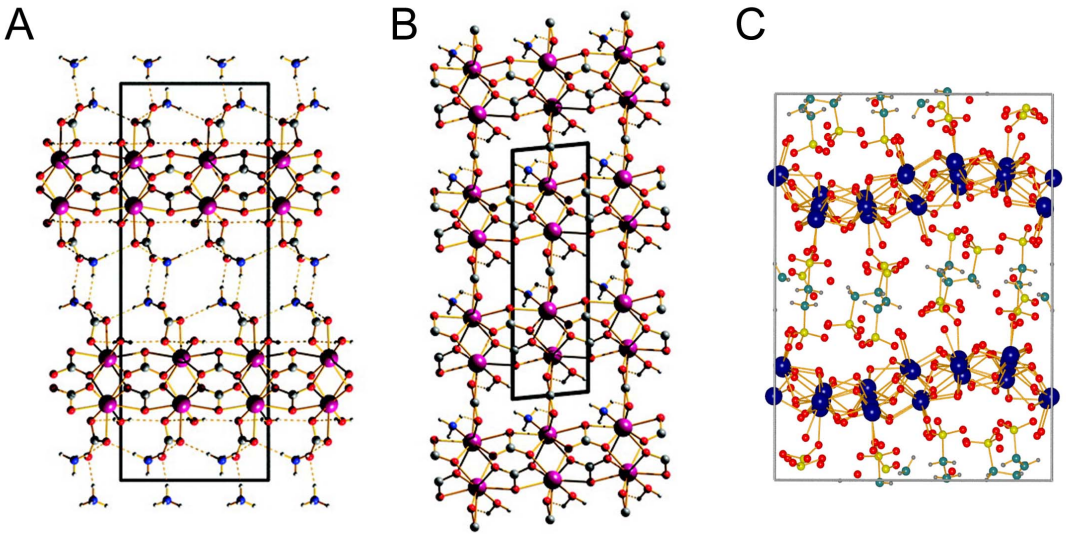

Figure 1.1.3. Crystallographic images of the anionic, neutral, and cationic structures of A) SLUG-7, B) SLUG-8, and C) SLUG-27, respectively. The unit cell of each structure is outlined. (SLUG-7 and SLUG-8: Gd = purple, C = gray, N = blue, O = red, H = light gray; SLUG-27: Er = blue, O = red, S = yellow, C = teal).

1.1.2. Synthesis Methods

A variety of synthesis methods of MOFs have been reported: hydro/solvothermal, microwave-assisted, mechanochemical, electrochemical, and sonochemical.[14–16] Here we will focus on hydro/solvothermal methods. Hydrothermal and solvothermal syntheses refer to high temperature conditions in a conventional autoclave and are the most often practiced synthesis techniques. When water is the reaction solvent, the term 'hydrothermal' is used and for any other solvent the term 'solvothermal' is employed. The use of a Teflon-lined steel autoclave allows a reaction to take place in a closed vessel under autogenous pressure above the boiling point of the solvent.

These conditions mimic the high temperature, high pressure conditions of natural geologic processes under which minerals form.[17] In fact, two naturally occurring metal oxalate ($C_2O_4^{2-}$) minerals: stepanovite [$NaMgFe(C_2O_4)_3 \cdot$8-9 H_2O] and zhemchuzhnikovite [$NaMg(Fe_{0.4}Al_{0.6})(C_2O_4)_3 \cdot 8\ H_2O$], which were discovered in a Siberian coal mine, exhibit MOF structures.[18] Metal oxalate minerals are the largest group of organic minerals. Each oxalate oxygen has a coordination number of four, which typically results in layered structures.[19] The choice of synthesis solvent plays many roles: structure direction, solubility, and pH determination.[20] This effect is nicely demonstrated by the characterization of four different structures synthesized from magnesium nitrate hexahydrate and 3,5-pyridinedicarboxylic acid in four different solvents [dimethylformamide (DMF), DMF/methanol, ethanol/water, and DMF/ethanol] (Figure 1.1.4).[21] The choice of solvent affected the dimensionality of the structures and the connectivity of the frameworks. As also demonstrated by this work, combinations of solvents with different polarities can be used to ensure dissolution of the starting materials. The final pH of a reaction mixture can influence the oxidation state of the metal, the extent of solubility of the reagents, and the extent of deprotonation of the organic linker, thus controlling the final structural framework.[20]

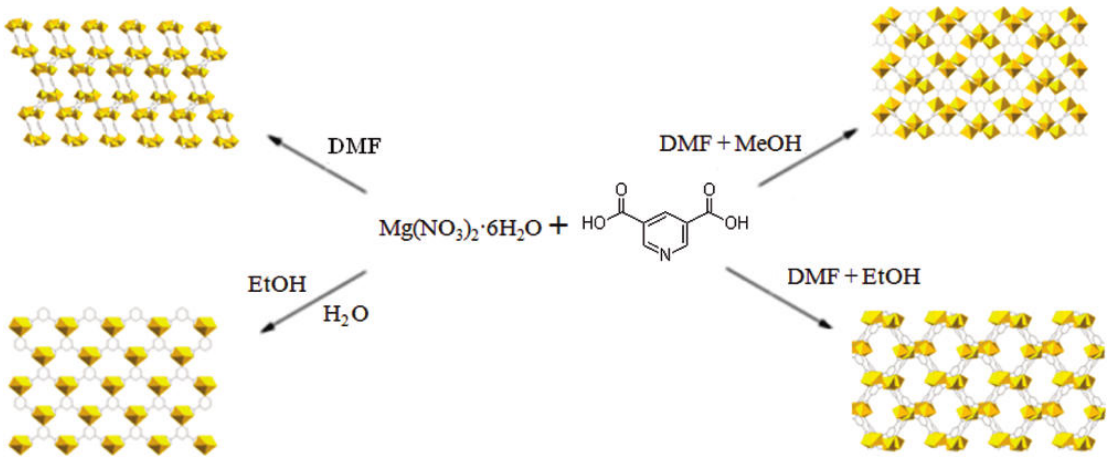

Figure 1.1.4. Four different structures as a result of differing solvent systems.[21]

Other factors to consider when synthesizing MOFs are the temperature, synthesis time, and reagent ratios. By cycling the reaction temperature, a phenomenon known as crystal ripening occurs: at high temperatures, small crystals formed in solution will dissolve more readily than larger crystals; as the temperature cools, the dissolved small crystals then redeposit onto the larger ones previously formed resulting in larger crystals (crystal growth).[15,22] The ratio of metal to organic linker starting material is important because it can affect the dimensionality of the structures, simply due to availability of reagents when the frameworks are ordered.[20] These parameters must be fine-tuned for each synthesis in a trial and error process in order to optimize the final conditions.

Another synthesis technique in MOFs is postsynthetic modification (PSM). This term refers to the modification of an assembled or synthesized MOF which preserves the lattice structure.[23] Types of PSM include the removal or exchange of guest molecules,

removal of auxiliary ligands to leave behind an unsaturated metal center, functionalization of the organic linker, and metal doping.[23,24] One of the reasons for PSM instead of pre-synthesis is due to the fact that not all functionalizations are compatible with high temperature and pressure solvothermal conditions.[24] These modifications provide MOFs with specialized functionalities and applications. Multiple examples of possible ligand functionalizations are provided in Figure 1.1.5.[25] The dibromination and triazolation reactions in Figure 1.1.5a-b are 'proof of concept' syntheses that demonstrate the wide possibilities of PSM.[26,27] The diamine and aminoalcohol functionalized MOFs in Figure 1.1.5c-d demonstrated an increased ability in selective CO_2 uptake compared to the parent UiO-66-type MOF.[28] Lastly, the amino/sulfo modification on a MIL-101 framework in Figure 1.1.5e was shown to produce an efficient acid-base catalyst for tandem deacetalization-Knoevenagel condensation reactions.[29] The area of MOF PSM is still growing, and is demonstrating the usefulness of these modifications on the potential applications of MOFs.

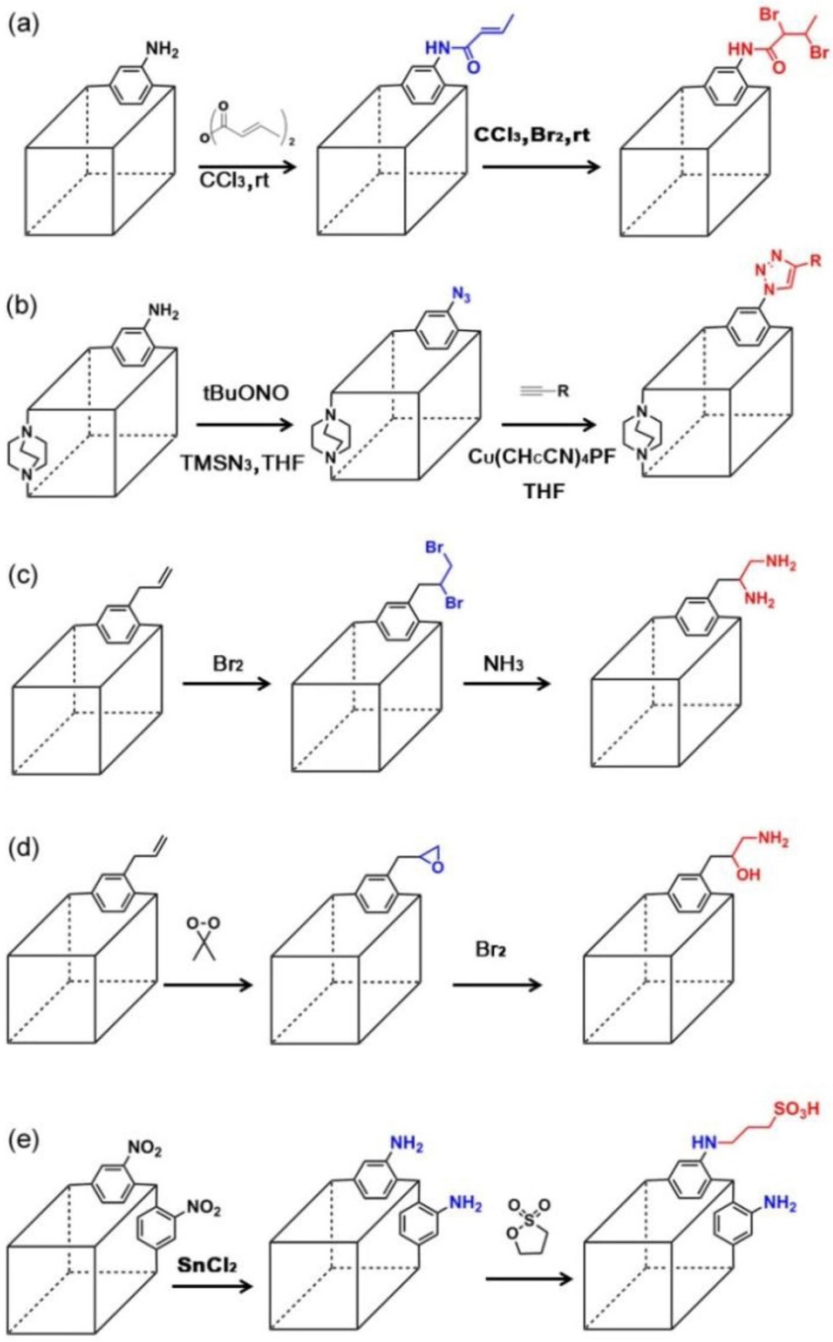

Figure 1.1.5. Various two-step tandem PSMs to introduce functional groups on the organic linker such as: a) -dibromine, b) -triazole, c) -diamine, d) α-amino-β-hydroxy, and e) -sulfonic acid.[25–29]

1.1.3. Applications

The intrinsic pore volume of MOFs lends itself to various applications (Figure 1.1.6): ion exchange/adsorption, sensing, catalysis, and gas storage.[3,30–37] The applications of ion exchange/adsorption and sensing are particularly attractive for the selective removal or detection of hazardous pollutants in water, respectively. Exposed metal nodes in MOFs can act as adsorptive sites or heterogeneous catalysts for organic reactions. MOFs are appealing candidates for gas storage because their high pore volumes and surface areas allow the storage of gases at lower pressures than conventional pressurized tanks. Examples of the various applications of MOFs and their chemistry will be discussed herein.

Figure 1.1.6. The many applications of MOFs.

As was discussed in section 1.1.1, the combination of metal and organic linker can lead to an anionic or cationic framework that is charge-balanced by an extra-framework ion. MOFs can be deliberately designed to exchange their extra-framework ion for or adsorb a potentially hazardous pollutant. In designing the MOF, it is important that the exchanged 'guest' species is relatively benign and does not pose a risk if it is released in water. Some pollutants that have been targeted by MOFs for ion exchange/adsorption are heavy metal cations such as Pb^{2+}, Cd^{2+}, and Hg^{2+}, and oxyanions such as perchlorate (ClO_4^-) and dichromate ($Cr_2O_7^{2-}$).[38] A postsynthetically-modified MOF {$[Zn_3L_3(BPE)_{1.5}]_n$, L = 4,4'-azoxydibenzoate, BPE = bis(4-pyridyl)ethylene} was reported to have 99% removal efficiency for Pb^{2+} ions from water against background ions, with an uptake capacity of 616 mg Pb^{2+}/g adsorbent.[39] The selective uptake of Pb^{2+} is attributed to the decoration of the framework with O^- groups. Two MOFs {**FJI-H9**: $[Me_2NH_2^+][Ca_2(thb^{2-})_2(CH_3COO^-)(DMA)]$, thb = 2,5-thiophenedicarboxylate, DMA = dimethylacetamide and **FJI-H12**: $[Co_3(Timt)_4(NCS)_6(H_2O)_{14}(EtOH)]_n$, Timt = 2,4,6-tri(1-imidazolyl)-1,3,5-triazine} from the Hong group were reported to exhibit over 99% and 86% removal of Cd^{2+} and Hg^{2+} ions, respectively.[40,41] These removals correspond to uptake capacities of 286 mg Cd^{2+}/g and 439 mg Hg^{2+}/g, respectively. The propensity of FJI-H9 and FJI-H12 for Cd^{2+} and Hg^{2+} is due to the dangling sulfurs from the thiophenyl and NCS^- ligands, respectively. The studies showed that although the two MOFs exhibited uptake of both Cd^{2+} and Hg^{2+}, FJI-H9 preferred Cd^{2+} and FJI-H12 preferred Hg^{2+}. The authors make the argument that the selectivity is dictated by the shape of the pore

channels of the respective MOFs.[40] Thus far, these three examples of heavy metal ion remediation have been for ion adsorption (by the organic linker) but not exchange. Other factors that make MOFs attractive candidates for pollutant remediation (other than their selectivity) are their reusability/regenerability. Colinas from the Oliver group reported anion exchange of NO_3^- for ClO_4^- from the two dimensional material [Ag-4,4'-bipyridine$^+$][NO_3^-] in 99% efficiency (353 mg ClO_4^-/g), and the ability for regeneration of the original material at least seven times with a minimal drop in exchange efficiency.[42] The cationic framework MONT-1 {[Ag(μ_3-abtz)$^+$](NO_3^-)(H_2O)$_{0.125}$]$_n$, abtz = 1-(4-aminobenzyl)-1,2,4-triazole} showed a 99% ion exchange of NO_3^- for $Cr_2O_7^{2-}$ (211 mg $Cr_2O_7^{2-}$/g) and regenerability of up to five times, retaining 73% in exchange efficiency.[43] The MONT-1 material was regenerated by adding the dichromate exchanged samples to a 200-fold molar nitrate solution; after 24 hours, almost 95% of the dichromate ions were released back into solution and MONT-1 was regenerated. This section hopefully demonstrates the ability of MOFs to act as robust ion adsorbents of hazardous aqueous species.

MOFs can be employed as two different types of sensors: luminescent or electromechanical.[35] Luminescent MOFs can be 'turn-on' or 'turn-off' sensors, which refer to the luminescence of an otherwise non-emissive framework or the quenching or shift in signal of an initially luminescence framework upon uptake of an analyte, respectively. A post-synthetically functionalized Zr-terephthalate-based MOF (UiO-66@N_3) was shown to be a selective turn-on probe for hydrogen sulfide (H_2S) detection within living cells.[44] Hydrogen sulfide is an important biological signaling

molecule, and its real-time detection could give insight into its physiological role. A Cd-based MOF {$[Cd_3(L)(2,2'\text{-bipyridine})_2 \cdot 4\ DMA]_n$, L = hexa[4-carboxyphenyl)oxamethyl]-3-oxapentanate, DMA = dimethylacetamide} was reported to have recyclable turn-off capabilities in the presence of benzene (C_6H_6) and nitrobenzene ($C_6H_5NO_2$) vapors.[45] The samples were regenerated by heating under vacuum at 80 °C for three hours. Further examples of luminescent lanthanide-based MOFs as sensors will be discussed in section 1.3.2. Electromechanical sensing MOFs are still in their inception. Thin films of the MOF HKUST-1 {$[Cu_3(BTC)_2(H_2O)_3]_n$, BTC = 1,3,5-benzenetricarboxylate} were reported to be grown on a microcantilever surface.[46] The cantilever incorporated a built-in piezoresistive sensor for stress-based detection. The slight distortions in the MOF crystal structure when water, methanol, or ethanol vapors were adsorbed could be measured and correlated with the concentrations of the adsorbed molecules. In another study, a thin film of HKUST-1 was grown on a quartz crystal microbalance surface.[47] The MOF was exposed to pyridine (C_5H_5N) vapors and analysis of the measurements resulted in determination of the diffusion coefficient of the gas. These examples show the 'proof of concept' of MOFs as electrochemical sensors. An ideal MOF sensor should be sensitive to only one analyte. Because many of these examples of sensors show responses to multiple analytes, more work in fine-tuning the specificity of analyte detection is needed.

The role of MOFs as catalysts is usually due to unsaturated metal nodes within the framework that can stabilize an incoming organic molecule for a reaction. One of the

first reports of MOF catalysis was the use of Cd(4,4'-bipyridine)$_2$(NO_3)$_2$ for the cyanosilylation of various aldehydes.[6] Other organic transformations that have been reported with MOF catalysts are alkene oxidation, oxidative coupling, ketal formation, and esterification.[48–51] The pores of MOFs may also aid catalysis by orienting molecules, stabilizing transition states, or excluding larger molecules.[33]

MOFs can be used to either store gases for alternative fuels (H_2, CH_4) or separate gas (CO_2) for clean air. In order to increase the pore volume of MOFs for gas adsorption, long organic linkers with multiple benzene rings are typically employed.[32] The Cu-based MOF, NU-100, was reported to have a substantial surface area of 6,143 m^2/g and storage capacities of 164 mg H_2/g and 2,315 mg CO_2/g.[52] A sol-gel synthesis of the MOF HKUST-1 was reported to have a surface area of 1,193 m^2/g and storage capacity of 177 mg CH_4/g.[53] The Department of Energy (DOE) has published technical targets for hydrogen and methane storage in vehicles outlining parameters such as kg H_2/kg system, system cost, durability and operability conditions, etc.[54] MOFs are potential candidates for hydrogen and methane storage systems, but no material that meets all the DOE criteria has yet to be reported.

1.1.4. Characterization Techniques

Due to the inherent crystallinity and porosity of MOFs, several analytical techniques are suitable for characterizing their structures: X-ray diffraction (XRD), microscopy, thermogravimetric analysis (TGA), Fourier-Transform infrared spectroscopy (FTIR), and gas adsorption analysis.[33,55] X-rays are a powerful tool because the wavelength

(typically 1.5418 Å for Cu-Kα X-ray source) of this electromagnetic radiation is the same order of magnitude as the atomic spacing in crystalline solids. Crystals are solid, repeating units with long-range atomic order. Single crystal X-ray diffraction (SCXRD) is perhaps the most valuable technique used because it allows the ordered atomic structure of crystalline materials to be solved. Crystals suitable for SCXRD must be single (as the name implies) and on the order of at least ~ 50 micrometers. The diffraction pattern produced by SCXRD is then solved and refined. This technique requires access to a single crystal facility and the skills of a crystallographer in solving and refining the final structure.

Another XRD technique is powder X-ray diffraction (PXRD). This is a simpler technique to use which gives limited but useful information on the structure. When X-rays interact with a randomly oriented, homogenously ground powder sample, they diffract and produce a fingerprint powder pattern. The use of Bragg's law ($2d \sin\theta = n\lambda$) allows for the relative determination of d-spacing within a two-dimensional or three-dimensional structure, as well as insight on additional reflections and structural information (Figure 1.1.7).[55] The values of d and θ are inversely proportional, thus in a PXRD pattern, a smaller θ value corresponds to a larger d-spacing. PXRD is a quick and practical technique that can be used to verify a synthesis or known mineral phase.

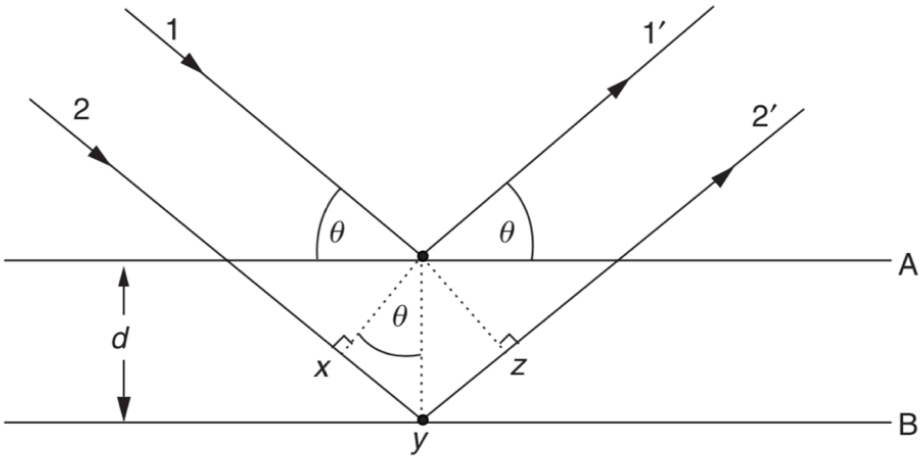

Figure 1.1.7. Derivation of Bragg's law, depicting incident X-rays (1, 2) interacting with the d-spacing of atoms and their resulting reflections (1', 2').[55]

Optical microscopy and scanning electron microscopy (SEM) are useful techniques for visualizing the crystal morphology and surface texture of a sample. Different crystal morphologies from a synthesis can indicate multiple crystal structures present. Transmission electron microscopy (TEM) is capable of identifying the structures of nanocrystalline MOFs and the distribution of nanoparticles within a sample.[56] These microscopy techniques have different resolution limits: ~ 1 μm for optical, ~ 10 nm for SEM, and ~ 1 nm for TEM. SEM and TEM both utilize an electron beam as the source of imaging. In the case of SEM, electrons are bombarded against the sample, and result in secondary (ionized) and backscattered (reflected) electrons. These types of electrons are independently detected and provide insight into the sample's atomic composition and topography, respectively. In TEM, electrons pass through the sample

to produce high resolution images. A combination of these microscopy techniques complements the data from XRD.

TGA reveals the thermal stability of a structure, i.e. how much temperature the framework can withstand before collapsing. TGA data is typically graphed as percent mass loss of a sample versus temperature. The analysis usually first shows the decomposition of guest and/or coordinated molecules and then the loss of the organic linker. The final product after heating to ~ 600 °C is typically a metal oxide. In conjunction with variable temperature (VT)-PXRD, information about how the structure changes as it is heated can be revealed.

FTIR uses infrared electromagnetic radiation to probe bond vibrations within molecules. These vibrations occur at characteristic frequencies (wavenumbers, cm^{-1}) and thus certain bonds or functional groups can be identified using this technique. FTIR is particularly useful for identifying functional groups on the organic linker, as well as demonstrating ion exchange.

Gas adsorption isotherms can give pore volume measurements and surface area measurements of MOFs. There are a few different methods for gas adsorption volumetry. Simply, a general procedure is as follows: a known volume of pure, inert gas (such as N_2) is admitted to a calibrated and confined volume containing the adsorbent (MOF).[57] As adsorption takes place, the pressure in the confined volume falls until equilibrium is established. First, a monolayer of adsorbed molecules comes

into contact with the surface layer of the adsorbent. The gas molecules continue to fill the pore volume so more than one layer of molecules is in direct contact with the adsorbent surface. The amount of gas adsorbed is the difference in the volume of the container and the volume that the sample takes up in the container. The adsorption isotherm can then be classified into one of eight characteristic types, which is related to pore structure and size (e.g. micropore/mesopore/macropore) (Figure 1.1.8).[57] Because new characteristic types of isotherms have been identified since the original six types, two additional isotherms have been added to the types I to VI. Type I isotherms are indicative of microporous solids with relatively small external surfaces. Type II isotherms are produced by the physisorption of gases on nonporous or microporous solids. Type III isotherms are representative of no identifiable monolayer formation. The adsorbent-adsorbate interactions are relatively weak and the adsorbed molecules are clustered around favorable sites on the surface of a nonporous or macroporous solid. Type IV isotherms are given by mesoporous adsorbents. Type V isotherms are attributed to relatively weak adsorbent-adsorbate interactions, similar to those in type III isotherms. The adsorbed molecules cluster around favorable sites on the surface and continue to fill the pores of microporous or mesoporous adsorbents. Lastly, Type VI isotherms describe a layer-by-layer adsorption on a highly uniform, nonporous surface. The hysteresis loops observed in the type IV(a) and V isotherms occur when the adsorption and desorption curves do not coincide. This can result due to network effects such as pore blocking. Further calculations using the Brunauer-Emmett-Teller (BET) method can yield internal surface area measurements of the framework.

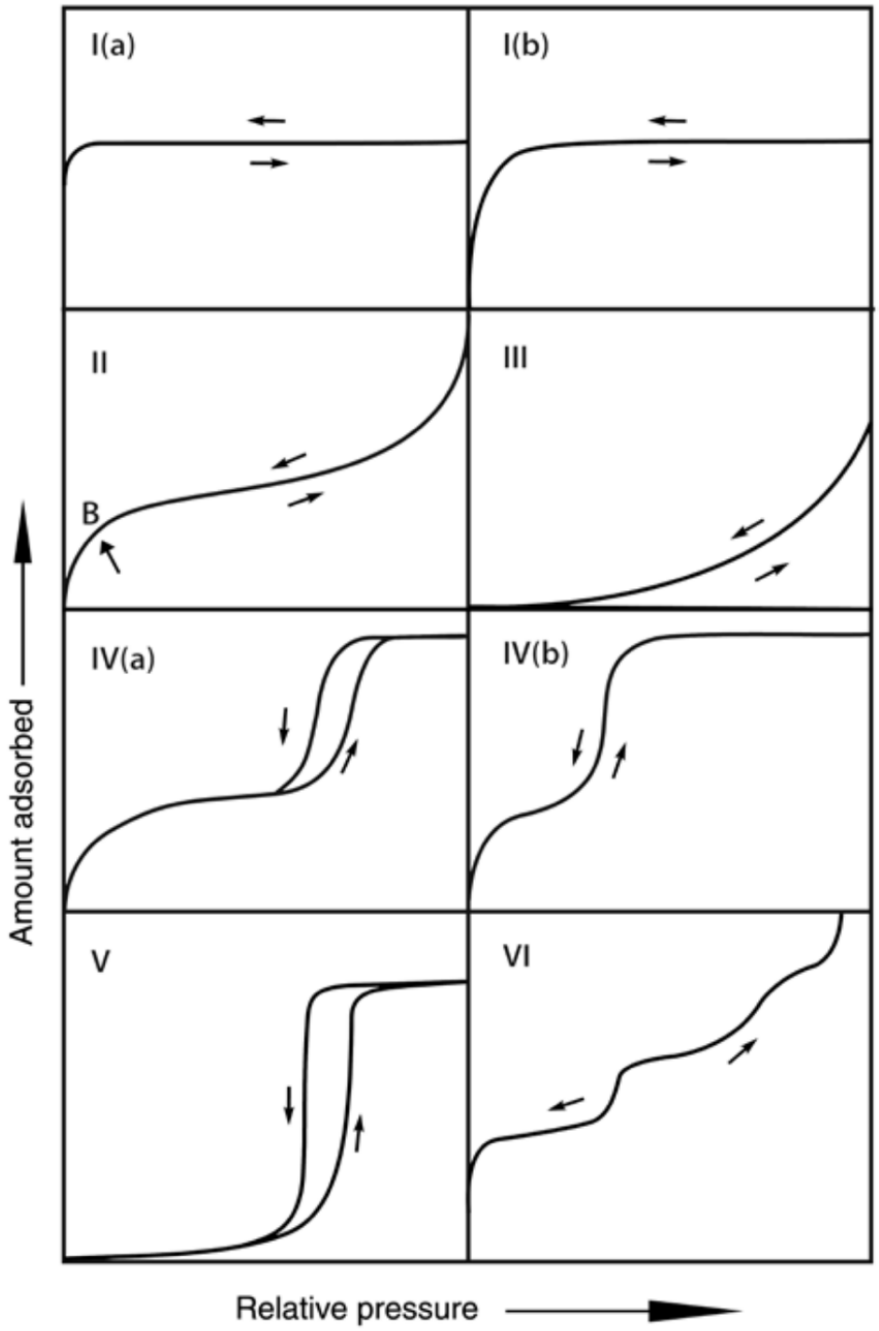

Figure 1.1.8. Classification of the eight different types of physisorption isotherms.[57]

1.2. Rare Earth Elements

1.2.1. Rare Earth History, Properties, and Chemistry

The rare earth elements (REEs) or rare earth metals (REMs) are comprised of the *d*-block elements scandium (Sc) and yttrium (Y) and the fifteen lanthanoid elements in the first row of the *f*-block on the periodic table (Figure 1.2.1). The lanthanoid elements range from lanthanum (La) to lutetium (Lu). The term 'lanthanoid' meaning 'like lanthanum' is preferred by the International Union of Pure and Applied Chemistry (IUPAC) as opposed to 'lanthanide' when referring to the neutral elements.[58] In this work, 'lanthanide' will be used to refer to the 3+ ions of the lanthanoids. The history of the REEs can be traced back to the late 18th century to a mine in Ytterby, a village on the Swedish island of Resarö.[59] Chemist and mineralogist Johan Gadolin is credited with discovering the first RE oxide, yttria (Y_2O_3), in a mineral that was later named after him as gadolinite.[60] Subsequent work revealed that gadolinite contained the oxides of at least 10 additional REEs.[61] It was not until the early 20th century that the periodic table of the elements was rearranged by number of protons rather than atomic mass, due to the work of Henry Moseley with X-ray spectroscopy. It was due to this new way of organizing the periodic table that left a gap for the fourteen elements between lanthanum and hafnium to be recognized and discovered. In fact, the term lanthanoid originates from the Greek word *lanthaneien*, which means "lying hidden".[62] By 1907, all of the lanthanoid elements with the exception of radioactive promethium had been identified.[59] The REEs were so difficult to separate from minerals due to the chemical similarities

among the elements. These metals are often found in the 3+ oxidation state and have similar sizes and chemical properties.

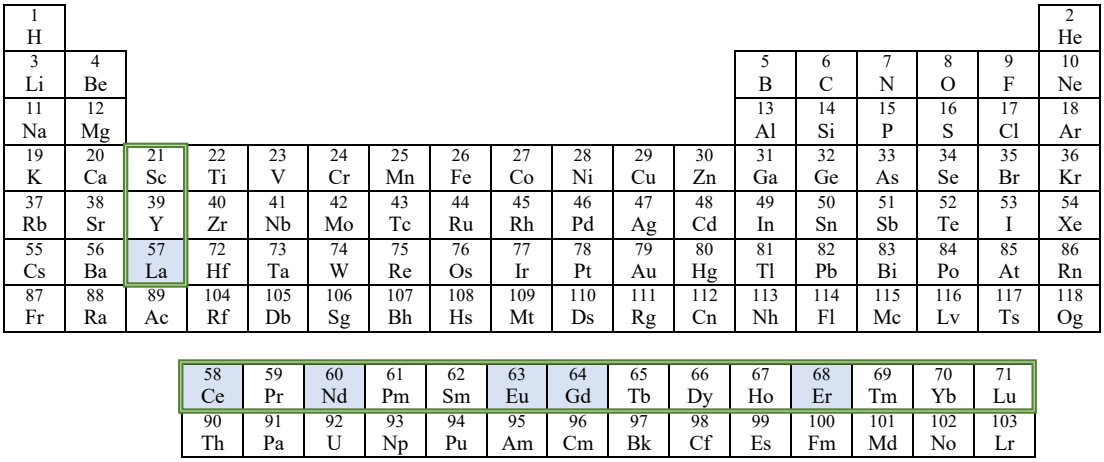

Figure 1.2.1. Periodic table of the elements. The rare earth elements are outlined in green, and the lanthanoids that will be discussed in this work are highlighted in blue.

Some basic properties of the lanthanoids are presented in Table 1.2.1. As can be seen from their electron configurations, the lanthanides (with the exception of La^{3+}) contain electrons in the *f* orbitals (Figure 1.2.2).[63] The 4*f* orbitals lie close to the nucleus, compared to the surrounding 5*s* and 5*p* orbitals. As a result, the 4*f* orbitals are typically not involved in bonding, and the lanthanoids first lose the higher energy $6s^2$ and $5d^1$ electrons to result in a 3+ oxidation state. The fact that the 4*f* orbitals are 'buried' also gives rise to the lanthanide contraction, a term used to describe the decrease in atomic radius from La to Lu. The 5*s* and 5*p* orbitals penetrate the 4*f* subshell and are not shielded from the increasing nuclear charge of the lanthanoids, thus resulting in the contraction of atomic radius.[59]

Table 1.2.1. Basic properties of the lanthanoids. The elements that will be discussed in this work are highlighted in blue

Element	Symbol	Atomic Number	Electron Configuration of Ln^{3+}	Atomic Mass	Effective Ionic Radius[64] (Å) (C.N. = 8)
Lanthanum	La	57	[Xe]	138.91	1.160
Cerium	Ce	58	[Xe]$4f^1$	140.12	1.143
Praseodymium	Pr	59	[Xe]$4f^2$	140.91	1.126
Neodymium	Nd	60	[Xe]$4f^3$	144.24	1.109
Promethium	Pm	61	[Xe]$4f^4$	(145)	1.093
Samarium	Sm	62	[Xe]$4f^5$	150.36	1.079
Europium	Eu	63	[Xe]$4f^6$	151.96	1.066
Gadolinium	Gd	64	[Xe]$4f^7$	157.25	1.053
Terbium	Tb	65	[Xe]$4f^8$	158.93	1.040
Dysprosium	Dy	66	[Xe]$4f^9$	162.50	1.027
Holmium	Ho	67	[Xe]$4f^{10}$	164.93	1.015
Erbium	Er	68	[Xe]$4f^{11}$	167.26	1.004
Thulium	Tm	69	[Xe]$4f^{12}$	168.93	0.994
Ytterbium	Yb	70	[Xe]$4f^{13}$	173.05	0.985
Lutetium	Lu	71	[Xe]$4f^{14}$	174.97	0.977

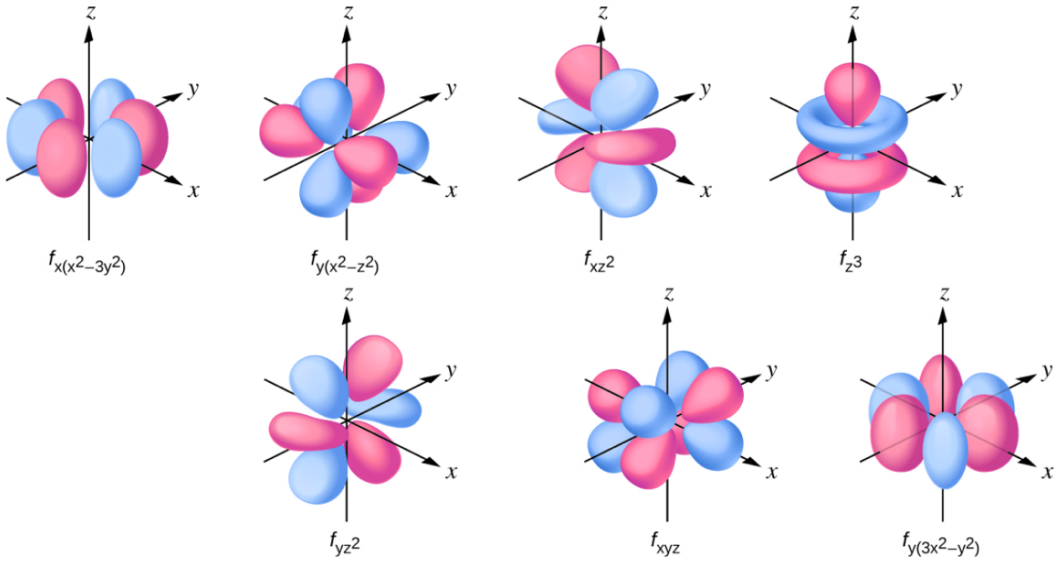

Figure 1.2.2. Depiction of the seven *f* orbitals. The general set is made of the orbitals:

$f_{x(x^2-3y^2)}$, $f_{y(x^2-z^2)}$, f_{xz^2}, f_{z^3}, f_{yz^2}, f_{xyz}, and $f_{y(3x^2-y^2)}$.[59,63]

The light emissive properties of a lanthanide ion are governed by two conditions: 1) the ease in which its excited states can be populated and 2) the minimization of non-radiative energy transfer paths.[65] To meet the first requirement, sensitization of the ion via the surroundings is often used (this will be further discussed in section 1.3.1 as the 'antenna effect'). The second requirement refers to the energy gap between the lowest lying excited state of the metal ion and the highest sublevel of its ground state (Figure 1.2.3: the difference between labeled energy states).[66] The smaller this gap, the easier it is to close by non-radiative deactivation processes, such as through vibrations of bound ligands. The sizeable energy gaps belonging to Eu^{3+} and Tb^{3+} correspond to energy differences which fall in the visible region (corresponding to wavelengths of approximately 620 nm and 550 nm, respectively). The other

lanthanides have emissions which correspond to near-infrared or ultraviolet wavelengths. Lanthanide luminescence will be further discussed in section 1.3.

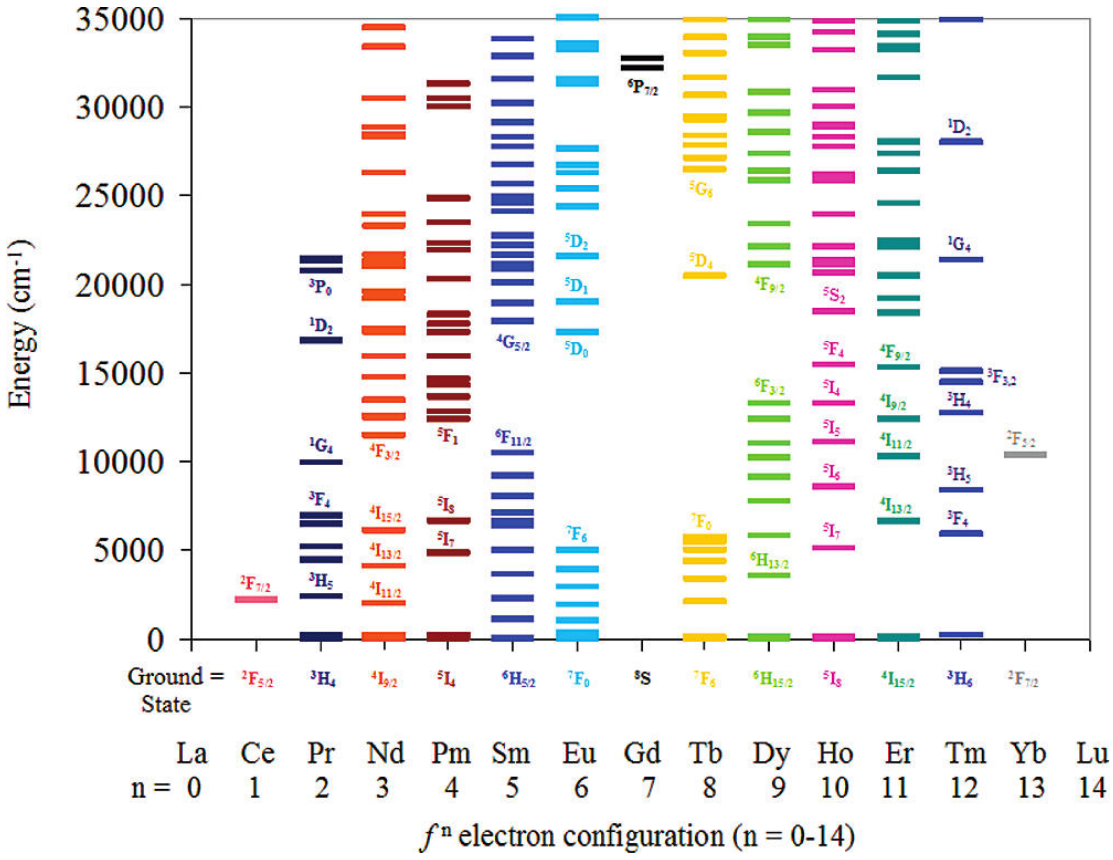

Figure 1.2.3. Partial electronic energy level diagrams of the lanthanides, showing possible *f-f* transitions.[66]

The lanthanides are classified as 'hard' acids and therefore show a preference in binding to 'hard' bases such as oxygen and fluorine rather than 'soft' bases with elements such nitrogen, phosphorus, or sulfur.[59] Due to the size of the lanthanides, they adopt high coordination numbers in their compounds (usually 8-9, but up to 12).[61] As a result of these two characteristics, the lanthanides are often found

coordinated to hydroxide and water molecules, which are able to fill up the lanthanide coordination sphere without being too bulky of a ligand. Terminal and bridging oxygen coordination has been observed.[67] Coordination to O-donor ligands such as carboxylates, alkoxides, nitrates, and sulfates are also well documented.[68]

1.2.2. Lanthanide MOFs

One of the first lanthanide-based MOFs to be reported was by Yaghi and his group in 1999: the structure of $Tb(bdc)NO_3 \cdot 2$ DMF (bdc = 1,4-benzenedicarboxylate) was reported and briefly characterized.[69] In this structure, there are two distinct Tb^{3+} centers, each one coordinated by eight oxygens from a combination of benzenedicarboxylates, nitrates, and DMF molecules. Due to the similar characteristic properties of the lanthanides, it is not uncommon for lanthanide MOFs to be isomorphous, meaning that the structures crystallize in the same space group, have the same unit cell dimensions, and the positions of atoms within the structure are the same except for a replacement of one or more atoms.[70] An example of this effect is the isomorphous series of fourteen structures (based on lanthanides = La – Lu, with the exception of Pm) with the general formula $[Ln(TC)_3(H_2O)_2][HPy \cdot TC]_n$ (TC = 2-thiophenecarboxylate; HPy = pyridinium).[71] Each lanthanide center is coordinated by eight carboxylate oxygens. The authors also demonstrated achieving luminescent color-tuning from red to green by varying the Eu^{3+}:Tb^{3+} ratio in a series of heterobimetallic structures. However, isomorphous structures will not always form with lanthanides under similar reaction conditions. For example, under similar reaction conditions, combinations of lanthanide nitrate salts (Ln = La, Pr, Nd, Sm, Eu,

Gd, Dy, Er) and the ligand 4,8-disulfonyl-2,6-naphthalenedicarboxylic acid produced three distinct structures (Figure 1.2.4).[72] The authors characterized the eight structures but do not discuss possible reasons for the structural diversity reported. The authors also report that syntheses with lanthanide nitrate salts of Tb, Ho, and Yb with the ligand were explored, but no suitable products were obtained. In chapter 4 of this work, some insights into the structural diversity of lanthanide-based structures will be presented.

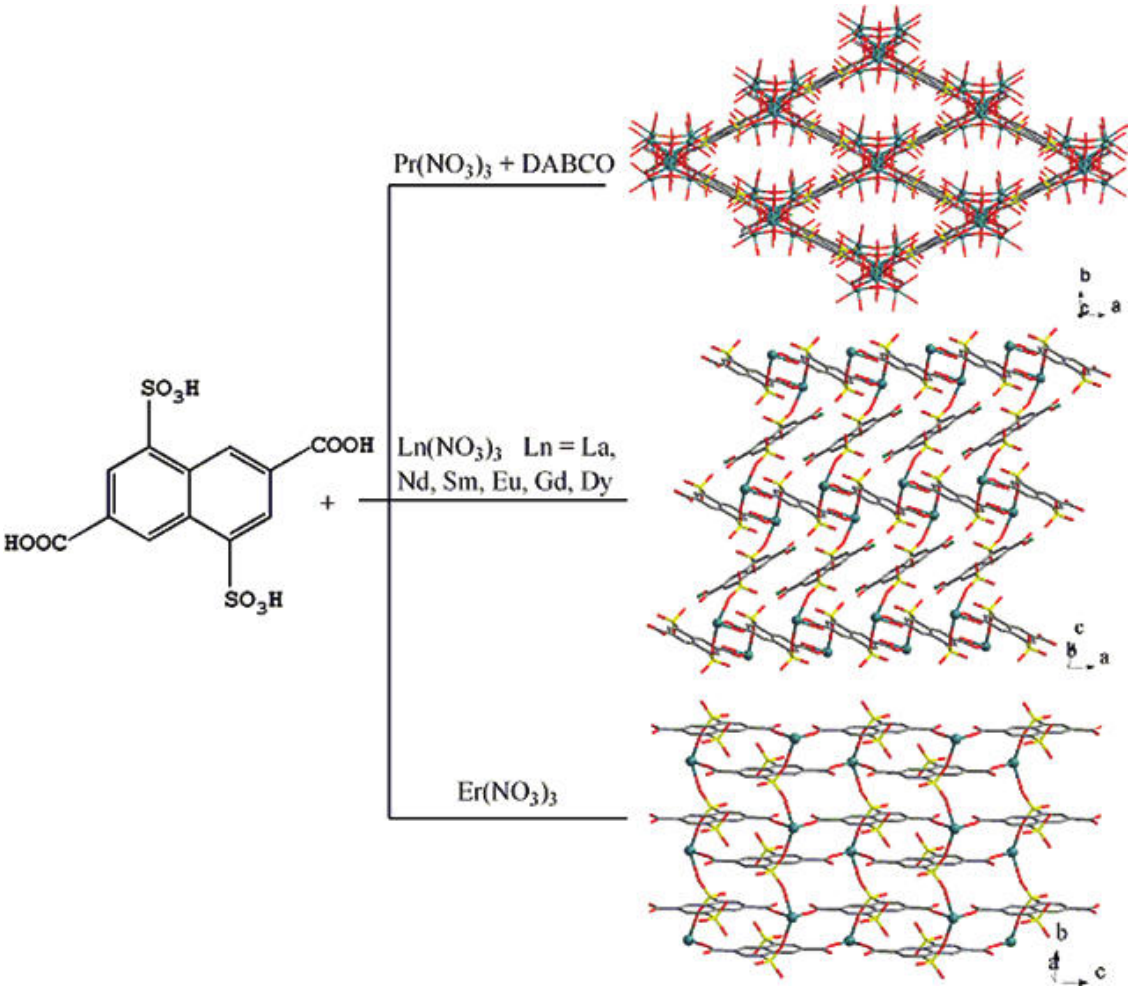

Figure 1.2.4. Structural diversity of lanthanides with the ligand 4,8-disulfonyl-2,6-naphthalenedicarboxylic acid under similar reaction conditions.[72]

1.2.3. Layered Rare Earth Hydroxides (LREHs)

Layered rare earth hydroxides (LREHs) are a subclass of layered double hydroxides (LDHs). LDHs have the general formula $[M^{2+}_{1-x}M^{3+}_{x}(OH)_2]^{x+}$ $[A^{n-}_{x/n}\cdot y\ H_2O]^{x-}$, where M is a divalent or trivalent metal, respectively, *x* is in the range of 0.2 to 0.33, and A is an *n*-valent anion.[73] LDHs thus consist of two-dimensional cationic layers with anions in the interlamellar space, which are held by electrostatic forces and hydrogen bonding (Figure 1.2.6).[73,74] The first family of LREH structures was reported by Monge and her group in 2006.[75] LREHs have the general formula $[RE_4(OH)_{10}(H_2O)_4]_nA_n$, where RE is a rare earth trivalent ion, and A is an intercalated anion (Figure 1.2.7).[75] LREHs are similar to LDHs in that they consist of cationic metal aquahydroxy layers intercalated by anions, such as halides (Cl^-, Br^-), nitrate, sulfate, organodicarboxylates, and organodisulfonates.[76] LREHs have applications in anion exchange, as the anions between the cationic layers are electrostatically bound and can be readily exchanged. Typically, LREHs are not as robust as MOFs. This is evidenced by qualitative but not quantitative characterizations of anion exchange.[77–79] For example, structures of $RE(OH)_{2.5}Cl_{0.5}\cdot 0.8\ H_2O$ (RE = Eu, Tb) were reported to readily exchange the interlayer chloride ions for various anions {NO_3^-, SO_4^{2-}, dodecylsulfonate ($C_{12}H_{25}OSO_3^-$)}.[77] The anion exchange was characterized with PXRD and FTIR. The authors show that this exchange is possible, but do not quantify the extent of anion uptake by the materials.

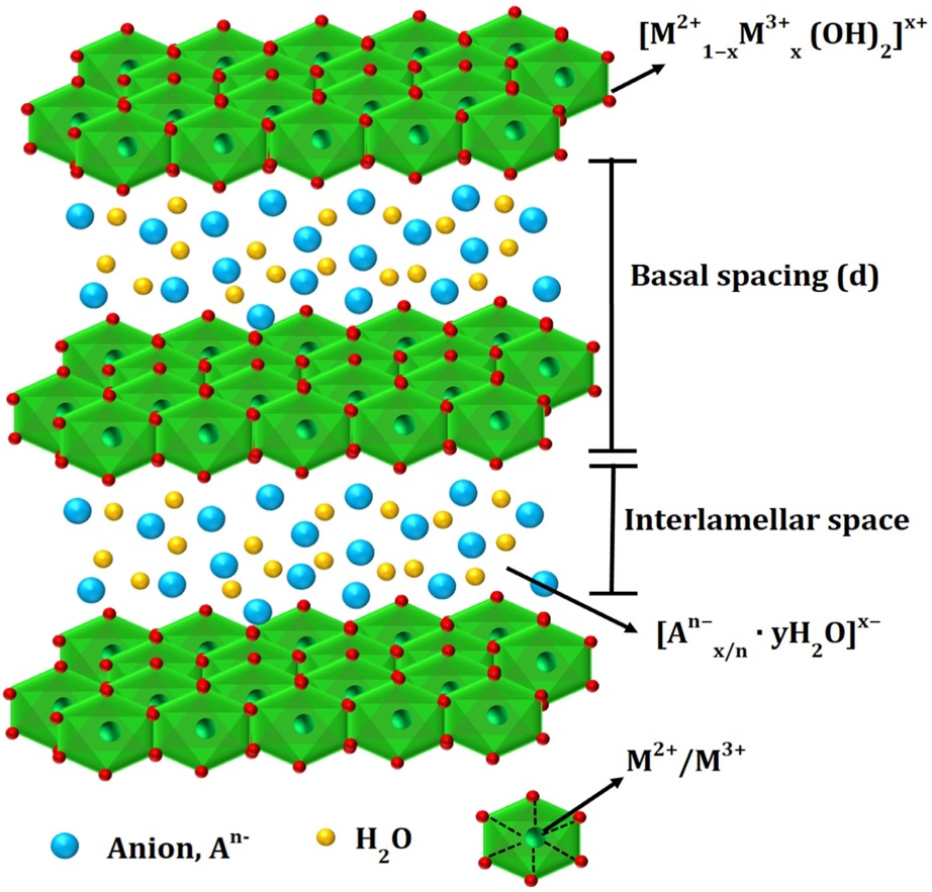

Figure. 1.2.6. General structure of a LDH, showing the anions in the interlamellar spaces between the cationic layers.[73]

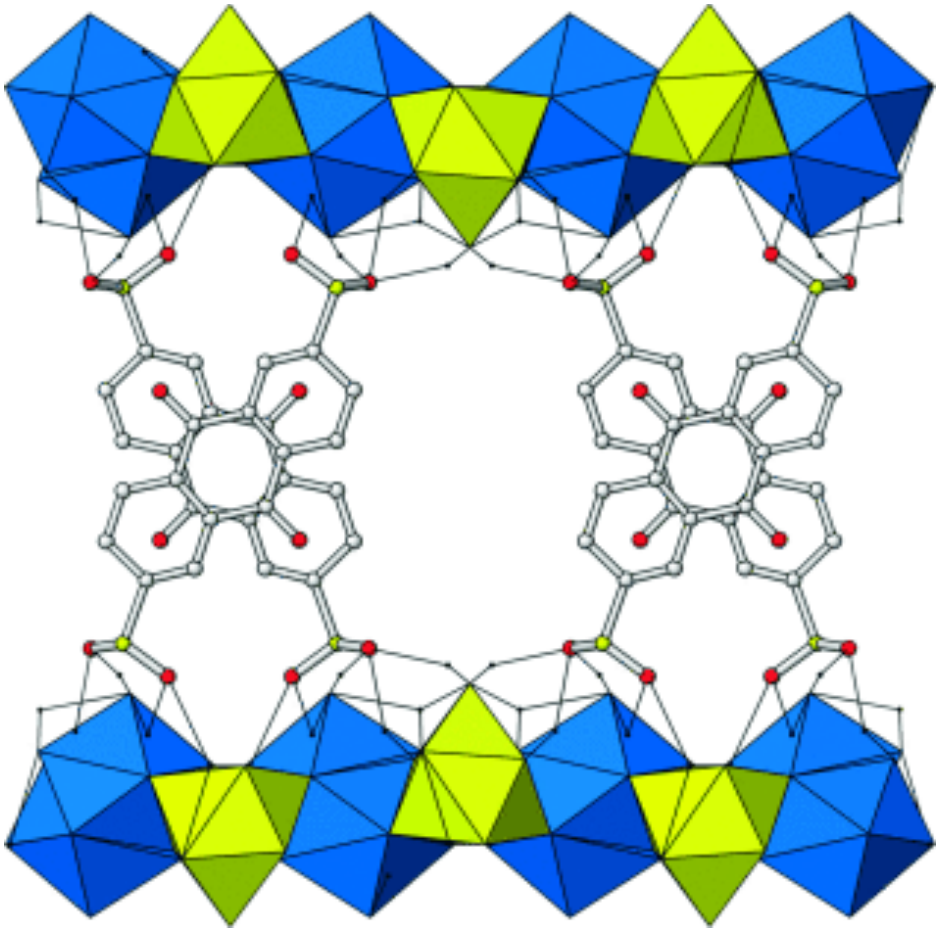

Figure 1.2.7. Structure of LREH: $[RE_4(OH)_{10}(H_2O)_4]^{2+}$ layers intercalated with organic linker anthraquinonedisulfonate [$RE(OH)_7H_2O$ = blue polyhedra, $RE(OH)_6H_2O$ = green polyhedra].[75]

1.3. Luminescent Lanthanide MOFs

1.3.1. Luminescence Background and Pathways

Luminescence is the emission of light by a substance that has not been heated. There are two types of luminescence: fluorescence and phosphorescence (Figure 1.3.1).[80] High energy light (usually ultraviolet light) excites an electron from the singlet

ground state to an excited singlet state. In the case of fluorescence, the electron falls back to a lower energy state, resulting in the emission of a photon of visible light. The electron in the excited orbital is the opposite spin of the second electron in the ground state orbital; this is called a spin-allowed transition and occurs rapidly.[81] In the case of phosphorescence, the excited electron will migrate to a lower energy triplet state (this migration is known as intersystem crossing, which results in the reversal of the electron spin orientation) before returning to the ground state and emitting light. The process of intersystem crossing occurs due to spin-orbit coupling. The electron in this excited triplet state is the same spin as the ground state electron, which makes this a spin-forbidden transition.[81] It is because of this forbidden transition at a lower energy state that phosphorescence usually has a longer lifetime than fluorescence (typically on the order of milliseconds or seconds versus nanoseconds, respectively) and emits at longer wavelengths.

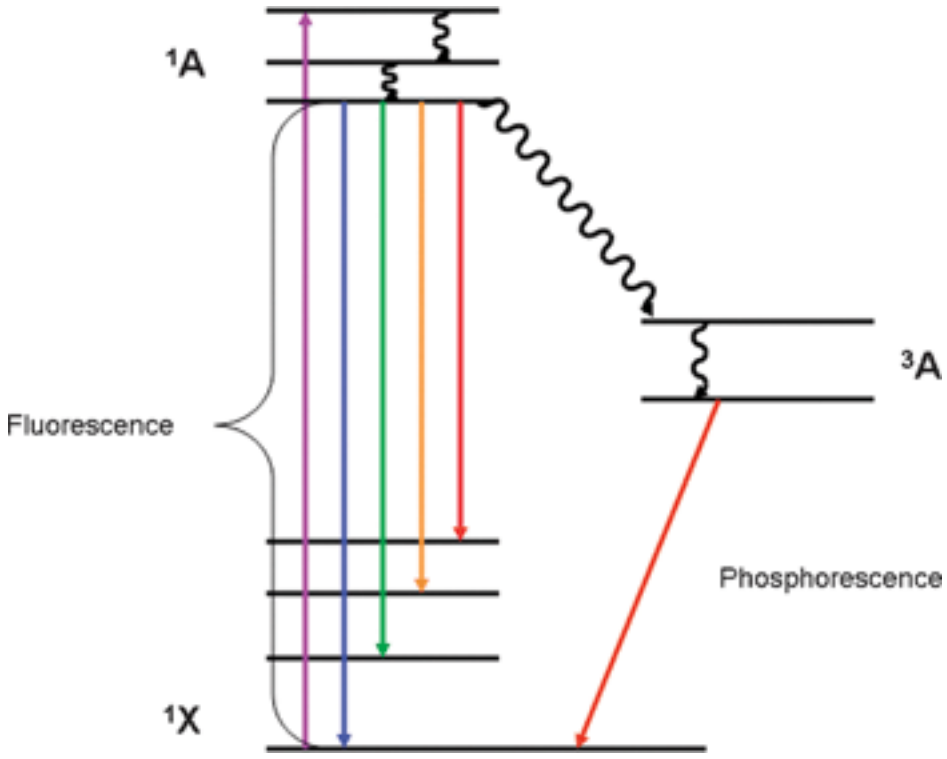

Figure 1.3.1. Jablonski diagram depicting the general schematic for fluorescence and phosphorescence pathways.[80]

In an insightful review on luminescent MOFs, Allendorf et al. describe five distinct modes for generating MOF luminescence (Figure 1.3.2).[80] The five possible modes are as follows: 1) conjugated organic linkers can directly emit light after absorbing in the UV or visible region; 2) framework metal ions (such as Ln^{3+}) in proximity to an organic fluorophore can produce an antenna effect and emit sharp luminescence; 3) adsorbed lumiphores can be entrapped in a MOF pore and luminesce in an otherwise non-emissive framework; 4) lumiphores can be covalently bound to the MOF framework; 5) exciplex formation can produce broad luminescence due to π-π interactions between adjacent conjugated linkers or between a linker and guest

molecule. The focus in this work will be on the luminescence emitted from lanthanide ions via the antenna effect.

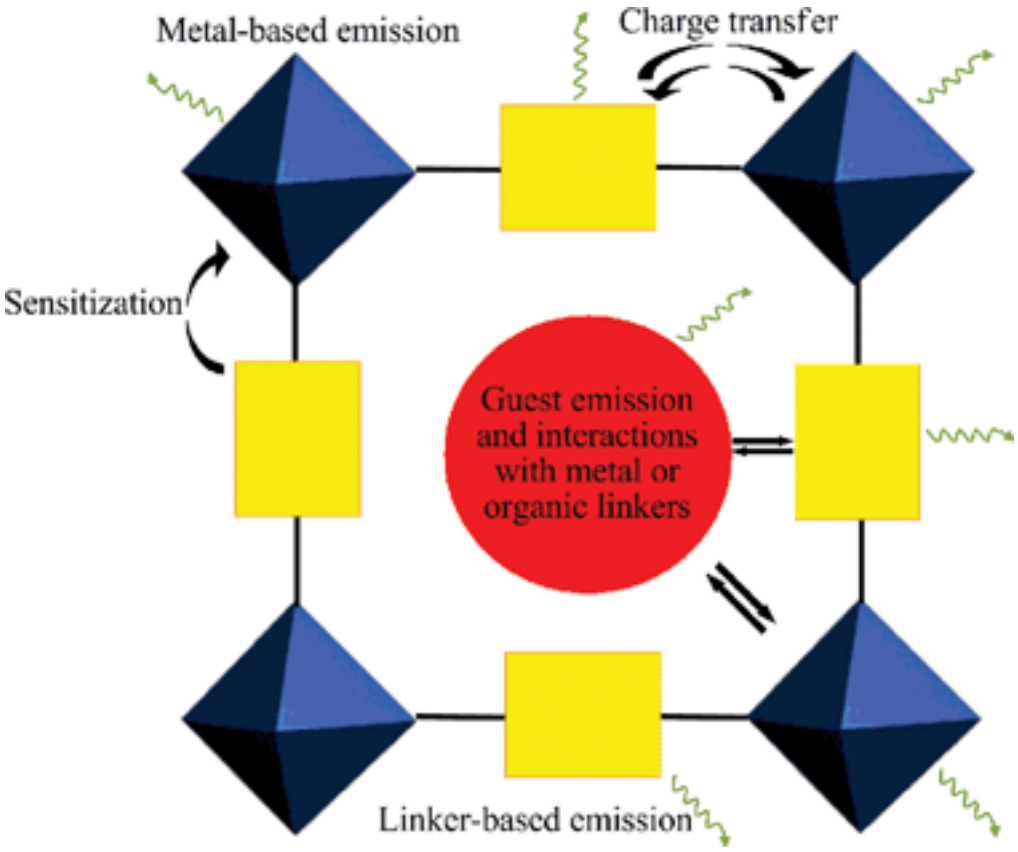

Figure 1.3.2. Five possible pathways of luminescence in MOFs (metal SBU = blue polyhedra; organic linker = yellow rectangle; guest species = red circle; light emission = green wavy arrows; electron transfer = black arrows).[80]

The antenna effect is further illustrated in Figure 1.3.3. Recall the two conditions for lanthanide luminescence: 1) the ease in which the excited states can be populated and 2) the minimization of non-radiative energy transfer paths.[65] Conjugated organic linkers such as those with benzene rings are excellent sensitizers which are capable of

transferring their excited energy to the lanthanide ion (activator). The electron in the excited lanthanide energy state may undergo radiative (photoluminescence) or non-radiative (dropping to a lower energy state without photoluminescence) de-activation.

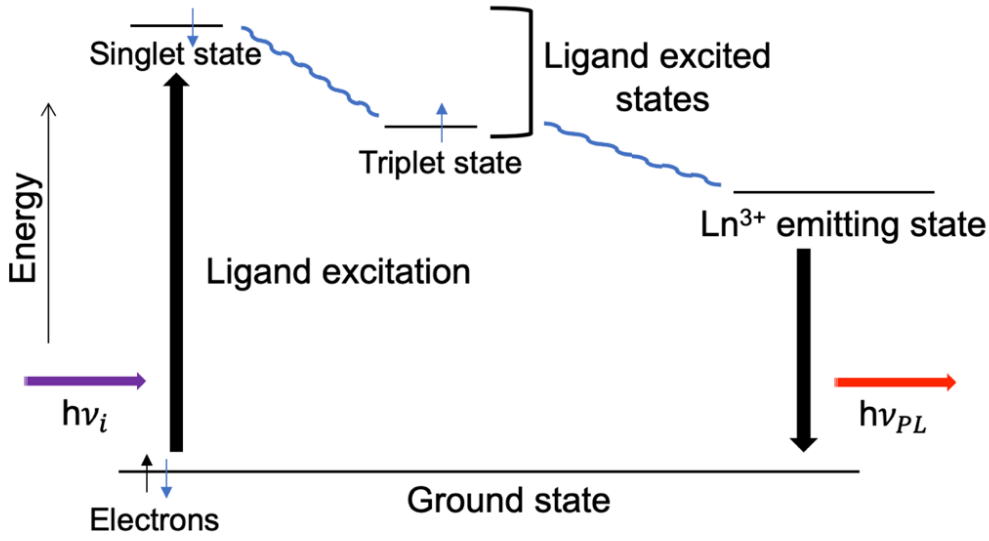

Figure 1.3.3. Schematic of the antenna effect. An organic linker is excited with incident, high energy light ($h\nu_i$) and the energy is transferred to a lanthanide ion excited state which photoluminesces at a longer wavelength ($h\nu_{PL}$).

Solid state luminescence is arguably advantageous over solution luminescence due to the predictability of structure. In the case of MOFs, the organic linkers are stabilized within the framework which reduce the non-radiative decay rate.[66] This also results in a bound organic linker which can readily charge transfer to the emitting lanthanide. In a crystalline solid, the ligand-ligand interactions are also rigidly controlled and can affect the luminescence of a MOF. Luminescent materials can be characterized in

three ways: solid state luminescence spectroscopy, quantum yield, and fluorescence lifetime. Solid state luminescence spectroscopy reveals the atomic transitions that occur within the lanthanide emitter. The wavelengths of emitted light can be correlated with the electronic energy diagram and specific transitions can be identified. In Eu^{3+}-containing materials, the most intense transition typically occurs at ~ 620 nm and corresponds to the $^5D_0 \rightarrow {}^7F_2$ transition.[82] The quantum yield or quantum efficiency of a luminescent material is defined as the ratio of photons emitted to photons absorbed. In a study of 41 different Eu^{3+} and Tb^{3+} chelates with aromatic ligands, the highest quantum yields reported were 0.38 and 0.58 for each metal, respectively.[83] These luminescence experiments were conducted in aqueous solution and the study also reported lower quantum yields for Ln^{3+} chelates with less than nine coordinating atoms as a result of water molecules filling empty coordination sites. The luminescence lifetime is a measurement of the average time the molecule stays in its exited state before emitting a photon. The lifetimes of lanthanide emissive transitions sensitized through the antenna effect are usually on the order of a millisecond.[80]

1.3.2. Applications of Luminescent Lanthanide MOFs

The applications of MOFs as luminescent and electromechanical sensors were previously described in section 1.1.3. Here, new applications of luminescent lanthanide-based MOFs such as white light emission and thermometry will be described. Combinations of Eu^{3+} and Tb^{3+} within a framework have proven to be an attractive area for luminescent applications in order to tailor luminescence emissions.

Solid-state white light emitting materials have been sought after due to their broad applications in displays and lighting.[84] White light can be produced by the combination of primary color emissions of red, green, and blue from different compounds. Qian and his group exploited this idea by constructing a MOF with Eu^{3+} and Tb^{3+} (red and green emitters, respectively) and a known blue emitter, the organic linker pyridine-2,6,-dicarboxylic acid (PDA).[85] The MOF $La_2(PDA)_3(H_2O)_5$ was doped with 1-2% molar amounts of Eu^{3+} and Tb^{3+} into the framework, and resulted in an isomorphous structure with a white light emission very close to pure white light.

The use of lanthanide MOFs as colorimetric luminescent temperature probes are advantageous due to their fast response, high sensitivity, and noninvasiveness.[84] Two types of isomorphous heterobimetallic Eu^{3+}/Tb^{3+} structures were reported based on the dicarboxylate ligands 6-(4-carboxyphenyl)-nicotinic acid and [2,2'-bipyridine]-5,5'-dicarboxylic acid.[86] Each material contains a ratio of $Eu_{0.05}Tb_{0.95}$ with each ligand and resulted in a color change from green at 25 K to red at 300 K. The lanthanide ions are sensitized by the ligands, and Eu^{3+} is further sensitized by the Tb^{3+} ions within the framework, as the excited Tb^{3+} electrons are transferred to the lower lying Eu^{3+} excited states. The authors reported that the material with the latter ligand has a higher temperature-sensitive range due to the higher activation energy of the deactivation channel between the ligand and Tb^{3+}. The applications of luminescent lanthanide MOFs continue to grow, and by understanding their structures, we can gain insight into their functions and properties.

1.4. Concluding Remarks

In this chapter, we reviewed the structural details, applications, and characterization techniques of metal-organic frameworks. We discussed the properties and chemistry of the lanthanoid elements, as well as their applications in luminescent metal-organic frameworks and layered rare earth hydroxides. These types of inorganic-organic hybrid structures based on lanthanide metals are relatively new and thus there are many possibilities for novel structures and applications to be explored. Combinations of sensitizers and lanthanide emitters will continue to evolve and as a result, new and exciting applications of luminescent lanthanide-based materials will likely emerge.

1.5. References

(1) Zhou, H.-C.; Kitagawa, S. Metal–Organic Frameworks (MOFs). *Chem. Soc. Rev.* **2014**, *43* (16), 5415–5418. https://doi.org/10.1039/C4CS90059F.

(2) Zhou, H.-C.; Long, J.; Yaghi, O. M. Introduction to Metal–Organic Frameworks. *Chem. Rev.* **2012**, *112* (2), 673–674. https://doi.org/10.1021/cr300014x.

(3) Howarth, A. J.; Liu, Y.; Hupp, J. T.; Farha, O. K. Metal–Organic Frameworks for Applications in Remediation of Oxyanion/Cation-Contaminated Water. *CrystEngComm* **2015**, *17* (38), 7245–7253. https://doi.org/10.1039/C5CE01428J.

(4) Eddaoudi, M.; Moler, D. B.; Li, H.; Chen, B.; Reineke, T. M.; O'Keeffe, M.; Yaghi, O. M. Modular Chemistry: Secondary Building Units as a Basis for the

Design of Highly Porous and Robust Metal−Organic Carboxylate Frameworks. *Acc. Chem. Res.* **2001**, *34* (4), 319–330. https://doi.org/10.1021/ar000034b.

(5) Gable, R. W.; Hoskins, B. F.; Robson, R. A New Type of Interpenetration Involving Enmeshed Independent Square Grid Sheets. The Structure of Diaquabis-(4,4′-Bipyridine)Zinc Hexafluorosilicate. *J. Chem. Soc. Chem. Commun.* **1990**, *0* (23), 1677–1678. https://doi.org/10.1039/C39900001677.

(6) Fujita, M.; Kwon, Y. J.; Washizu, S.; Ogura, K. Preparation, Clathration Ability, and Catalysis of a Two-Dimensional Square Network Material Composed of Cadmium(II) and 4,4'-Bipyridine. *J. Am. Chem. Soc.* **1994**, *116* (3), 1151–1152. https://doi.org/10.1021/ja00082a055.

(7) Yaghi, O. M.; Li, H. Hydrothermal Synthesis of a Metal-Organic Framework Containing Large Rectangular Channels. *J. Am. Chem. Soc.* **1995**, *117* (41), 10401–10402. https://doi.org/10.1021/ja00146a033.

(8) Web of Science Search Results for "Metal-Organic Frameworks." January 2019.

(9) Kuppler, R. J.; Timmons, D. J.; Fang, Q.-R.; Li, J.-R.; Makal, T. A.; Young, M. D.; Yuan, D.; Zhao, D.; Zhuang, W.; Zhou, H.-C. Potential Applications of Metal-Organic Frameworks. *Coord. Chem. Rev.* **2009**, *253* (23), 3042–3066. https://doi.org/10.1016/j.ccr.2009.05.019.

(10) Eddaoudi, M.; Kim, J.; Rosi, N.; Vodak, D.; Wachter, J.; O'Keeffe, M.; Yaghi, O. M. Systematic Design of Pore Size and Functionality in Isoreticular MOFs and Their Application in Methane Storage. *Science* **2002**, *295* (5554), 469–472. https://doi.org/10.1126/science.1067208.

(11) Oliver, S. R. J. Cationic Inorganic Materials for Anionic Pollutant Trapping and Catalysis. *Chem. Soc. Rev.* **2009**, *38* (7), 1868–1881. https://doi.org/10.1039/B710339P.

(12) Rogow, D. L.; Swanson, C. H.; Oliver, A. G.; Oliver, S. R. J. Two Related Gadolinium Aquo Carbonate 2-D and 3-D Structures and Their Thermal, Spectroscopic, and Paramagnetic Properties. *Inorg. Chem.* **2009**, *48* (4), 1533–1541. https://doi.org/10.1021/ic801844b.

(13) Sergo, K. M.; Han, C. S.; Bresler, M. R.; Citrak, S. C.; Abdollahian, Y.; Fei, H.; Oliver, S. R. J. Erbium Hydroxide Ethanedisulfonate: A Cationic Layered Material with Organic Anion Exchange Capability. *Inorg. Chem.* **2015**, *54* (8), 3883–3888. https://doi.org/10.1021/acs.inorgchem.5b00073.

(14) Dey, C.; Kundu, T.; Biswal, B. P.; Mallick, A.; Banerjee, R. Crystalline Metal-Organic Frameworks (MOFs): Synthesis, Structure and Function. *Acta Crystallogr. Sect. B Struct. Sci. Cryst. Eng. Mater.* **2014**, *70* (1), 3–10. https://doi.org/10.1107/S2052520613029557.

(15) Stock, N.; Biswas, S. Synthesis of Metal-Organic Frameworks (MOFs): Routes to Various MOF Topologies, Morphologies, and Composites. *Chem. Rev.* **2012**, *112* (2), 933–969.

(16) Meek, S. T.; Greathouse, J. A.; Allendorf, M. D. Metal-Organic Frameworks: A Rapidly Growing Class of Versatile Nanoporous Materials. *Adv. Mater.* **2011**, *23* (2), 249–267. https://doi.org/10.1002/adma.201002854.

(17) Rabenau, A. The Role of Hydrothermal Synthesis in Preparative Chemistry. *Angew. Chem. Int. Ed. Engl.* **1985**, *24* (12), 1026–1040. https://doi.org/10.1002/anie.198510261.

(18) Huskić, I.; Pekov, I. V.; Krivovichev, S. V.; Friščić, T. Minerals with Metal-Organic Framework Structures. *Sci. Adv.* **2016**, *2* (8), e1600621. https://doi.org/10.1126/sciadv.1600621.

(19) Echigo, T.; Kimata, M. Crystal Chemistry and Genesis of Organic Minerals: A Review of Oxalate and Polycyclic Aromatic Hydrocarbon Minerals. *Can. Mineral.* **2010**, *48* (6), 1329–1357. https://doi.org/10.3749/canmin.48.5.1329.

(20) Seetharaj, R.; Vandana, P. V.; Arya, P.; Mathew, S. Dependence of Solvents, PH, Molar Ratio and Temperature in Tuning Metal Organic Framework Architecture. *Arab. J. Chem.* **2016**. https://doi.org/10.1016/j.arabjc.2016.01.003.

(21) Banerjee, D.; Finkelstein, J.; Smirnov, A.; Forster, P. M.; Borkowski, L. A.; Teat, S. J.; Parise, J. B. Synthesis and Structural Characterization of Magnesium Based Coordination Networks in Different Solvents. *Cryst. Growth Des.* **2011**, *11* (6), 2572–2579. https://doi.org/10.1021/cg200327y.

(22) Myerson, A. S.; Ginde, R. 2 - Crystals, Crystal Growth, and Nucleation. In *Handbook of Industrial Crystallization (Second Edition)*; Myerson, A. S., Ed.; Butterworth-Heinemann: Woburn, 2002; pp 33–65. https://doi.org/10.1016/B978-075067012-8/50004-5.

(23) Wang, Z.; M. Cohen, S. Postsynthetic Modification of Metal–Organic Frameworks. *Chem. Soc. Rev.* **2009**, *38* (5), 1315–1329. https://doi.org/10.1039/B802258P.

(24) Tanabe, K. K.; Cohen, S. M. Postsynthetic Modification of Metal–Organic Frameworks—a Progress Report. *Chem. Soc. Rev.* **2011**, *40* (2), 498–519. https://doi.org/10.1039/C0CS00031K.

(25) Yin, Z.; Wan, S.; Yang, J.; Kurmoo, M.; Zeng, M.-H. Recent Advances in Post-Synthetic Modification of Metal–Organic Frameworks: New Types and Tandem Reactions. *Coord. Chem. Rev.* **2019**, *378*, 500–512. https://doi.org/10.1016/j.ccr.2017.11.015.

(26) Wang, Z.; Cohen, S. M. Tandem Modification of Metal–Organic Frameworks by a Postsynthetic Approach. *Angew. Chem. Int. Ed.* **2008**, *47* (25), 4699–4702. https://doi.org/10.1002/anie.200800686.

(27) Savonnet, M.; Bazer-Bachi, D.; Bats, N.; Perez-Pellitero, J.; Jeanneau, E.; Lecocq, V.; Pinel, C.; Farrusseng, D. Generic Postfunctionalization Route from Amino-Derived Metal−Organic Frameworks. *J. Am. Chem. Soc.* **2010**, *132* (13), 4518–4519. https://doi.org/10.1021/ja909613e.

(28) Kronast, A.; Eckstein, S.; Altenbuchner, P. T.; Hindelang, K.; Vagin, S. I.; Rieger, B. Gated Channels and Selectivity Tuning of CO2 over N2 Sorption by Post-Synthetic Modification of a UiO-66-Type Metal–Organic Framework. *Chem. – Eur. J.* **2016**, *22* (36), 12800–12807. https://doi.org/10.1002/chem.201602318.

(29) Liu, H.; Xi, F.-G.; Sun, W.; Yang, N.-N.; Gao, E.-Q. Amino- and Sulfo-Bifunctionalized Metal–Organic Frameworks: One-Pot Tandem Catalysis and the Catalytic Sites. *Inorg. Chem.* **2016**, *55* (12), 5753–5755. https://doi.org/10.1021/acs.inorgchem.6b01057.

(30) Khan, N. A.; Hasan, Z.; Jhung, S. H. Adsorptive Removal of Hazardous Materials Using Metal-Organic Frameworks (MOFs): A Review. *J. Hazard. Mater.* **2013**, *244–245*, 444–456. https://doi.org/10.1016/j.jhazmat.2012.11.011.

(31) Langmi, H. W.; Ren, J.; North, B.; Mathe, M.; Bessarabov, D. Hydrogen Storage in Metal-Organic Frameworks: A Review. *Electrochimica Acta* **2014**, *128*, 368–392. https://doi.org/10.1016/j.electacta.2013.10.190.

(32) Suh, M. P.; Park, H. J.; Prasad, T. K.; Lim, D.-W. Hydrogen Storage in Metal–Organic Frameworks. *Chem. Rev.* **2012**, *112* (2), 782–835. https://doi.org/10.1021/cr200274s.

(33) Vitillo, J. G.; Atzori, C.; Civalleri, B.; Barbero, N.; Barolo, C.; Bonino, F. Design and Characterization of MOFs (Metal–Organic Frameworks) for Innovative Applications. *Hybrid Organic-Inorganic Interfaces* **2018**. https://doi.org/10.1002/9783527807130.ch10.

(34) U. Czaja, A.; Trukhan, N.; Müller, U. Industrial Applications of Metal–Organic Frameworks. *Chem. Soc. Rev.* **2009**, *38* (5), 1284–1293. https://doi.org/10.1039/B804680H.

(35) Kumar, P.; Deep, A.; Kim, K.-H. Metal Organic Frameworks for Sensing Applications. *TrAC Trends Anal. Chem.* **2015**, *73*, 39–53. https://doi.org/10.1016/j.trac.2015.04.009.

(36) Lee, J.; K. Farha, O.; Roberts, J.; A. Scheidt, K.; T. Nguyen, S.; T. Hupp, J. Metal–Organic Framework Materials as Catalysts. *Chem. Soc. Rev.* **2009**, *38* (5), 1450–1459. https://doi.org/10.1039/B807080F.

(37) Furukawa, H.; Cordova, K. E.; O'Keeffe, M.; Yaghi, O. M. The Chemistry and Applications of Metal-Organic Frameworks. *Science* **2013**, *341* (6149), 1230444. https://doi.org/10.1126/science.1230444.

(38) Kumar, P.; Pournara, A.; Kim, K.-H.; Bansal, V.; Rapti, S.; Manos, M. J. Metal-Organic Frameworks: Challenges and Opportunities for Ion-Exchange/Sorption Applications. *Prog. Mater. Sci.* **2017**, *86*, 25–74. https://doi.org/10.1016/j.pmatsci.2017.01.002.

(39) Yu, C.; Shao, Z.; Hou, H. A Functionalized Metal–Organic Framework Decorated with O− Groups Showing Excellent Performance for Lead(II) Removal from Aqueous Solution. *Chem. Sci.* **2017**, *8* (11), 7611–7619. https://doi.org/10.1039/C7SC03308G.

(40) Xue, H.; Chen, Q.; Jiang, F.; Yuan, D.; Lv, G.; Liang, L.; Liu, L.; Hong, M. A Regenerative Metal–Organic Framework for Reversible Uptake of Cd(II): From Effective Adsorption to in Situ Detection. *Chem. Sci.* **2016**, *7* (9), 5983–5988. https://doi.org/10.1039/C6SC00972G.

(41) Liang, L.; Chen, Q.; Jiang, F.; Yuan, D.; Qian, J.; Lv, G.; Xue, H.; Liu, L.; Jiang, H.-L.; Hong, M. In Situ Large-Scale Construction of Sulfur-Functionalized Metal–Organic Framework and Its Efficient Removal of Hg(II) from Water. *J. Mater. Chem. A* **2016**, *4* (40), 15370–15374. https://doi.org/10.1039/C6TA04927C.

(42) Colinas, I. R.; Silva, R. C.; Oliver, S. R. J. Reversible, Selective Trapping of Perchlorate from Water in Record Capacity by a Cationic Metal–Organic

Framework. *Environ. Sci. Technol.* **2016**, *50* (4), 1949–1954. https://doi.org/10.1021/acs.est.5b03455.

(43) Ding, B.; Guo, C.; Xin Liu, S.; Cheng, Y.; Xia Wu, X.; Mei Su, X.; Yuan Liu, Y.; Li, Y. A Unique Multi-Functional Cationic Luminescent Metal–Organic Nanotube for Highly Sensitive Detection of Dichromate and Selective High Capacity Adsorption of Congo Red. *RSC Adv.* **2016**, *6* (40), 33888–33900. https://doi.org/10.1039/C6RA03576K.

(44) Nagarkar, S. S.; Saha, T.; Desai, A. V.; Talukdar, P.; Ghosh, S. K. Metal-Organic Framework Based Highly Selective Fluorescence *Turn-on* Probe for Hydrogen Sulphide. *Sci. Rep.* **2014**, *4*, 7053. https://doi.org/10.1038/srep07053.

(45) Yi, F.-Y.; Wang, Y.; Li, J.-P.; Wu, D.; Lan, Y.-Q.; Sun, Z.-M. An Ultrastable Porous Metal–Organic Framework Luminescent Switch towards Aromatic Compounds. *Mater. Horiz.* **2015**, *2* (2), 245–251. https://doi.org/10.1039/C4MH00210E.

(46) Allendorf, M. D.; Houk, R. J. T.; Andruszkiewicz, L.; Talin, A. A.; Pikarsky, J.; Choudhury, A.; Gall, K. A.; Hesketh, P. J. Stress-Induced Chemical Detection Using Flexible Metal−Organic Frameworks. *J. Am. Chem. Soc.* **2008**, *130* (44), 14404–14405. https://doi.org/10.1021/ja805235k.

(47) Zybaylo, O.; Shekhah, O.; Wang, H.; Tafipolsky, M.; Schmid, R.; Johannsmann, D.; Wöll, C. A Novel Method to Measure Diffusion Coefficients in Porous Metal–Organic Frameworks. *Phys. Chem. Chem. Phys.* **2010**, *12* (28), 8093–8098. https://doi.org/10.1039/B927601G.

(48) Tonigold, M.; Lu, Y.; Bredenkötter, B.; Rieger, B.; Bahnmüller, S.; Hitzbleck, J.; Langstein, G.; Volkmer, D. Heterogeneous Catalytic Oxidation by MFU-1: A Cobalt(II)-Containing Metal–Organic Framework. *Angew. Chem. Int. Ed.* **2009**, *48* (41), 7546–7550. https://doi.org/10.1002/anie.200901241.

(49) Xiao, B.; Hou, H.; Fan, Y. Catalytic Applications of CuII-Containing MOFs Based on N-Heterocyclic Ligand in the Oxidative Coupling of 2,6-Dimethylphenol. *J. Organomet. Chem.* **2007**, *692* (10), 2014–2020. https://doi.org/10.1016/j.jorganchem.2007.01.010.

(50) Fei, H.; Rogow, D. L.; Oliver, S. R. J. Reversible Anion Exchange and Catalytic Properties of Two Cationic Metal−Organic Frameworks Based on Cu(I) and Ag(I). *J. Am. Chem. Soc.* **2010**, *132* (20), 7202–7209. https://doi.org/10.1021/ja102134c.

(51) Fei, H.; Paw U, L.; Rogow, D. L.; Bresler, M. R.; Abdollahian, Y. A.; Oliver, S. R. J. Synthesis, Characterization, and Catalytic Application of a Cationic Metal−Organic Framework: Ag2(4,4′-Bipy)2(O3SCH2CH2SO3). *Chem. Mater.* **2010**, *22* (6), 2027–2032. https://doi.org/10.1021/cm9032308.

(52) Farha, O. K.; Özgür Yazaydın, A.; Eryazici, I.; Malliakas, C. D.; Hauser, B. G.; Kanatzidis, M. G.; Nguyen, S. T.; Snurr, R. Q.; Hupp, J. T. *De Novo* Synthesis of a Metal–Organic Framework Material Featuring Ultrahigh Surface Area and Gas Storage Capacities. *Nat. Chem.* **2010**, *2* (11), 944–948. https://doi.org/10.1038/nchem.834.

(53) Tian, T.; Zeng, Z.; Vulpe, D.; Casco, M. E.; Divitini, G.; Midgley, P. A.; Silvestre-Albero, J.; Tan, J.-C.; Moghadam, P. Z.; Fairen-Jimenez, D. A Sol–Gel

Monolithic Metal–Organic Framework with Enhanced Methane Uptake. *Nat. Mater.* **2018**, *17* (2), 174–179. https://doi.org/10.1038/nmat5050.

(54) DOE Technical Targets for Onboard Hydrogen Storage for Light-Duty Vehicles https://www.energy.gov/eere/fuelcells/doe-technical-targets-onboard-hydrogen-storage-light-duty-vehicles (accessed Feb 12, 2019).

(55) West, A. R. *Solid State Chemistry and Its Applications*, Second Edition.; Wiley, 2014.

(56) Wiktor, C.; Meledina, M.; Turner, S.; Lebedev, O. I.; Fischer, R. A. Transmission Electron Microscopy on Metal–Organic Frameworks – a Review. *J. Mater. Chem. A* **2017**, *5* (29), 14969–14989. https://doi.org/10.1039/C7TA00194K.

(57) Thommes, M.; Kaneko, K.; Neimark, A. V.; Olivier, J. P.; Rodriguez-Reinoso, F.; Rouquerol, J.; Sing, K. S. W. Physisorption of Gases, with Special Reference to the Evaluation of Surface Area and Pore Size Distribution (IUPAC Technical Report). *Pure Appl. Chem.* **2015**, *87* (9–10), 1051–1069. https://doi.org/10.1515/pac-2014-1117.

(58) Holden, N.; Coplen, T. The Periodic Table of the Elements. *Chem. Int.* **2009**, *26* (1), 8–9. https://doi.org/10.1515/ci.2004.26.1.8.

(59) Cotton, S. *Lanthanides and Actinides*; Macmillan Physical Science Series; Macmillan Education LTD: London, 1991.

(60) Voncken, J. H. L. The Rare Earth Elements—A Special Group of Metals. In *The Rare Earth Elements: An Introduction*; Voncken, J. H. L., Ed.; SpringerBriefs in

Earth Sciences; Springer International Publishing: Cham, 2016; pp 1–13. https://doi.org/10.1007/978-3-319-26809-5_1.

(61) Kaltsoyannis, N.; Scott, P. *The f Elements*; Oxford University Press: New York, 1999.

(62) Vuojola, J.; Soukka, T. Luminescent Lanthanide Reporters: New Concepts for Use in Bioanalytical Applications. *Methods Appl. Fluoresc.* **2014**, *2* (1), 012001. https://doi.org/10.1088/2050-6120/2/1/012001.

(63) 2.2: Atomic Orbitals and Quantum Numbers https://chem.libretexts.org/Courses/Oregon_Institute_of_Technology/OIT%3A_CHE_202_-_General_Chemistry_II/Unit_2%3A_Electrons_in_Atoms/2.2%3A_Atomic_Orbitals_and_Quantum_Numbers (accessed Feb 10, 2019).

(64) Shannon, R. D. Revised Effective Ionic Radii and Systematic Studies of Interatomic Distances in Halides and Chalcogenides. *Acta Crystallogr. A* **1976**, *32* (5), 751–767. https://doi.org/10.1107/S0567739476001551.

(65) Bünzli, J.-C. G.; Piguet, C. Taking Advantage of Luminescent Lanthanide Ions. *Chem. Soc. Rev.* **2005**, *34* (12), 1048–1077. https://doi.org/10.1039/B406082M.

(66) Cui, Y.; Yue, Y.; Qian, G.; Chen, B. Luminescent Functional Metal–Organic Frameworks. *Chem. Rev.* **2012**, *112* (2). https://doi.org/10.1021/cr200101d.

(67) Bünzli, J.-C. G. *Handbook on the Physics and Chemistry of the Rare Earths: Including Actinides*; Elsevier: Amsterdam, 2016; Vol. 50.

(68) Soni, P. L.; Soni, V. *Coordination Chemistry: Metal Complexes Transition Metal Chemistry with Lanthanides and Actinides*; CRC Press: Boca Raton, FL, 2013.

(69) Reineke, T. M.; Eddaoudi, M.; O'Keeffe, M.; Yaghi, O. M. A Microporous Lanthanide–Organic Framework. *Angew. Chem. Int. Ed.* **1999**, *38* (17), 2590–2594. https://doi.org/10.1002/(SICI)1521-3773(19990903)38:17<2590::AID-ANIE2590>3.0.CO;2-H.

(70) Isomorphous crystals - Online Dictionary of Crystallography http://reference.iucr.org/dictionary/Isomorphous_crystals (accessed Feb 19, 2019).

(71) Batrice, R. J.; Adcock, A. K.; Cantos, P. M.; Bertke, J. A.; Knope, K. E. Synthesis and Characterization of an Isomorphous Lanthanide-Thiophenemonocarboxylate Series (Ln = La–Lu, except Pm) Amenable to Color Tuning. *Cryst. Growth Des.* **2017**, *17* (9), 4603–4612. https://doi.org/10.1021/acs.cgd.7b00400.

(72) Liu, Q.-Y.; Wang, W.-F.; Wang, Y.-L.; Shan, Z.-M.; Wang, M.-S.; Tang, J. Diversity of Lanthanide(III)–Organic Extended Frameworks with a 4,8-Disulfonyl-2,6-Naphthalenedicarboxylic Acid Ligand: Syntheses, Structures, and Magnetic and Luminescent Properties. *Inorg. Chem.* **2012**, *51* (4), 2381–2392. https://doi.org/10.1021/ic2023727.

(73) Mishra, G.; Dash, B.; Pandey, S. Layered Double Hydroxides: A Brief Review from Fundamentals to Application as Evolving Biomaterials. *Appl. Clay Sci.* **2018**, *153*, 172–186. https://doi.org/10.1016/j.clay.2017.12.021.

(74) Duan, X.; Evans, D. G. *Layered Double Hydroxides*; Springer Science & Business Media, 2006.

(75) Gándara, F.; Perles, J.; Snejko, N.; Iglesias, M.; Gómez-Lor, B.; Gutiérrez-Puebla, E.; Monge, M. Á. Layered Rare-Earth Hydroxides: A Class of Pillared Crystalline Compounds for Intercalation Chemistry. *Angew. Chem. Int. Ed.* **2006**, *45* (47), 7998–8001. https://doi.org/10.1002/anie.200602502.

(76) Liang, J.; Ma, R.; Sasaki, T. Layered Rare Earth Hydroxides (LREHs): Synthesis and Structure Characterization towards Multifunctionality. *Dalton Trans.* **2014**, *43* (27), 10355–10364. https://doi.org/10.1039/C4DT00425F.

(77) Geng, F.; Xin, H.; Matsushita, Y.; Ma, R.; Tanaka, M.; Izumi, F.; Iyi, N.; Sasaki, T. New Layered Rare-Earth Hydroxides with Anion-Exchange Properties. *Chem. – Eur. J.* **2008**, *14* (30), 9255–9260. https://doi.org/10.1002/chem.200800127.

(78) Lee, K.-H.; Byeon, S.-H. Extended Members of the Layered Rare-Earth Hydroxide Family, RE2(OH)5NO3·nH2O (RE = Sm, Eu, and Gd): Synthesis and Anion-Exchange Behavior. *Eur. J. Inorg. Chem.* **2009**, *2009* (7), 929–936. https://doi.org/10.1002/ejic.200801052.

(79) Geng, F.; Ma, R.; Sasaki, T. Anion-Exchangeable Layered Materials Based on Rare-Earth Phosphors: Unique Combination of Rare-Earth Host and Exchangeable Anions. *Acc. Chem. Res.* **2010**, *43* (9), 1177–1185. https://doi.org/10.1021/ar900289v.

(80) D. Allendorf, M.; A. Bauer, C.; K. Bhakta, R.; T. Houk, R. J. Luminescent Metal–Organic Frameworks. *Chem. Soc. Rev.* **2009**, *38* (5), 1330–1352. https://doi.org/10.1039/B802352M.

(81) *Principles of Fluorescence Spectroscopy*; Lakowicz, J. R., Ed.; Springer US: Boston, MA, 2006. https://doi.org/10.1007/978-0-387-46312-4.

(82) Binnemans, K. Interpretation of Europium(III) Spectra. *Coord. Chem. Rev.* **2015**, *295*, 1–45. https://doi.org/10.1016/j.ccr.2015.02.015.

(83) Latva, M.; Takalo, H.; Mukkala, V.-M.; Matachescu, C.; Rodríguez-Ubis, J. C.; Kankare, J. Correlation between the Lowest Triplet State Energy Level of the Ligand and Lanthanide(III) Luminescence Quantum Yield. *J. Lumin.* **1997**, *75* (2), 149–169. https://doi.org/10.1016/S0022-2313(97)00113-0.

(84) Cui, Y.; Chen, B.; Qian, G. Lanthanide Metal-Organic Frameworks for Luminescent Sensing and Light-Emitting Applications. *Coord. Chem. Rev.* **2014**, *273* (Supplement C), 76–86. https://doi.org/10.1016/j.ccr.2013.10.023.

(85) Rao, X.; Huang, Q.; Yang, X.; Cui, Y.; Yang, Y.; Wu, C.; Chen, B.; Qian, G. Color Tunable and White Light Emitting Tb3+ and Eu3+ Doped Lanthanide Metal–Organic Framework Materials. *J. Mater. Chem.* **2012**, *22* (7), 3210–3214. https://doi.org/10.1039/C2JM14127B.

(86) Zhao, D.; Yue, D.; Jiang, K.; Zhang, L.; Li, C.; Qian, G. Isostructural Tb3+/Eu3+ Co-Doped Metal–Organic Framework Based on Pyridine-Containing Dicarboxylate Ligands for Ratiometric Luminescence Temperature Sensing. *Inorg. Chem.* **2019**, *58* (4), 2637–2644. https://doi.org/10.1021/acs.inorgchem.8b03225.

Chapter 2

Experimental Methods of Lanthanide Metal-Organic Structures

2.1. Solvothermal Syntheses of Ln-BPDC MOFs (SLUG-43 – 48)

Lanthanum (III) nitrate hexahydrate [$La(NO_3)_3 \cdot 6H_2O$, Alfa Aesar, 99%], cerium (III) nitrate hexahydrate [$Ce(NO_3)_3 \cdot 6H_2O$, Spectrum, 99%], neodymium (III) nitrate hexahydrate [$Nd(NO_3)_3 \cdot 6H_2O$, Alfa Aesar, 99.9%], europium (III) nitrate hexahydrate [$Eu(NO_3)_3 \cdot 6H_2O$, Strem Chemicals, 99.9%], gadolinium (III) nitrate hexahydrate [$Gd(NO_3)_3 \cdot 6H_2O$, Strem Chemicals, 99.9%], erbium (III) nitrate pentahydrate [$Er(NO_3)_3 \cdot 5H_2O$, Acros Organics, 99.9%], 4-(4'-carboxy)phenylbenzoic acid [$HO_2C(C_6H_4)_2CO_2H$, Combi-Blocks, 98%] and N,N-dimethylformamide [$(CH_3)_2NCHO$, Macron Fine Chemicals, Analytical Reagent] were used as-received.

$[Ln(BPDC)_2^-][NH_2(CH_3)_2^+]$ (Ln = La, Ce, Nd, Eu, Gd, Er which we denote as **SLUG-43**, **-44**, **-45**, **-46**, **-47**, and **-48**, respectively, for the University of California, Santa Cruz – structure number) were synthesized under solvothermal conditions. A mixture of $Ln(NO_3)_3 \cdot xH_2O$ (0.200 g), 4,4'-H_2BPDC (0.226 g), and 10.0 mL DMF was stirred until homogeneous, transferred into an autoclave and heated statically under autogenous pressure for 3 days at 140 to 150 °C, then slow cooled to room

temperature at a rate of 0.1 °C/min. After vacuum filtering and rinsing with ethanol, lustrous, block-shaped crystals suitable for single crystal X-ray diffraction (SCXRD) were collected among a powder of smaller crystals of the same phase.

2.2. Solvothermal Syntheses of Ln-NDC MOFs (SLUG-49 – 52)

Lanthanum (III) nitrate hexahydrate [$La(NO_3)_3 \cdot 6H_2O$, Alfa Aesar, 99%], neodymium (III) nitrate hexahydrate [$Nd(NO_3)_3 \cdot 6H_2O$, Alfa Aesar, 99.9%], europium (III) nitrate hexahydrate [$Eu(NO_3)_3 \cdot 6H_2O$, Strem Chemicals, 99.9%], gadolinium (III) nitrate hexahydrate [$Gd(NO_3)_3 \cdot 6H_2O$, Strem Chemicals, 99.9%], 2,6-naphthalenedicarboxylic acid [$HO_2C(C_{10}H_6)CO_2H$], TCI America, > 98%] and N,N-dimethylformamide [$(CH_3)_2NCHO$, Macron Fine Chemicals, Analytical Reagent] were used as-received.

[$Ln_2(NDC)_2(DMF)_2 \cdot x$ DMF] (Ln = La, Nd, Eu, Gd, which we denote as **SLUG-49**, **-50**, **-51**, and **-52**, respectively, for the University of California, Santa Cruz – structure number) were synthesized under solvothermal conditions. A mixture of $Ln(NO_3)_3 \cdot xH_2O$ (0.200 g or equimolar amount of other metal salt), 2,6-H_2NDC (0.197 g) and 10.0 mL DMF was stirred until homogeneous, transferred into an autoclave and heated statically under autogenous pressure for 3 days at 110 to 125 °C, then slow cooled to room temperature at a rate of 0.1 °C/min. After vacuum filtering and rinsing with ethanol, lustrous, block-shaped crystals suitable for SCXRD were collected among a powder of smaller crystals of the same phase.

2.3. Hydrothermal Syntheses of Nd-ADS LREHs (SLUG-28 – 30)

Neodymium (III) nitrate hexahydrate [$Nd(NO_3)_3 \cdot 6H_2O$, Alfa Aesar, 99.9%], 1,2-ethanedisulfonate disodium salt [$NaO_3S(CH_2)_2SO_3Na$, EDS-Na_2, Acros Organics, 99%], 1,3-propanedisulfonate disodium salt [$NaO_3S(CH_2)_3SO_3Na$, PDS-Na_2, Sigma-Aldrich], 1,4-butanedisulfonate disodium salt [$NaO_3S(CH_2)_4SO_3Na$, BDS-Na_2, Oakwood Chemical] and sodium hydroxide pellets (NaOH, Fisher Chemical, 99%) were used as-received for the syntheses. Adipic acid [$HO_2C(CH_2)_4CO_2H$, TCI America, 99%] was used as-received for the anion exchange reactions.

$[Nd_2(OH)_4(OH_2)_2^{2+}][^{-}O_3S(CH_2)_2SO_3^{-}]$ (which we denote as **SLUG-28** for University of California, Santa Cruz – structure number), **$[Nd_2(OH)_4(OH_2)_2^{2+}][^{-}O_3S(CH_2)_3SO_3^{-}]$ (SLUG-29)** and **$[Nd_2(OH)_4(OH_2)_2^{2+}][^{-}O_3S(CH_2)_4SO_3^{-}]$** (**SLUG-30**) were synthesized under hydrothermal conditions. A reactant mixture of $Nd(NO_3)_3 \cdot 6H_2O$ (2.43 g, 5.55 mmol), the respective α,ω-alkanedisulfonate [EDS-Na_2 (1.30 g, 5.55 mmol) / PDS-Na_2 (1.37 g, 5.55 mmol) / BDS-Na_2 (1.45 g, 5.55 mmol)] and H_2O (10.0 mL, 555 mmol) was adjusted to pH = 7 with NaOH. The mixture was stirred at room temperature until homogenous before transferring to a 23 mL capacity Teflon-lined stainless steel autoclave. The autoclave was heated statically at 150 °C for 3 days under autogenous pressure followed by slow cooling (0.1 °C·min^{-1}) to room temperature. Vacuum filtration and rinsing with water/ethanol afforded a white powder of small crystals for all three compounds. Beige-colored rod-shaped crystals suitable for single crystal XRD analysis were obtained for SLUG-28 from a 1 : 1 :

0.75 : 100 molar ratio of $Nd(NO_3)_3 \cdot 6H_2O$: EDS-Na_2 : 4,4'-bipyridine ($C_{10}H_8N_2$) : H_2O, respectively.

Anion exchanges with SLUG-28, -29, and -30 were carried out by placing ~ 200 mg of the respective SLUG-n material in 50 mL H_2O containing an eight-fold molar excess (with respect to SLUG-28, -29, or -30) of adipic acid. The reaction mixture was allowed to slowly stir at room temperature for 24 hours. The solid products were isolated *via* vacuum filtration and rinsed with H_2O and ethanol.

2.4. Characterization Methods

2.4.1. Single Crystal X-ray Diffraction

Pale yellow, almost colorless, crystals of SLUG-43 (La-BPDC), SLUG-44 (Ce-BPDC), SLUG-46 (Eu-BPDC), SLUG-47 (Gd-BPDC), SLUG-49 (La-NDC), SLUG-50 (Nd-NDC), SLUG-51 (Eu-NDC), and SLUG-52 (Gd-NDC) were secured to a Mitegen micromount using Paratone oil. Their SCXRD data was collected at 100 K using a Rigaku Oxford Diffraction (ROD) Synergy-S X-ray diffractometer equipped with a HyPix-6000HE hybrid photon counting (HPC) detector and microfocused Mo-$K\alpha_1$ radiation (λ = 0.71073 Å). For all samples, data collection strategies to ensure completeness and desired redundancy were determined using CrysAlis^{Pro}.[1] Data processing was performed using CrysAlis^{Pro} and included numerical absorption corrections determined *via* face-indexing for all samples, applied using the SCALE3 ABSPACK scaling algorithm.[2] All structures were solved *via* intrinsic phasing methods using ShelXT and refined using ShelXL in the Olex2 graphical user interface.[3–5] Space groups were unambiguously verified by PLATON.[6] The final

structural refinement included anisotropic temperature factors on all non-hydrogen atoms. All hydrogen atoms were attached *via* the riding model at calculated positions using suitable HFIX commands.

An arbitrary sphere of data was collected on a colorless rod-like crystal of SLUG-28 (Nd-EDS), having approximate dimensions of 0.134 × 0.078 × 0.022 mm^3, on a Bruker APEX-II diffractometer using a combination of ω- and φ-scans of 0.5°.[7] Data were corrected for absorption and polarization effects and analyzed for space group determination.[8] The structure was solved by dual-space methods and expanded routinely.[3] The model was refined by full-matrix least-squares analysis of F^2 against all reflections.[4] All non-hydrogen atoms were refined with anisotropic atomic displacement parameters. Unless otherwise noted, hydrogen atoms were included in calculated positions. Atomic displacement parameters for the hydrogens were tied to the equivalent isotropic displacement parameter of the atom to which they are bonded [U_{iso}(H) = 1.5U_{eq}(C) for methyl, 1.2U_{eq}(C) for all others].

2.4.2. Powder X-ray Diffraction

Powder X-ray diffraction (PXRD) patterns were obtained on a Rigaku Miniflex II Plus diffractometer with Cu-Kα radiation (λ = 1.5418 Å) from 2° to 35° or 60° (2θ) at a rate of 2° per minute and a step size of 0.02°.

2.4.3. Fourier-Transform Infrared Spectroscopy

Fourier transform infrared (FTIR) spectroscopy of the materials was collected on a PerkinElmer spectrophotometer using KBr pellets.

2.4.4. Thermogravimetric Analysis

Thermogravimetric analysis (TGA) was performed on a TA Q500 Thermoanalyzer. Samples were heated in a platinum pan at a ramp rate of 10 °C/min under nitrogen flow. The samples for *ex situ* variable temperature (VT-) PXRD were heated in a tube furnace to the designated temperature at a rate of 2 °C/min in air.

2.4.5. Photoluminescence

Steady-state photoluminescence spectrum was obtained at room temperature on an Edinburgh Instruments FLS980 spectrophotometer. Absolute PLQE measurements of both bulk and microscopic crystals were performed on FLS 920 spectrophotometer with an integrating sphere ($BaSO_4$ coating) using single photon counting mode. The focal length of the monochromator was 300 mm. Samples were excited at 320 nm (Eu-BPDC, SLUG-46) or 362 nm (Eu-NDC, SLUG-51) using a 450W Xenon lamp with 3 mm excitation slit width and detected by a Hamamatsu R928p photomultiplier tube. The emission was obtained using 0.2 nm scan step, 0.2 s scan dwell time, and 0.1 mm emission slit width. The PLQEs were calculated by the equation: $\varphi = k_f/k_a$, in which k_f means the number of emitted photons and k_a means the number of absorbed photons.

2.5. References

(1) *CrysAlisPro*; Rigaku Oxford Diffraction; 2017.

(2) *SCALE3 ABSPACK*; Rigaku Oxford Diffraction; 2017.

(3) Sheldrick, G. M. SHELXT – Integrated Space-Group and Crystal-Structure Determination. *Acta Crystallogr. Sect. Found. Adv.* **2015**, *71* (1), 3–8. https://doi.org/10.1107/S2053273314026370.

(4) Sheldrick, G. M. Crystal Structure Refinement with SHELXL. *Acta Crystallogr. Sect. C Struct. Chem.* **2015**, *71* (1), 3–8. https://doi.org/10.1107/S2053229614024218.

(5) Dolomanov, O. V.; Bourhis, L. J.; Gildea, R. J.; Howard, J. a. K.; Puschmann, H. OLEX2: A Complete Structure Solution, Refinement and Analysis Program. *J. Appl. Crystallogr.* **2009**, *42* (2), 339–341. https://doi.org/10.1107/S0021889808042726.

(6) Spek, A. L. Structure Validation in Chemical Crystallography. *Acta Crystallogr. D Biol. Crystallogr.* **2009**, *65* (2), 148–155. https://doi.org/10.1107/S090744490804362X.

(7) *APEX-3*; Bruker AXS: Madison, Wisconsin, USA, 2016.

(8) Krause, L.; Herbst-Irmer, R.; Sheldrick, G. M.; Stalke, D. *J. Appl. Cryst.* **2015**, *48*, 3.

Chapter 3

Characterizations and Luminescent Properties of Lanthanide Metal-Organic Structures

Abstract

In this chapter, the three projects Ln-BPDC, Ln-NDC, and Nd-ADS are presented. The Ln-BPDC (SLUG-43–48) project consists of six anionic, isomorphous MOFs with the formula $[Ln(BPDC)_2^-][NH_2(CH_3)_2^+]$ (Ln = La, Ce, Nd, Eu, Gd, Er). The materials all possess the same 3-D structure and crystallize in the orthorhombic space group *Pbcn*. All exhibit thermal stability up to 300 °C and decompose to Ln_2O_3 after 800 °C. The Eu-BPDC structure exhibits strong fluorescence in the 612-620 nm range and a quantum yield of 2.11%. The Ln-NDC (SLUG-49–52) project consists of four neutral structures that each crystallize in distinct space groups. Their formulas are $[La_6(NDC)_9(DMF)_3 \cdot 6\ DMF]$, $[Nd_2(NDC)_3(DMF)_2]$, $[Eu_2(NDC)_3(DMF)_2 \cdot DMF]$, and $[Gd_4(NDC)_6(DMF)_4]$. The NDC-based structures exhibit similar thermal decomposition profiles and infrared spectra. The Eu-NDC structure exhibits a sharp red-orange luminescence at 613 nm and a quantum yield of 3.56%. Lastly, the Nd-ADS (SLUG-28–30) project consists of three LREHs made of $[Nd_2(OH)_4(OH_2)_2^{2+}]$ layers with interlamellar α,ω-$[^-O_3S(CH_2)_nSO_3^-]$ anions (n = 2 to 4). These LREHs show an increase in thermal stability with increasing alkanedisulfonate chain length.

As an initial example of anion exchange, all three materials show exchange for adipate, $^{-}O_2C(CH_2)_4CO_2^{-}$. This work expands the chemistry of lanthanide MOFs and LREHs.

3.1. Ln-BPDC MOFs (SLUG-43–48)

3.1.1. Structures

SLUG-43 through 48 were synthesized solvothermally in high yield [80% to 89% based on Ln(III)] at a synthesis temperature range of 140 to 150 °C. Below this optimal temperature range, no crystalline product formed. Longer synthesis times resulted in higher crystallinity and slightly higher yield. The crystals were colorless blocks among a powder of the same phase. Single crystal structures of the MOFs based on La, Ce, Eu and Gd (SLUG-43, -44, -46 and -47, respectively) were obtained and solved (Figures 3.1.1 – 3.1.4). The crystal data for these structures are summarized in Table 3.1.1. The experimental PXRDs match the theoretical PXRD calculated from the single crystal data, verifying that this series of MOFs is isostructural. The similarity of the PXRD patterns for SLUG-45 and -48 (based on Nd and Er, respectively, Figure 3.1.5) support that they are isomorphous despite forming crystals too small for SCXRD analysis.

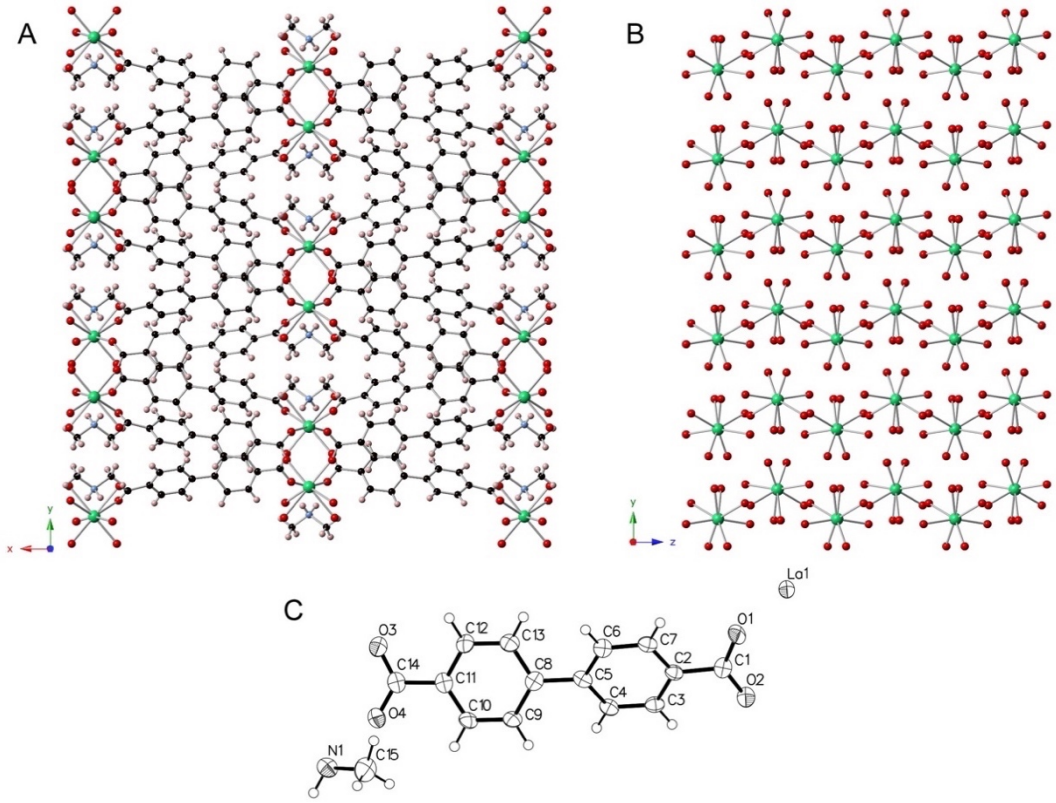

Figure 3.1.1. Crystallographic projections of SLUG-43 (La): A) View along the *c*-axis, showing the metal centers surrounded by $BPDC^{2-}$ ligands and the charge-balancing dimethylammonium ions (La – green; O – red; C – black; N – light blue; H – pink); B) View along the *a*-axis of one layer of isolated LaO_8 centers (C, N, and H omitted for clarity); C) ORTEP (Oak Ridge thermal ellipsoid plot) diagram of SLUG-43 and its atomic numbering scheme. Thermal ellipsoids are calculated at 50% probability.

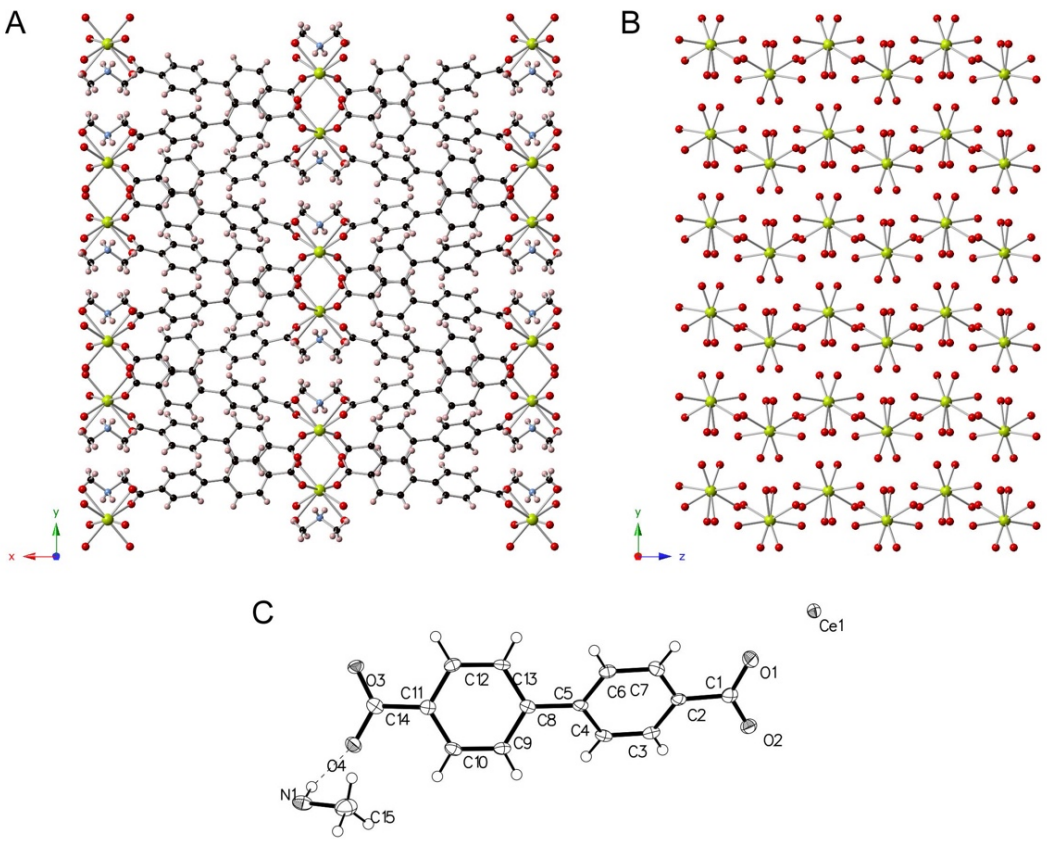

Figure 3.1.2. Crystallographic projections of SLUG-44 (Ce): A) View along the *c*-axis, showing the metal centers surrounded by $BPDC^{2-}$ ligands and the charge-balancing dimethylammonium ions (Ce – yellow; O – red; C – black; N – light blue; H – pink); B) View along the *a*-axis of one layer of isolated CeO_8 centers (C, N, and H omitted for clarity); C) ORTEP (Oak Ridge thermal ellipsoid plot) diagram of SLUG-44 and atomic numbering scheme. Thermal ellipsoids are calculated at 50% probability.

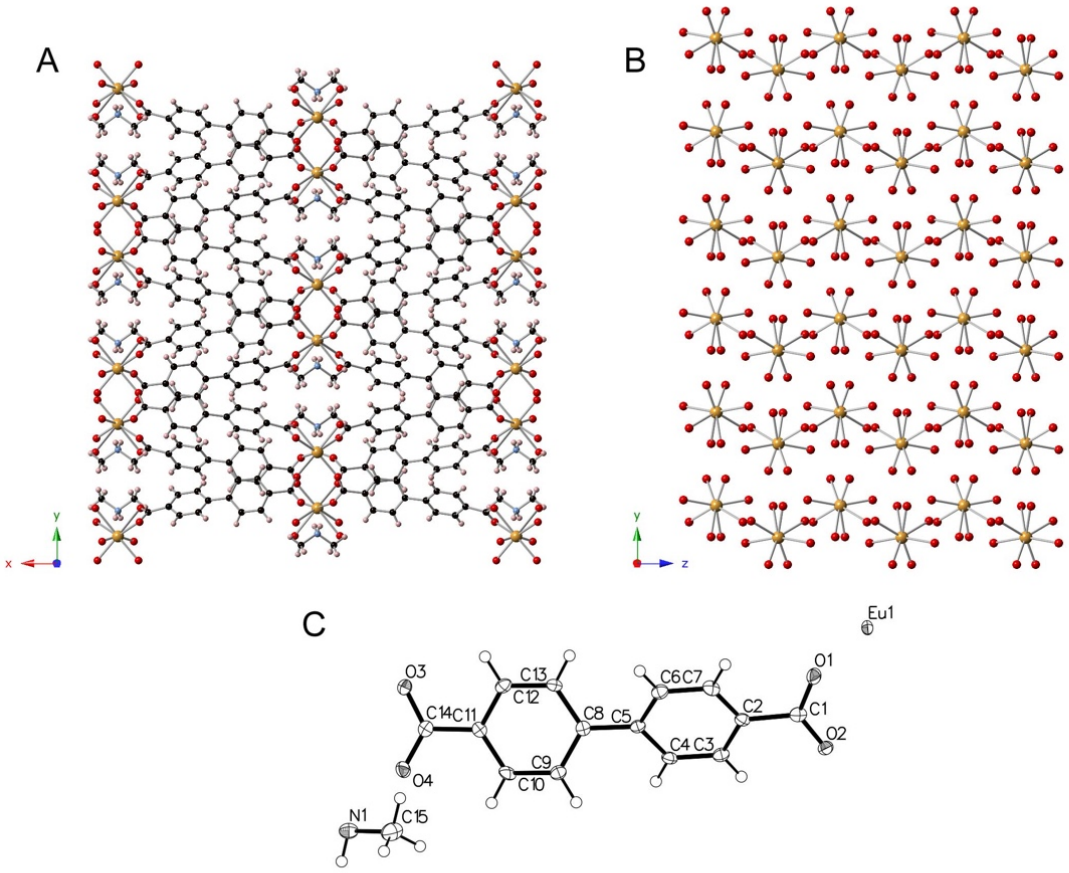

Figure 3.1.3. Crystallographic projections of SLUG-46 (Eu): A) View along the *c*-axis, showing the metal centers surrounded by $BPDC^{2-}$ ligands and the charge-balancing dimethylammonium ions (Eu – orange; O – red; C – black; N – light blue; H – pink); B) View along the *a*-axis of one layer of isolated EuO_8 centers (C, N, and H omitted for clarity); C) ORTEP (Oak Ridge thermal ellipsoid plot) diagram of SLUG-46 and atomic numbering scheme. Thermal ellipsoids are calculated at 50% probability.

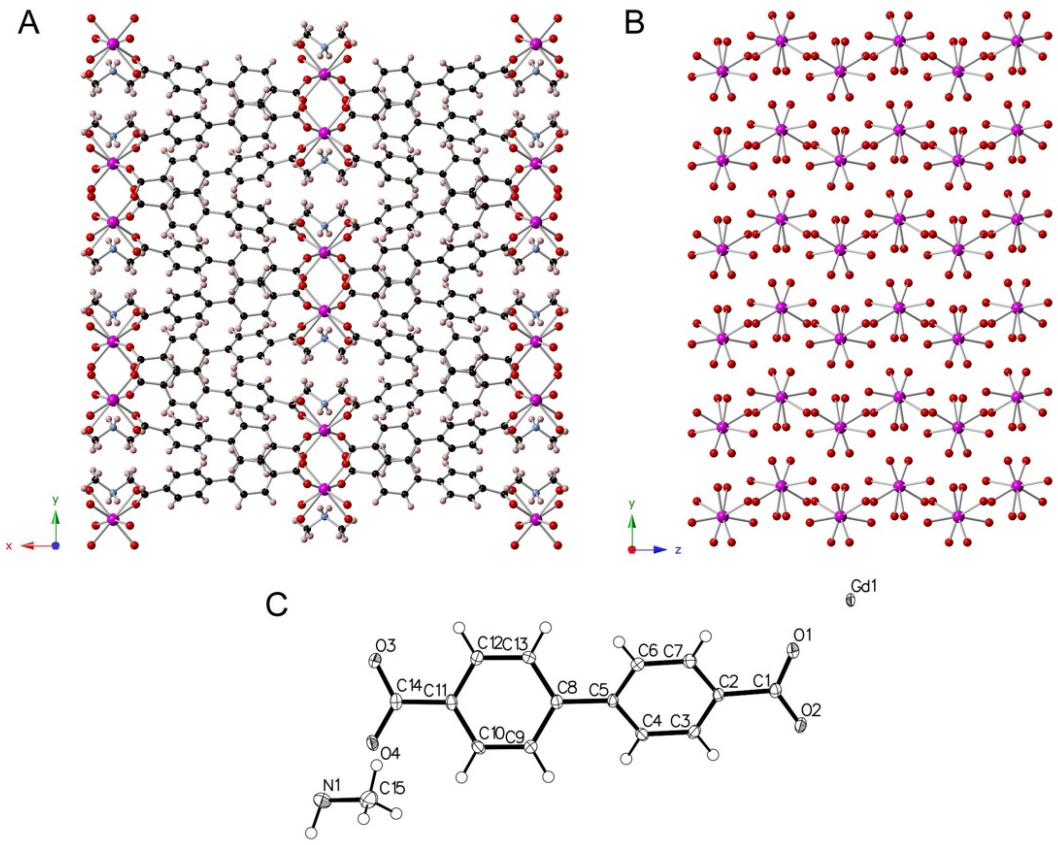

Figure 3.1.4. Crystallographic projections of SLUG-47 (Gd): A) View along the *c*-axis, showing the metal centers surrounded by $BPDC^{2-}$ ligands and the charge-balancing dimethylammonium ions (Gd – purple; O – red; C – black; N – light blue; H – pink); B) View along the *a*-axis of one layer of isolated GdO_8 centers (C, N, and H omitted for clarity); C) ORTEP (Oak Ridge thermal ellipsoid plot) diagram of SLUG-47 and atomic numbering scheme. Thermal ellipsoids are calculated at 50% probability.

Table 3.1.1. Crystal Data and Structure Refinement for SLUG-43, -44, -46 and -47

Material	SLUG-43	SLUG-44	SLUG-46	SLUG-47
Empirical Formula	$LaO_8C_{30}H_{24}N$	$CeO_8C_{30}H_{24}N$	$EuO_8C_{30}H_{24}N$	$GdO_8C_{30}H_{24}N$
Formula Weight ($g \cdot mol^{-1}$)	665.42	666.62	678.46	683.75
Temperature (K)	100	100	100	100
Crystal System	Orthorhombic	Orthorhombic	Orthorhombic	Orthorhombic
Space Group	*Pbcn*	*Pbcn*	*Pbcn*	*Pbcn*
a, b, c (Å)	28.1888(18), 11.7883(12), 7.7777(8)	28.0397(16), 11.7767(6), 7.7568(4)	27.844(2), 11.7069(5), 7.7599(4)	27.8139(14), 11.7109(6), 7.7452(4)
α, β, γ (°)	90, 90, 90	90, 90, 90	90, 90, 90	90, 90, 90
Volume ($Å^3$)	2584.5(4)	2561.4(2)	2529.5(2)	2522.8(2)
Z	8	8	8	8
ρ_{calc} ($g \cdot cm^{-3}$)	1.71	1.729	1.785	1.800
μ (mm^{-1})	1.709	1.833	2.541	2.686
F(000)	1328	1332	1352	1356
Crystal Dimensions (mm)	0.017 × 0.049 × 0.149	0.033 × 0.183 × 0.239	0.014 × 0.070 × 0.098	0.046 × 0.065 × 0.090
Index Ranges	$-34 \le h \le 35$, $-14 \le k \le 13$, $-9 \le l \le 9$	$-34 \le h \le 35$, $-14 \le k \le 14$, $-8 \le l \le 9$	$-34 \le h \le 23$, $-13 \le k \le 14$, $-9 \le l \le 9$	$-34 \le h \le 34$, $-14 \le k \le 14$, $-9 \le l \le 9$
Reflections Collected	8123	9025	8262	9912
Unique Data	2567 [$R_{int} = 0.0849$]	2611 [$R_{int} = 0.0357$]	2565 [$R_{int} = 0.0349$]	2574 [$R_{int} = 0.0319$]
Data / Restraints / Parameters	2567 / 0 / 187	2611 / 0 / 187	2565 / 0 / 187	2574 / 0 / 187

Goodness of Fit on F^2	1.005	1.081	1.200	1.065
Final R Factors [$I > 2\sigma(I)$]	$R_1 = 0.0514$ $wR_2 = 0.1162$	$R_1 = 0.0339$ $wR_2 = 0.0740$	$R_1 = 0.0407$ $wR_2 = 0.0768$	$R_1 = 0.0232$ $wR_2 = 0.0520$
Largest Residual Peak/Hole ($e \cdot Å^{-3}$)	2.02 / -0.90	1.22 / -0.85	1.35 / -0.82	0.872 / -0.339

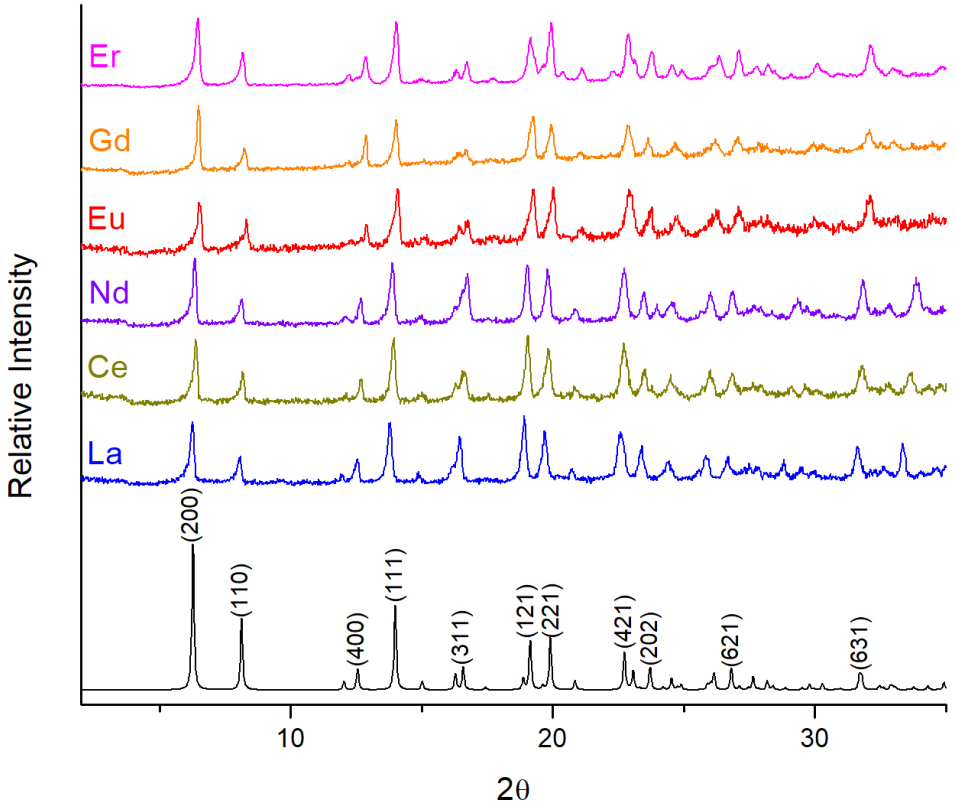

Figure 3.1.5. PXRD patterns of the isomorphous series SLUG-43-48 (La, Ce, Nd, Eu, Gd and Er, respectively), with the theoretical pattern for SLUG-43 (La) shown at the bottom.

The SCXRD studies reveal that the asymmetric unit of SLUG-43-48 contains one Ln(III) ion, two $BPDC^{2-}$ ligands and one dimethylammonium cation. The Ln(III) ion is eight-coordinated by the oxygens from six different $BPDC^{2-}$ ligands in a distorted square antiprismatic coordination geometry. The average Ln-O bond distance is 2.44(6) Å, well within the covalent range based on a search of the Cambridge Structural Database. The ligand $BPDC^{2-}$ is known to adopt up to seven different coordination modes.[1] In the present MOFs, all $BPDC^{2-}$ ligands exhibit the same type of binding mode (Figure 3.1.6). One end of the ligand participates in η^2 binding to one Ln(III) ion, while the other end μ-2 bridges between two Ln(III) ions, creating a three-dimensional framework. The Ln(III) ions are independent with no inorganic connectivity, but are centered about layers in the yz plane (Figure 3.1.1B). The dimethylammonium cations are electrostatically coordinated to each Ln(III) ion, balancing the net negative charge from each $[Ln^{3+}(BPDC^{2-})_2]^-$ unit.

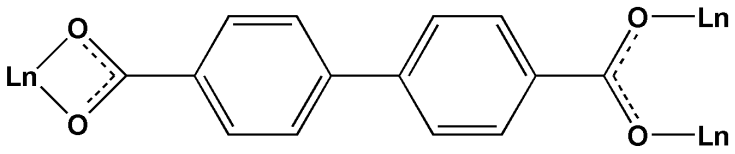

Figure 3.1.6. Binding mode for all $BPDC^{2-}$ ligands in SLUG-43–48.

3.1.2. Thermal Characterization

The SLUG-43–48 materials decompose similarly (Figures 3.1.7–3.1.12). Ln-BPDC begins to decompose at approximately 300 °C (Figure 3.1.7A). The first mass loss of

19.4% corresponds to a loss of dimethylammonium and likely the hydrocarbon portion of one of the linkers, with a theoretical mass loss of 19.7%. The VT-PXRD shows a low angle peak with two higher order reflections after the sample was heated to 375 °C (Figure 3.1.7B). It is possible that the Ln polyhedra have condensed into a layered structure. The second decomposition event at ~ 400 °C of 35.8% agrees well with the loss of an additional $BPDC^{2-}$ ligand (theoretical mass loss of 35.4%). The final decomposition event at ~ 600 °C of 18.5% agrees with the loss of the remaining organic (theoretical mass loss of 18.9%). As expected, the final solid is Ln_2O_3, confirmed by both PXRD after TGA heating and VT-PXRD (Figure 3.1.7B, top pattern). As a representative sample, SLUG-46 (Eu) was heated to 1000 °C to obtain a complete decomposition profile (Figure 3.1.10A).

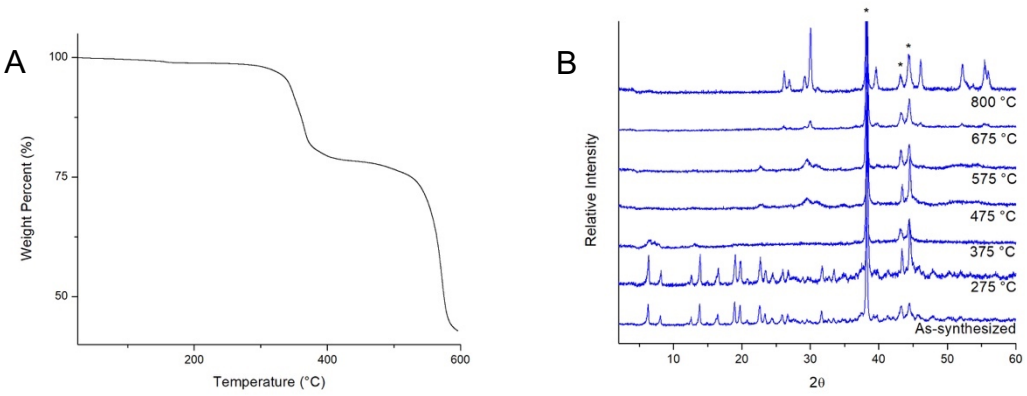

Figure 3.1.7. A) Thermogravimetric trace of SLUG-43 (La); B) *Ex situ* VT-PXRD of SLUG-43 (La), with asterisks denoting peaks due to the aluminum sample holder.

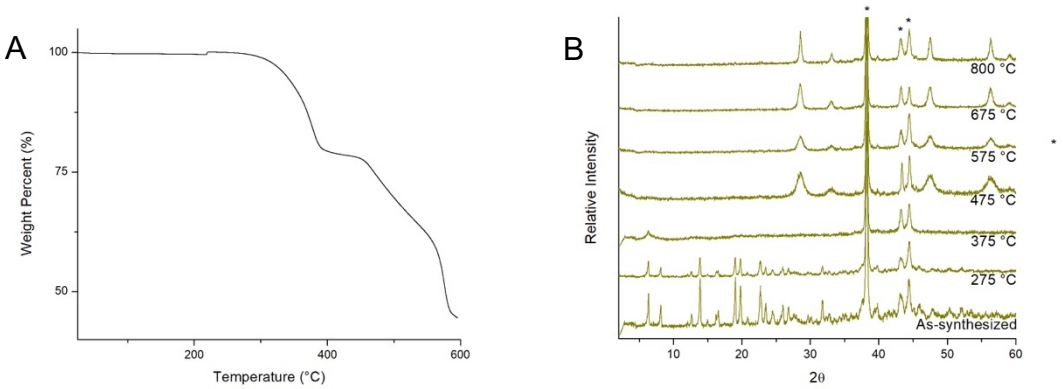

Figure 3.1.8. A) Thermogravimetric trace of SLUG-44 (Ce); B) *Ex situ* VT-PXRD of SLUG-44 (Ce), with asterisks denoting peaks due to the aluminum sample holder.

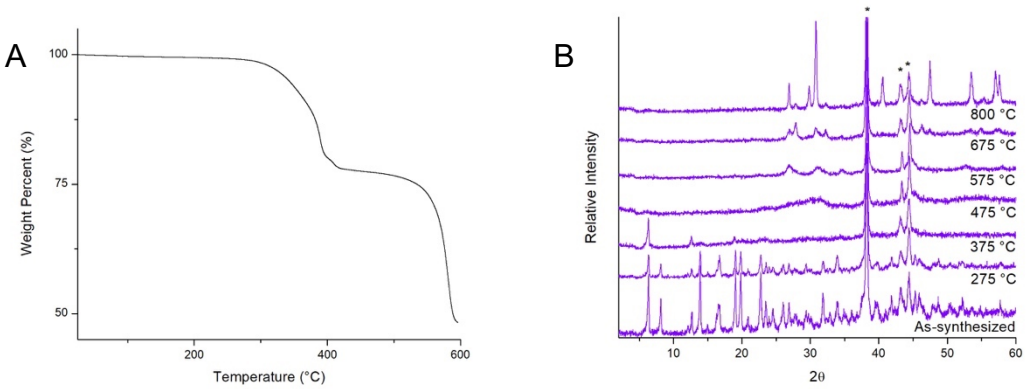

Figure 3.1.9. A) Thermogravimetric trace of SLUG-45 (Nd); B) *Ex situ* VT-PXRD of SLUG-45 (Nd), with asterisks denoting peaks due to the aluminum sample holder.

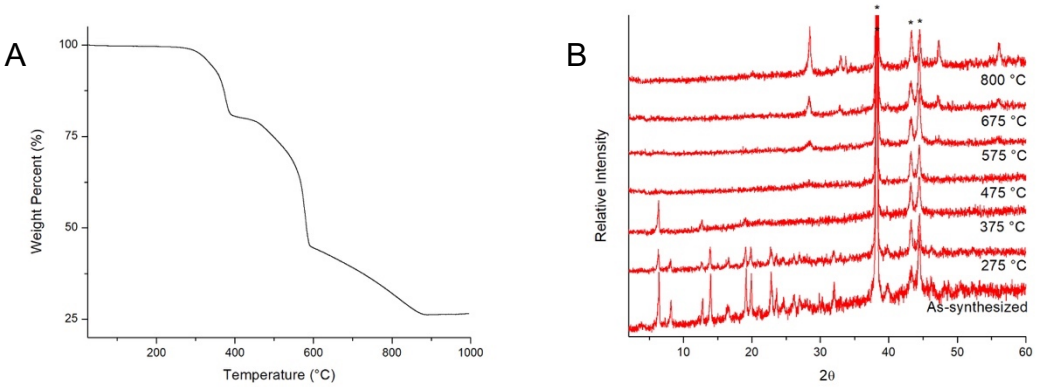

Figure 3.1.10. A) Thermogravimetric trace of SLUG-46 (Eu); B) *Ex situ* VT-PXRD of SLUG-46 (Eu), with asterisks denoting peaks due to the aluminum sample holder.

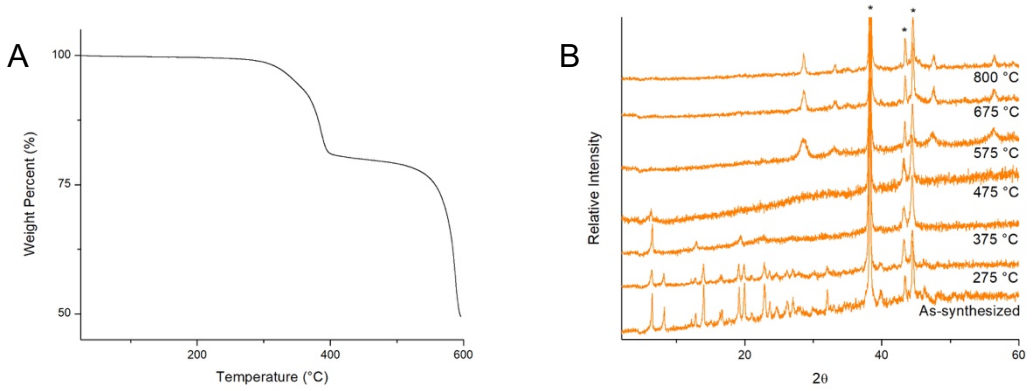

Figure 3.1.11. A) Thermogravimetric trace of SLUG-47 (Gd); B) *Ex situ* VT-PXRD of SLUG-47 (Gd), with asterisks denoting peaks due to the aluminum sample holder.

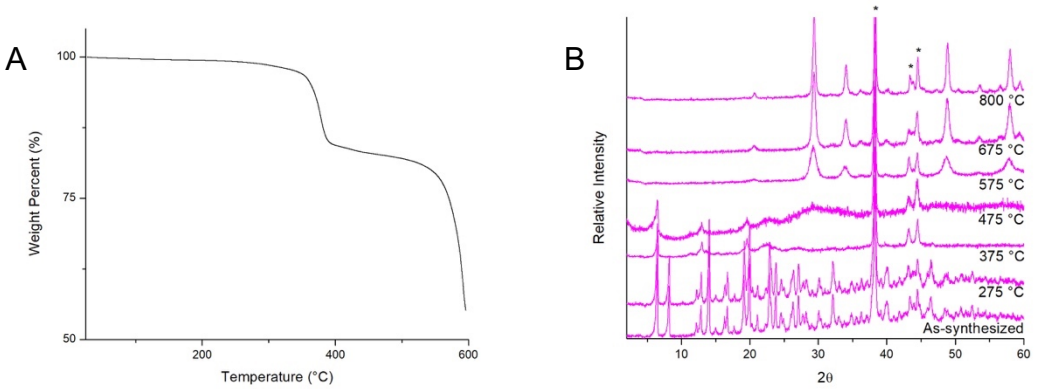

Figure 3.1.12. A) Thermogravimetric trace of SLUG-48 (Er); B) *Ex situ* VT-PXRD of SLUG-48 (Er), with asterisks denoting peaks due to the aluminum sample holder.

3.1.3. Vibrational Spectroscopy

All six materials have very similar IR spectra, owing to their isomorphous topology (Figure 3.1.13). Broad N-H stretching bands are visible centered around ~ 3130 and 3400 cm^{-1} due to the dimethylammonium countercations.[2,3] Four sharp peaks in the 1400 to 1650 cm^{-1} region are attributed to $(C{-}{-}O)_2$ stretching from the carboxylate in the $BPDC^{2-}$ ligands. The sharp peak at ~ 770 cm^{-1} is due to the characteristic C-H deformation of 1,4-disubstituted aromatics. The PXRD and FTIR of the free ligand H_2BPDC are shown in Figure 3.1.14, to demonstrate the differences with the synthesized materials. We posit that the luminescence of SLUG-46 (Eu) is due to a ligand-to-metal charge transfer (LMCT) process. FTIR of Eu-BPDC sample after heating to 375 °C (Figure 3.1.15) shows the partial loss of the peaks at 3100 cm^{-1} and 1650 cm^{-1}, corresponding to N-H and $(C{-}{-}O)_2$ stretching, respectively.

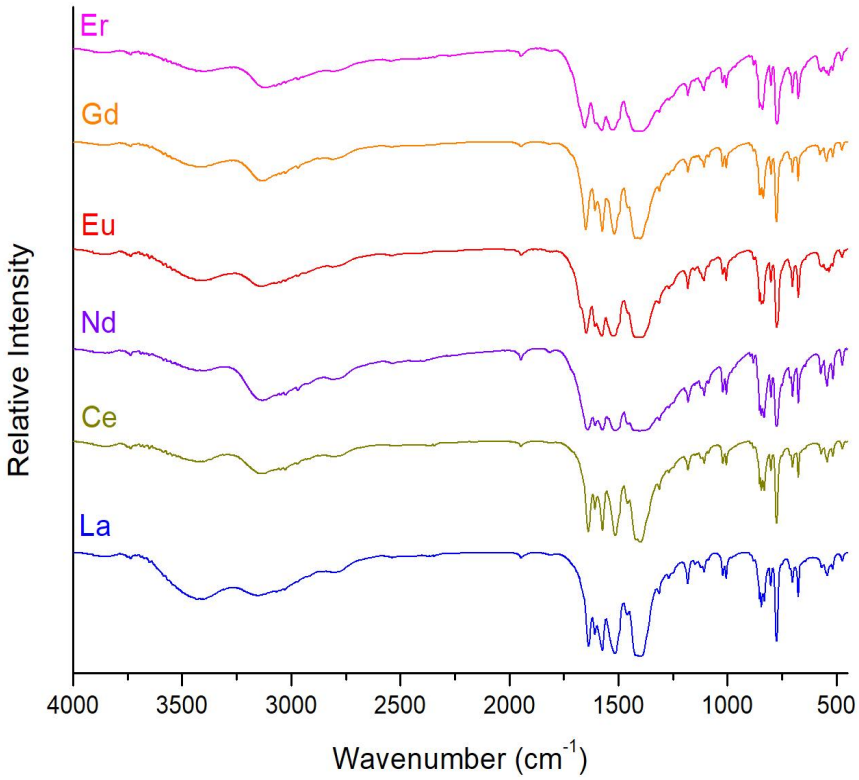

Figure 3.1.13. FTIR spectra of SLUG-43-48, further underscoring their isomorphous nature.

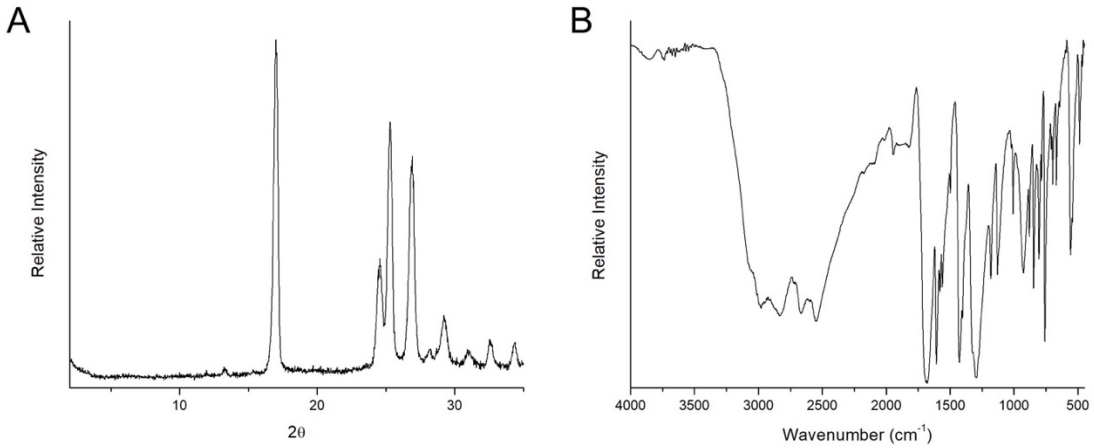

Figure 3.1.14. Characterizations of the free ligand H_2BPDC: A) PXRD pattern of H_2BPDC; B) FTIR spectrum of H_2BPDC.

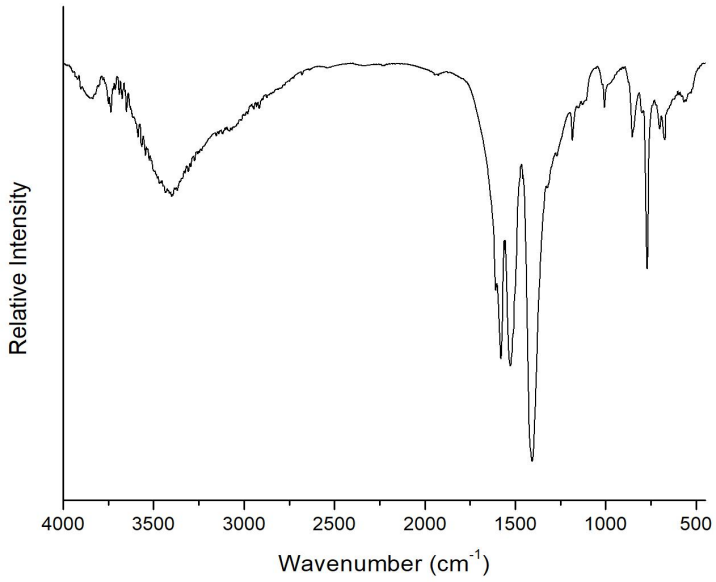

Figure 3.1.15. FTIR spectrum of the intermediate structure after heating SLUG-46 (Eu) to 375 °C.

3.1.4. Photoluminescence Spectroscopy

The Eu(III)-based MOF, SLUG-46, exhibits intense luminescence in the visible red-orange region (Figure 3.1.16–3.1.17). These emission bands are due to $^5D_0 \rightarrow {}^7F_J$ (J = 1, 2, 4) electronic transitions. The $^5D_0 \rightarrow {}^7F_3$ transition is weakly observed at 660 nm. These electronic transitions are known to be the most notable for Eu(III) complexes.[4] The intense $^5D_0 \rightarrow {}^7F_2$ transition is hypersensitive and indicates that Eu(III) is not at a site with a center of symmetry. SLUG-46 displays a quantum efficiency of 2.11%. As expected, none of the SLUG-43 (La), -44 (Ce), -45 (Nd), -47 (Gd) or -48 (Er) materials were fluorescent. The photoluminescence of SLUG-46 is quenched after the material is heated to 375 °C (Figure 3.1.17). As the organic is evolved, the LMCT process is likely disrupted and as a result, Eu(III) no longer emits light.

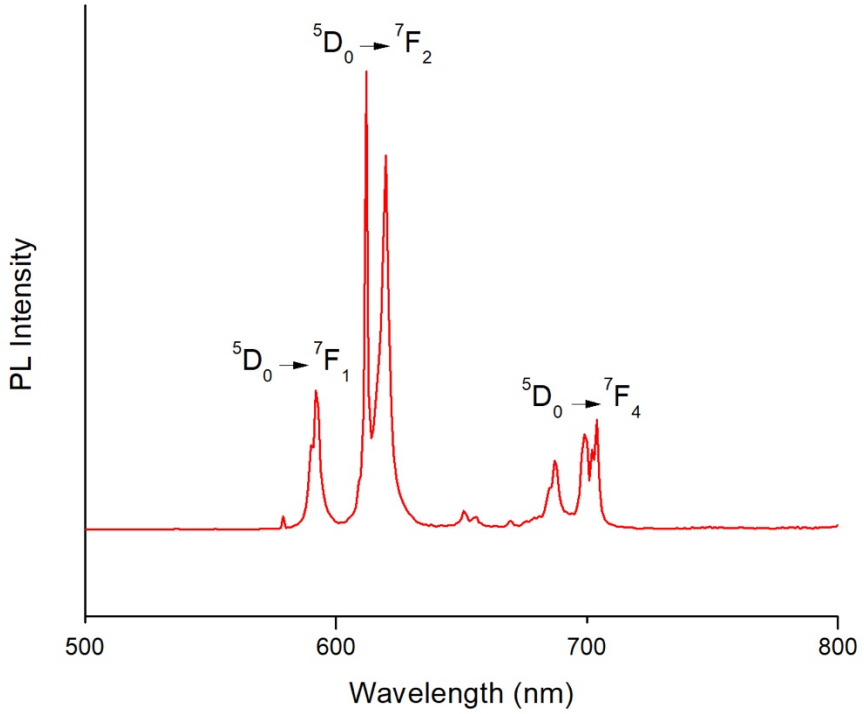

Figure 3.1.16. Solid-state fluorescence emission spectrum of SLUG-46 (Eu), excited at 320 nm.

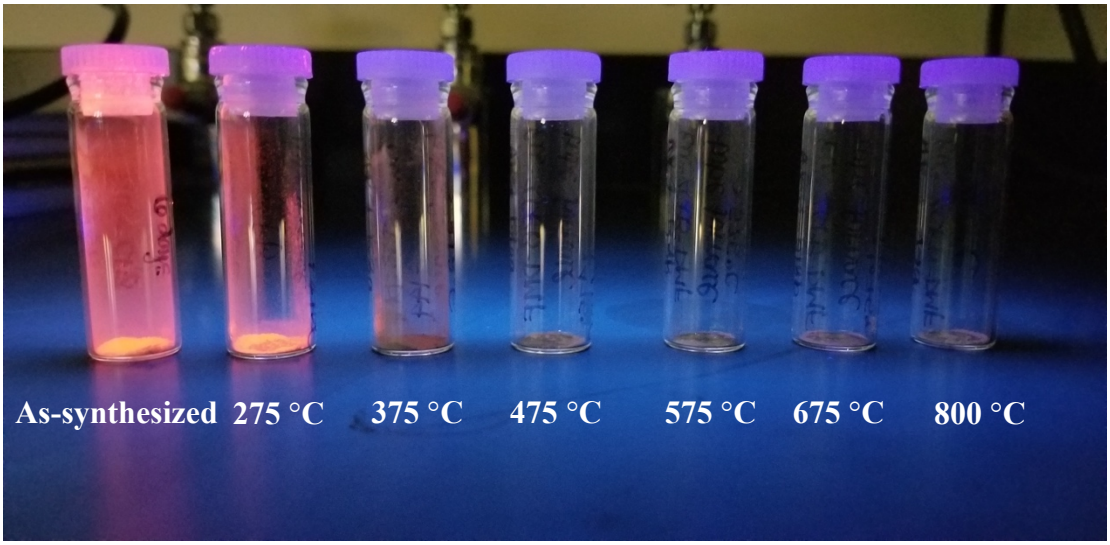

Figure 3.1.17. Optical image of SLUG-46 (Eu) and post-heating samples, illuminated under 254 nm light. The photoluminescence is quenched after heating to 375 °C, signifying a disruption of the LMCT process.

3.1.5. Other Investigations

A variety of synthesis conditions and ion exchanges were attempted with the Ln-BPDC materials. These investigations are presented in the Appendix (Table A1, A5), and include exchanges with ammonium bicarbonate (NH_4HCO_3), tetramethylammonium bromide [$(CH_3)_4NBr$], lead(II) nitrate [$Pb(NO_3)_2$], sodium perchlorate ($NaClO_4$), potassium permanganate ($KMnO_4$), and perfluorooctanoic acid (PFOA, $HO_2C_8F_{15}$).

3.2. Ln-NDC MOFs (SLUG-49–52)

3.2.1. Structures

SLUG-49 through 52 were synthesized solvothermally in good yields [70% to 85% based on Ln(III)] at a synthesis temperature of 110 to 125 °C. Below this optimal temperature, no crystalline product formed. Higher temperatures produced different crystal phases which could not be isolated. The crystals were colorless blocks among a powder of the same phase. Single crystal structures of the MOFs based on La, Nd, Eu, and Gd (SLUG-49 through 52) were obtained and solved (Figures 3.2.1–3.2.4) and the crystal data for these structures are summarized in Table 3.2.1. All four structures are neutral in charge and each crystallizes in a distinct space group and structure. Throughout the four structures, there are two distinct binding modes of the NDC ligand, which we refer to as type I and type II (Figure 3.2.5).

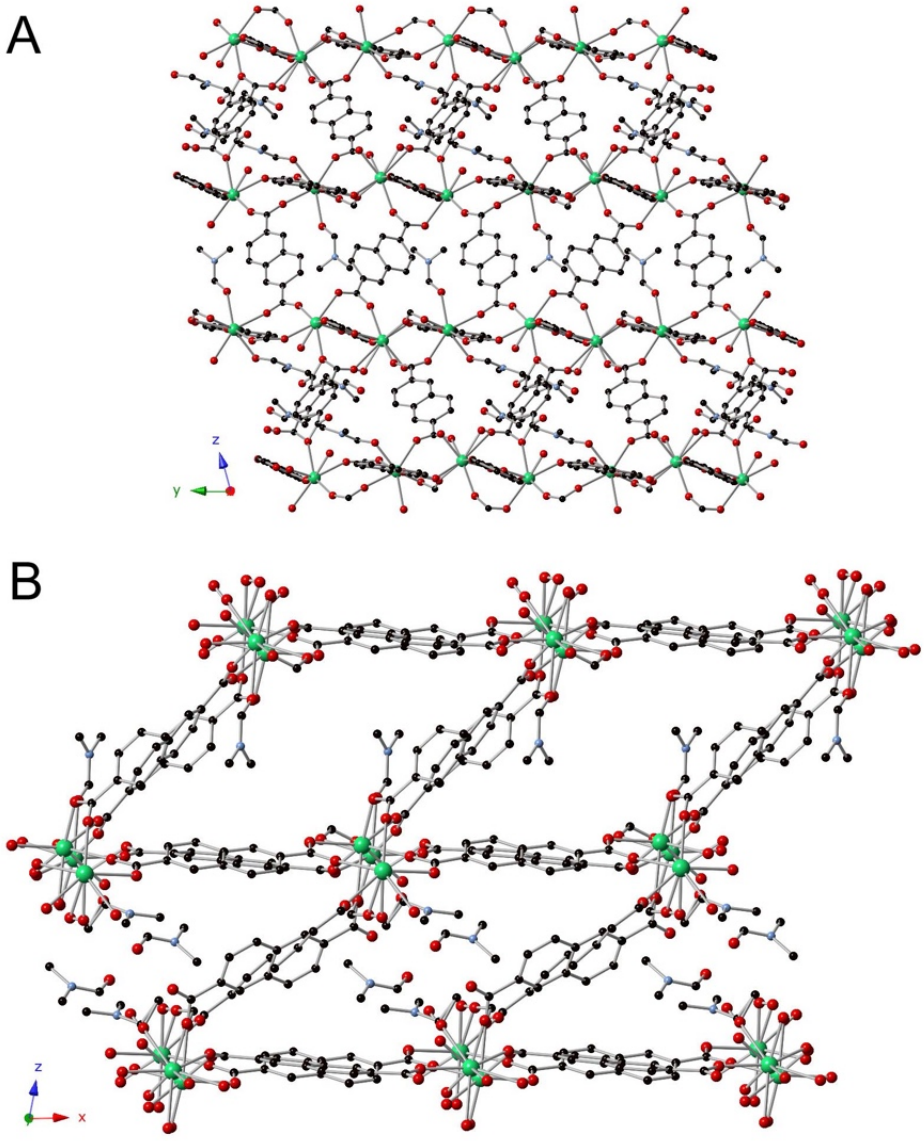

Figure 3.2.1. Crystallographic projections of SLUG-49 (La): A) View along the *a*-axis, highlighting the binding modes of NDC and 3-dimensionality of the structure; B) View along the *b*-axis, showing the three crystallographically distinct La centers and floating DMF molecules within the pores (La – green; O – red; C – black; N – light blue; H – omitted for clarity).

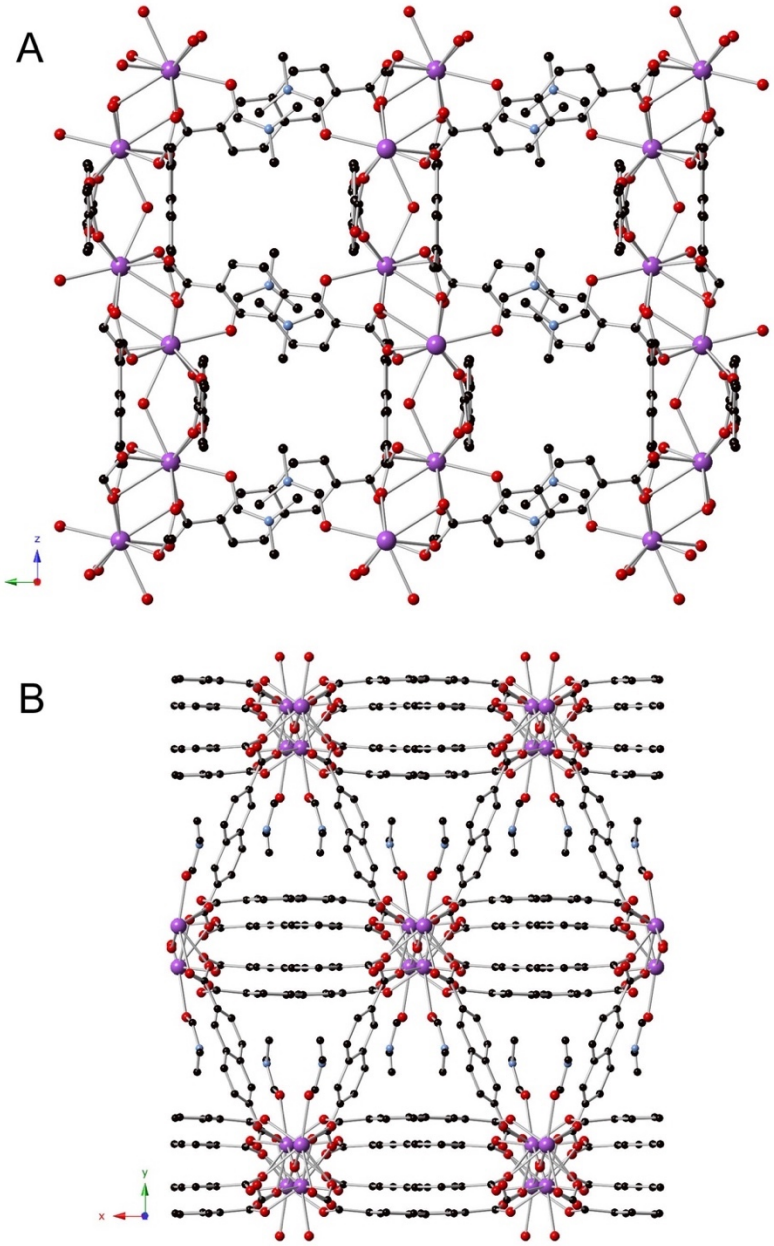

Figure 3.2.2. Crystallographic projection of SLUG-50 (Nd): A) View along the *a*-axis of the 3-dimensional structure; B) View along the *c*-axis, highlighting the various binding modes and pi stacking of NDC ligands, as well as the bound DMF molecules (Nd – purple; O – red; C – black; N – light blue; H – omitted for clarity).

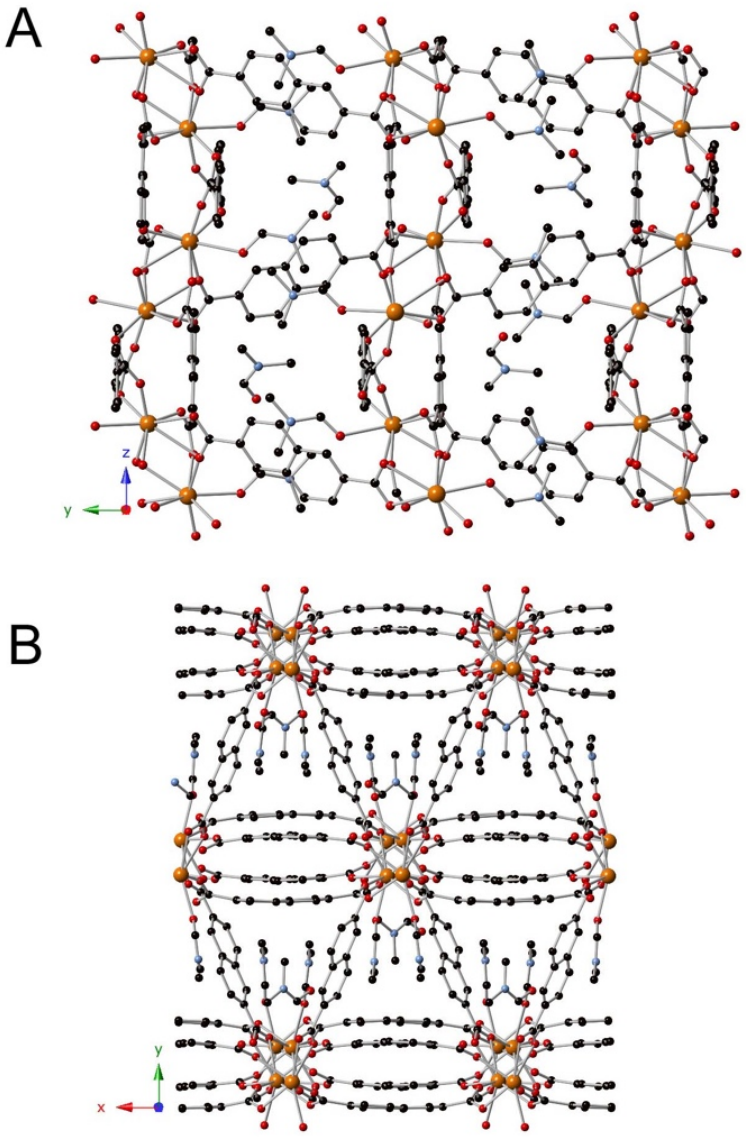

Figure 3.2.3. Crystallographic projections of SLUG-51 (Eu): A) View along the *a*-axis of the 3-dimensional structure; B) View along the *c*-axis, highlighting the various binding modes and pi-stacking of NDC ligands, as well as the bound and floating DMF molecules (Eu – orange; O – red; C – black; N – light blue; H – omitted for clarity).

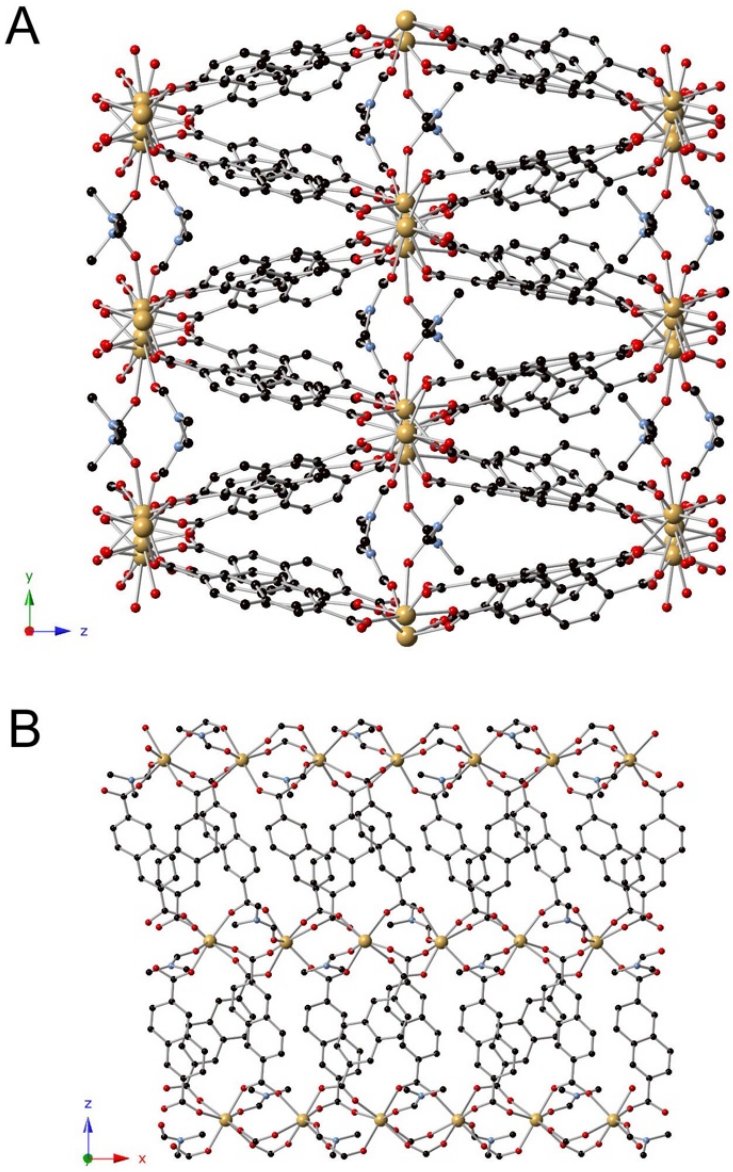

Figure 3.2.4. Crystallographic projections of SLUG-52 (Gd); A) View along the *a*-axis of the 3-dimensional structure; B) View along the *b*-axis, showing the various binding modes of the NDC ligands and the bound DMF molecules (Gd – yellow; O – red; C – black; N – light blue; H – omitted for clarity).

Table 3.2.1. Crystal Data and Structure Refinement for SLUG-49, -50, -51 and -52

Material	SLUG-49	SLUG-50	SLUG-51	SLUG-52
Empirical Formula	$La_6C_{135}H_{115}O_{47}N_9$	$NdC_{21}H_{16}O_{7.5}N$	$Eu_2C_{45}H_{39}O_{15}N_3$	$Gd_4C_{84}H_{64}O_{28}N_4$
Formula Weight ($g \cdot mol^{-1}$)	3448.81	546.59	1165.71	2206.39
Temperature (K)	100(2)	100(2)	100.01(10)	120(2)
Crystal System	Triclinic	Monoclinic	Monoclinic	Orthorhombic
Space Group	$P\bar{1}$	$C2/c$	$P2_1/n$	$Pca2_1$
a, b, c, (Å)	13.2526(8) 14.3785(8) 19.9214(10)	12.4204(5) 21.5953(7) 16.3081(6)	11.9185(3) 21.8730(5) 16.5342(4)	19.4366(9) 8.7643(4) 45.084(2)
α, β, γ (°)	70.927(5) 74.630(5) 75.542(5)	90 102.907(4) 90	90 100.476(2) 90	90 90 90
Volume ($Å^3$)	3403.5(4)	4263.7(3)	4238.51(18)	7679.9(6)
Z	1	8	4	4
ρ_{calc} ($g \cdot cm^{-3}$)	1.683	1.703	1.827	1.908
μ (mm^{-1})	14.980	2.480	3.009	3.500
F(000)	1706	2152	2304	4304
Index Ranges	$-12 \le h \le 15$ $-16 \le k \le 17$ $-23 \le l \le 23$	$-16 \le h \le 16$ $-27 \le k \le 29$ $-22 \le l \le 21$	$-14 \le h \le 14$ $-26 \le k \le 27$ $-20 \le l \le 20$	$-25 \le h \le 24$ $-11 \le k \le 11$ $-59 \le l \le 60$
Reflections Collected	32919	4360	30302	19057
Unique Data	9215 [R_{int} = 0.0589]	3954 [R_{int} = 0.0296]	6543 [R_{int} = 0.0249]	13636 [R_{int} = 0.0918]
Data / Restraints / Parameters	11945 / 56 / 1042	4360 / 38 / 316	8660 / 0 / 592	19057 / 25 / 1089
Goodness of Fit on F^2	1.043	1.075	1.025	0.875
Final R Factors [$I > 2\sigma(I)$]	R_1 = 0.0434 wR_2 = 0.1043	R_1 = 0.0254 wR_2 = 0.0675	R_1 = 0.0220 wR_2 = 0.0462	R_1 = 0.0536 wR_2 = 0.1267
Largest Residual Peak/Hole ($e \cdot Å^{-3}$)	1.121 / -1.196	1.043 / -0.640	0.639 / -0.720	2.065 / -1.440

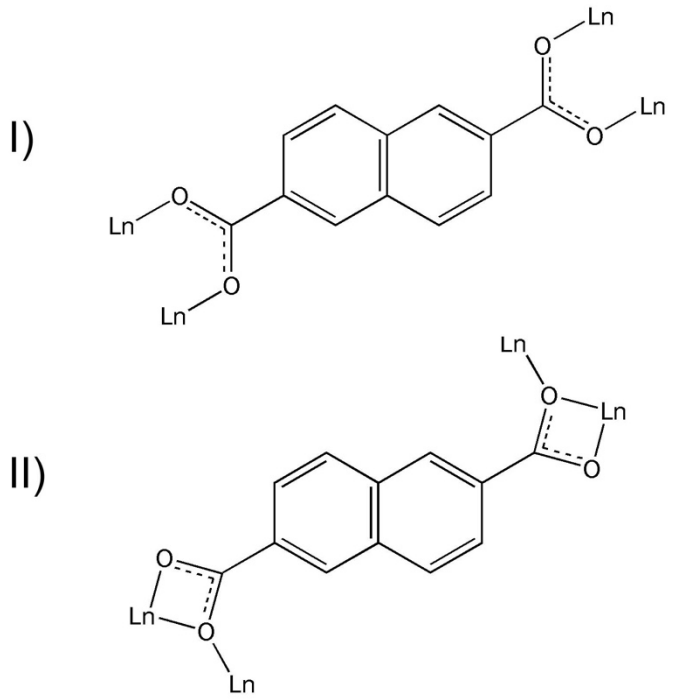

Figure 3.2.5. Two binding modes of the NDC ligand in SLUG-49 through 52. I) NDC μ_2-bridging four lanthanide metal ions; II) NDC bidentate bridging to one lanthanide metal ion and one of the oxygens from each carboxylate group also bridges to a second metal.

The SCXRD data reveals the La-based structure (SLUG-49) crystallizes in the $P\bar{1}$ space group. There are three distinct La^{3+} ions in the asymmetric unit of SLUG-49, each of which is coordinated to eight or nine oxygens. The first La^{3+} center is nine-coordinate: coordinated to seven oxygens from NDC ligands via type I coordination, one bridging oxygen, and an oxygen from a DMF molecule. The second type of La^{3+} center is coordinated by six oxygens from NDC via type I coordination, one oxygen

from a DMF molecule, and one terminal oxygen. The third La^{3+} center is coordinated to four NDC ligands via type I coordination, one bridging oxygen, 1 terminal oxygen, and two DMF molecules. SLUG-49 contains 6 disordered floating DMF molecules per formula unit. The Nd- and Eu-based structures (SLUG-50 and-51, respectively) are the most similar to each other. Both are in the monoclinic crystal system, but the structures crystallize in the $C2/c$ and $P2_1/n$ space groups, respectively. SLUG-50 contains a nine-coordinate Nd^{3+} center, surrounded by four NDC ligands with type I coordination, one NDC ligand with bidentate type II coordination, one bridging type II coordination, one DMF molecule, and one μ_2-bridging oxygen. SLUG-51 is characterized by an eight-coordinate Eu^{3+} center. Here, Eu^{3+} is surrounded by four NDC ligands with type I coordination, one bidentate type II coordination, one bridging type II coordination, and one DMF molecule. Another difference between these two structures is that SLUG-51 contains a floating DMF molecule in addition to the bound DMF found in SLUG-50. Lastly, the Gd-based SLUG-52 structure crystallizes in the $Pca2_1$ space group. Gd^{3+} is seven-coordinate, surrounded by six NDC ligands with type I coordination and one DMF molecule. Syntheses with the lanthanides cerium and erbium were also attempted but no crystals large enough for SCXRD could be isolated.

As evidenced by the SCXRD data, this group of structures is not isomorphous. The PXRD patterns of SLUG-49 through 52 are shown in Figure 3.2.6. Comparisons of the theoretical PXRDs with the as-synthesized materials are presented in Figures 3.2.7 – 3.2.10. One possible reason behind the diversity of these structures is due to

the rigidity of the NDC ligand. As NDC molecules coordinate to the Ln(III) centers, effects such as pi-stacking and an abundance of available coordinating DMF molecules compete to fill the coordination sphere of the lanthanides. These factors will be further discussed in chapter 4.2.

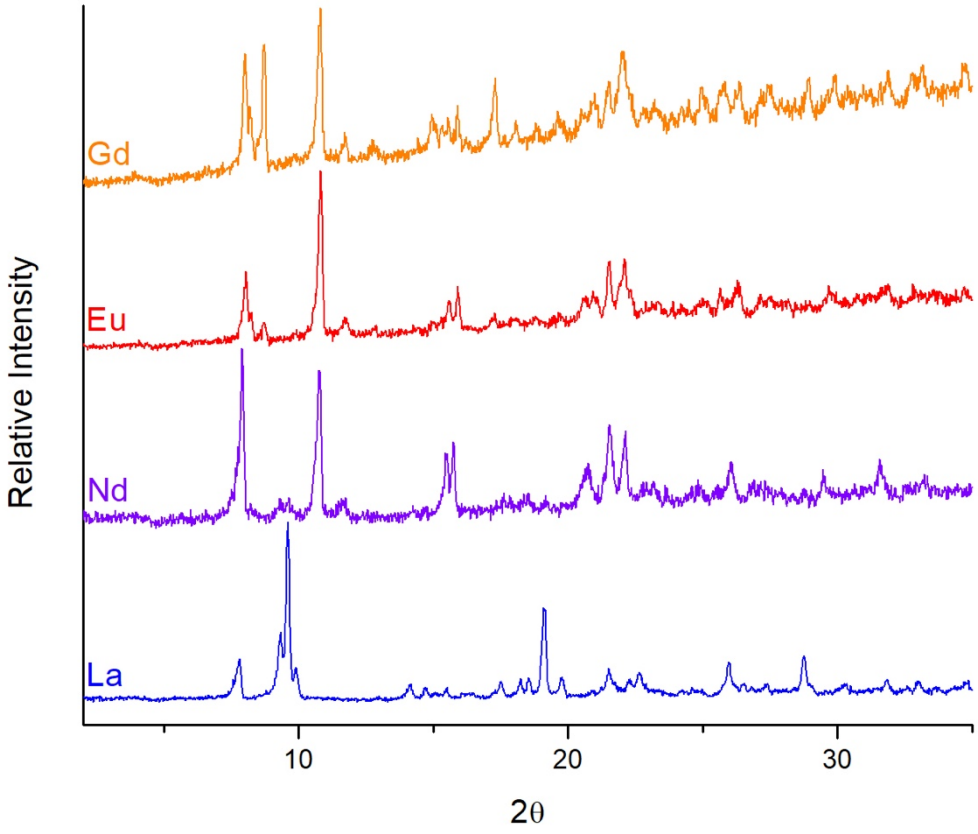

Figure 3.2.6. PXRD patterns of SLUG-49 through 52.

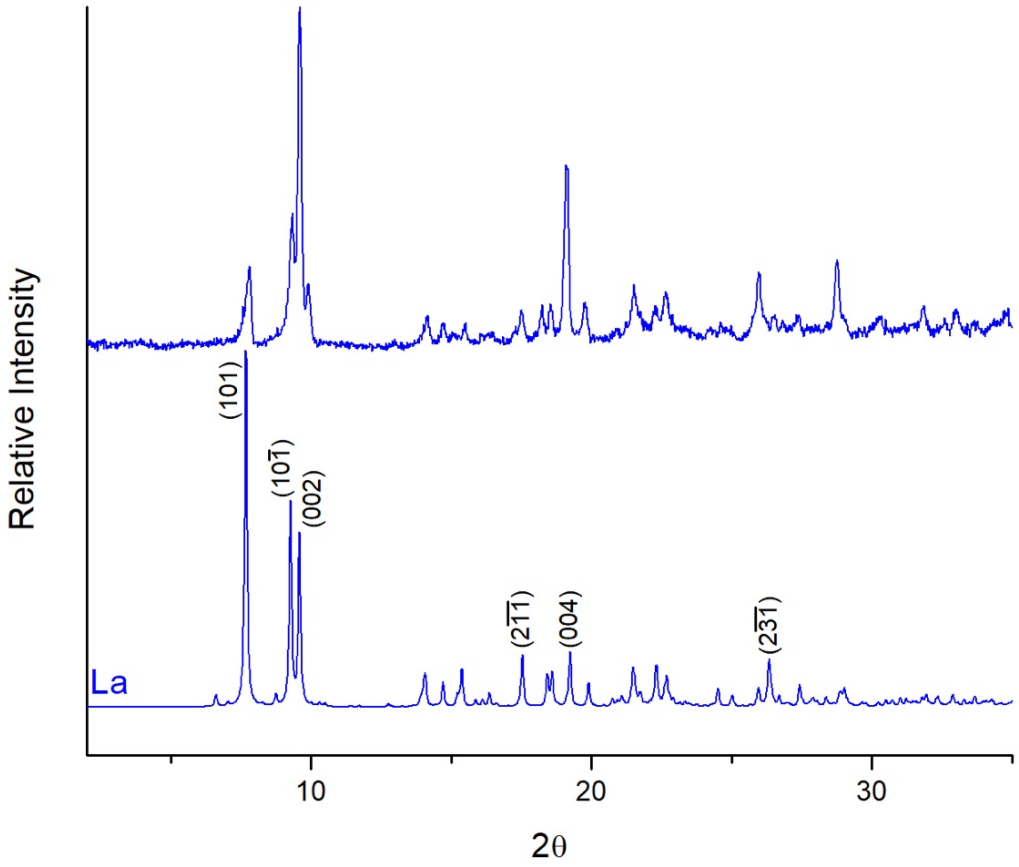

Figure 3.2.7. Comparison of the theoretical PXRD of SLUG-49 (La) (bottom) with as-synthesized (top).

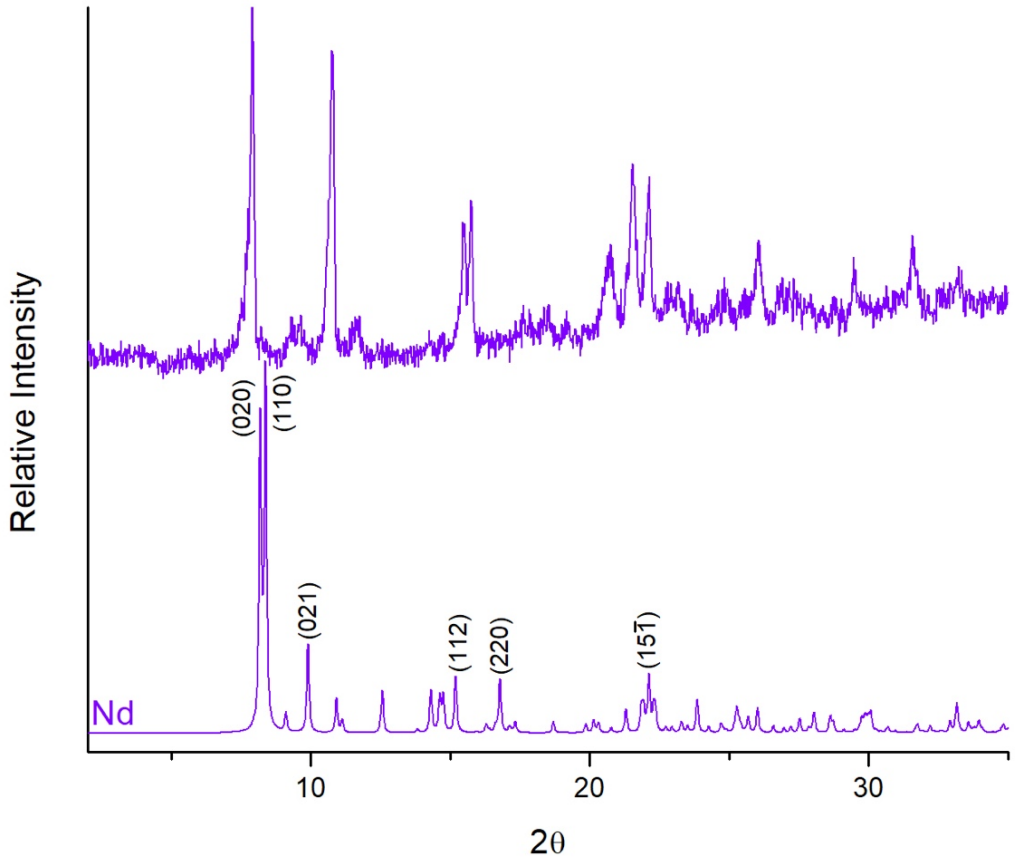

Figure 3.2.8. Comparison of the theoretical PXRD of SLUG-50 (Nd) (bottom) with as-synthesized (top).

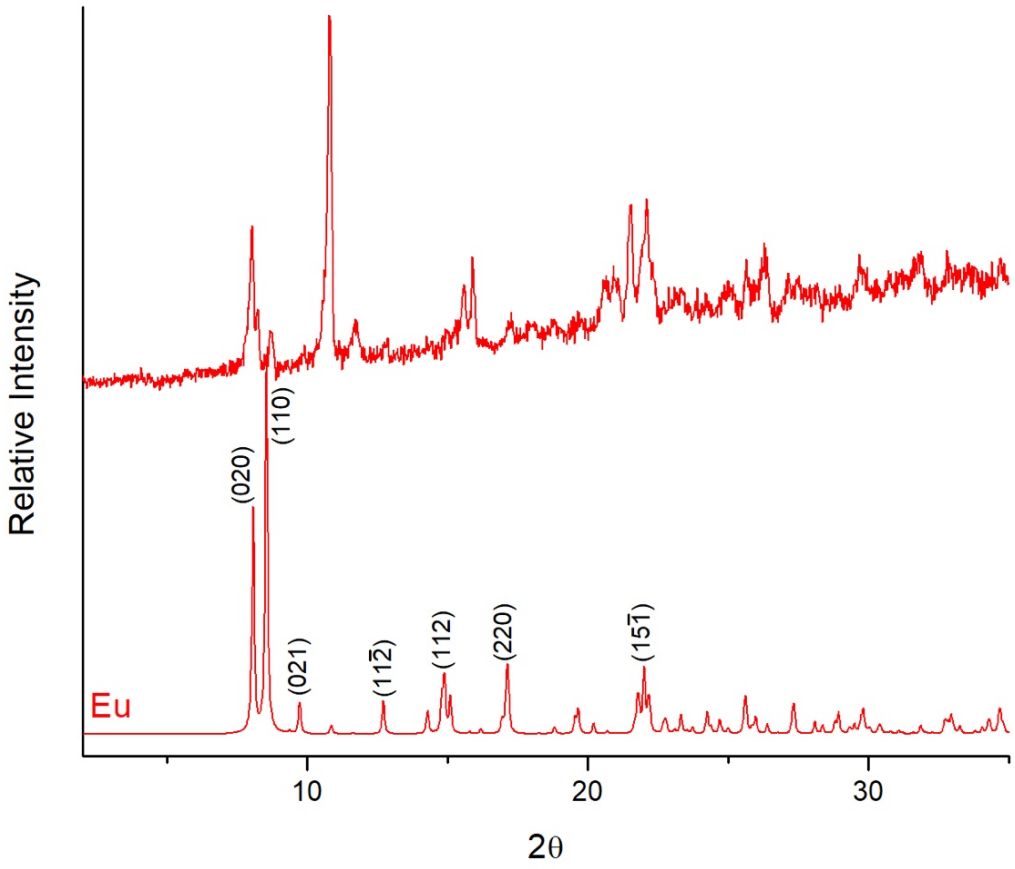

Figure 3.2.9. Comparison of the theoretical PXRD of SLUG-51 (Eu) (bottom) with as-synthesized (top).

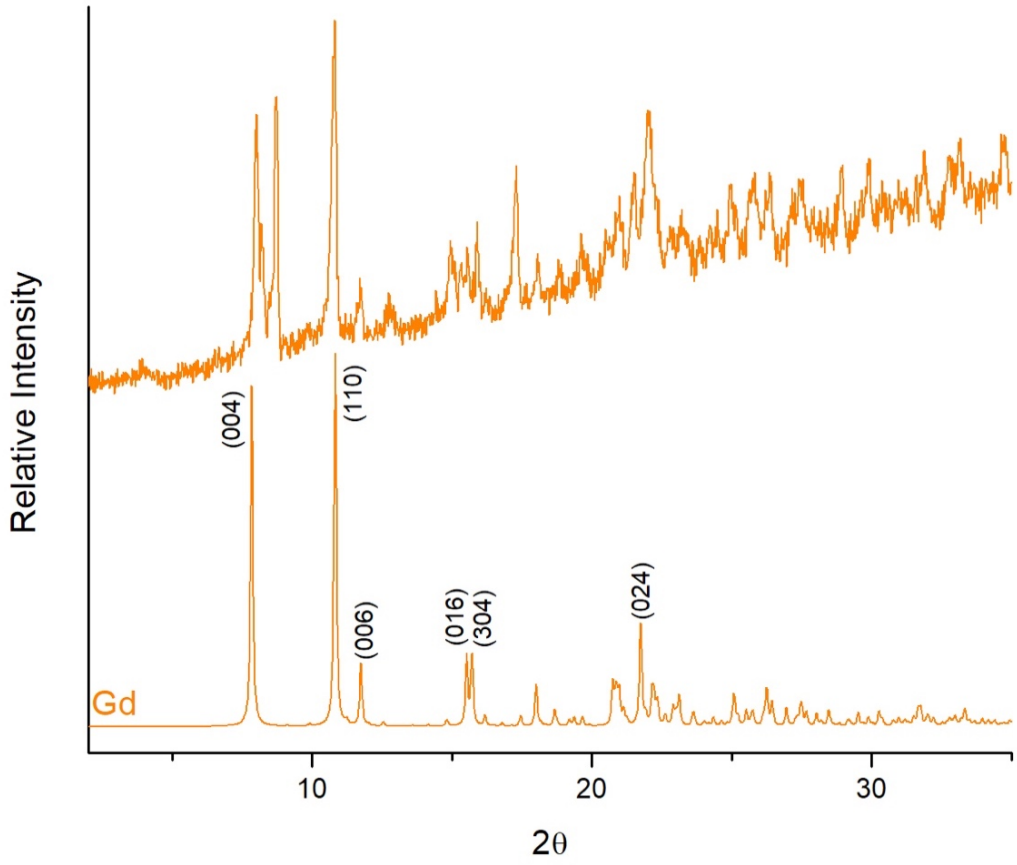

Figure 3.2.10. Comparison of the theoretical PXRD of SLUG-52 (Gd) (bottom) with as-synthesized (top).

3.2.2. Thermal Characterization

The four materials exhibit similar decomposition profiles, which can be characterized by the loss of DMF solvent, the loss of coordinated DMF molecules, and finally the loss of the organic NDC linker (Figures 3.2.11–3.2.14). In the case of SLUG-49 (La), a 12.7% mass loss by 210 °C is observed (Figure 3.2.11A). This corresponds nicely with the loss of six free DMF solvent molecules, which corresponds to a theoretical mass loss of 12.7%. An additional 7.8% mass is lost by 292 °C, which corresponds to

a theoretical mass loss of 7.3% of the three coordinated DMF molecules and an unknown intermediate in the VT-PXRD (Figure 3.2.11B). Lastly, there is a loss of 51.4% mass by 600 °C, which can be attributed to the loss of the organic NDC linkers (theoretical mass loss of 52.6%). VT-PXRD pattern shows that the final phase is La_2O_3 (Figure 3.2.11B, top pattern).

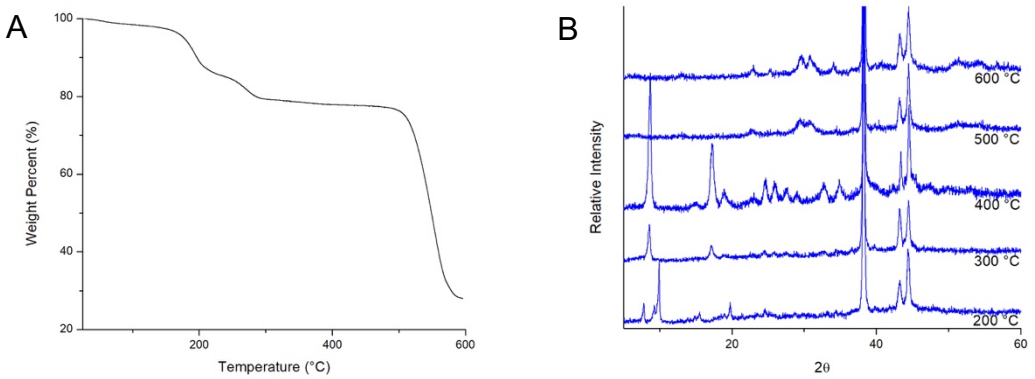

Figure 3.2.11. A) Thermogravimetric trace of SLUG-49 (La); B) *Ex situ* VT-PXRD of SLUG-49 (La).

In the case of SLUG-50 (Nd), a mass loss of 3.0% is observed at 180 °C due to the evolution of solvent DMF molecules. At 290 °C, an additional 13.1% mass loss is observed which corresponds to the loss of coordinated DMF molecules (theoretical loss of 13.4%). By 600 °C, the observed mass loss of 39.7% corresponds to the theoretical mass loss of 41% of the organic component.

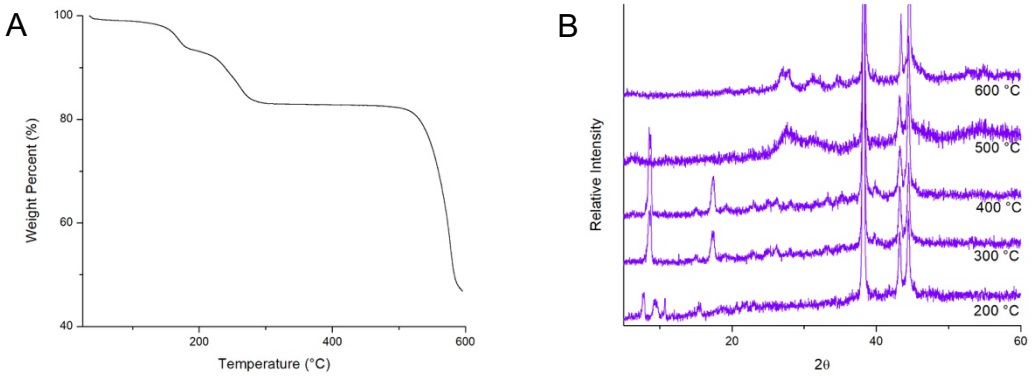

Figure 3.2.12. A) Thermogravimetric trace of SLUG-50 (Nd); B) *Ex situ* VT-PXRD of SLUG-50 (Nd).

SLUG-51 (Eu) is observed to lose 5.5% at 180 °C, which is attributed to the DMF solvent molecule, with a theoretical mass loss of 6.2%. At 310 °C, a mass loss of 12.4% is observed, which matches nicely with the theoretical loss of 12.5% and corresponds to the loss of two coordinated DMF molecules. By 600 °C, a mass loss of 29.5% is observed. This last loss corresponds to the loss of the organic component, with a theoretical mass loss of 38%. It is evident from the TGA and VT-PXRD (Figure 3.2.13) that not all of the organic component has been completely decomposed by 600 °C.

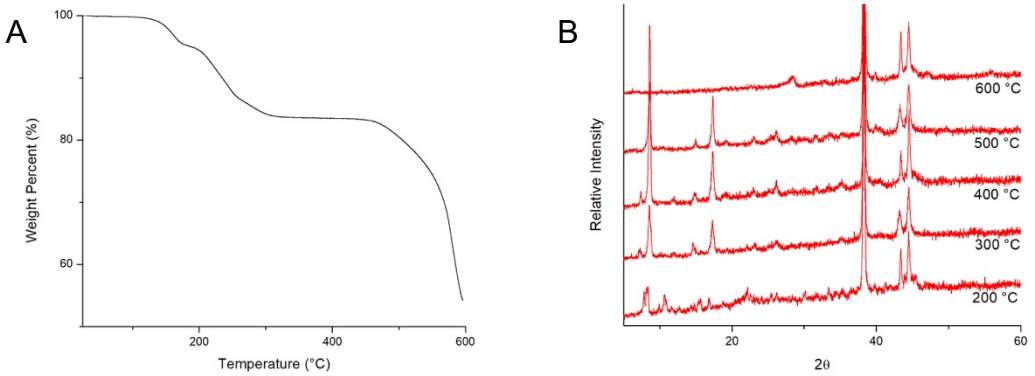

Figure 3.2.13. A) Thermogravimetric trace of SLUG-51 (Eu); B) *Ex situ* VT-PXRD of SLUG-51 (Eu).

By 172 °C, SLUG-52 (Gd) is observed to lose 6.1%, corresponding to the mass loss of two free DMF solvent molecules, a theoretical loss of 6.6%. The second mass loss is 10.3%, which is attributed to the loss of three coordinated DMF molecules, with a theoretical loss of 9.9%. At the final decomposition at 600 °C, a mass loss of 37.7% is observed. This corresponds to the partial loss of the organic component, which again is not completely decomposed (Figure 3.2.14).

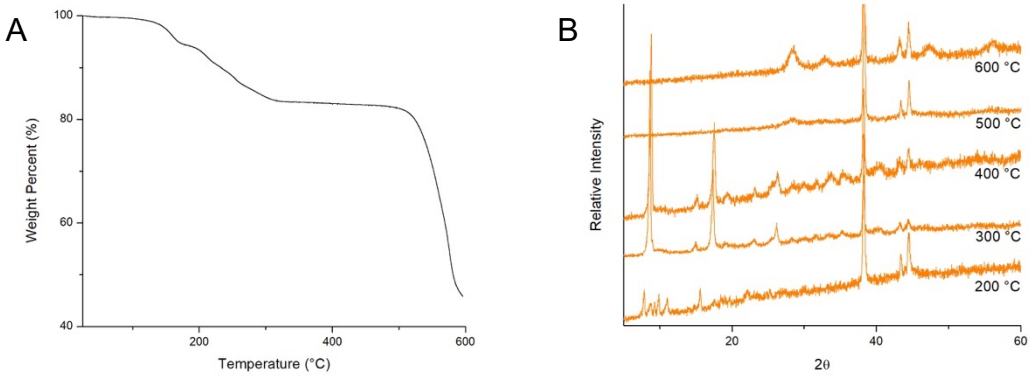

Figure 3.2.14. A) Thermogravimetric trace of SLUG-52 (Gd); B) *Ex situ* VT-PXRD of SLUG-52 (Gd).

3.2.3. Vibrational Spectroscopy

Although SLUG-49 through 52 display different structures, their IR spectra are very similar owing to their similar components: NDC ligands, and bound and floating DMF molecules (Figure 3.2.15). Between the range of 1680 to 1620 cm^{-1}, two bands are observed which correspond to the C=O stretch of DMF.[2] The peaks at ~ 1600 cm^{-1} correspond to asymmetrical $(C^{---}O)_2$ stretching from the carboxylate group on NDC. The sharp peaks near 1400 cm^{-1} are attributed to the C-N stretch of DMF. The bands between 790 and 770 cm^{-1} correspond to C-H bands on the β-substituted naphthalenes. The PXRD and FTIR of the free ligand H_2NDC are shown in Figure 3.2.16, to demonstrate the differences with the synthesized materials.

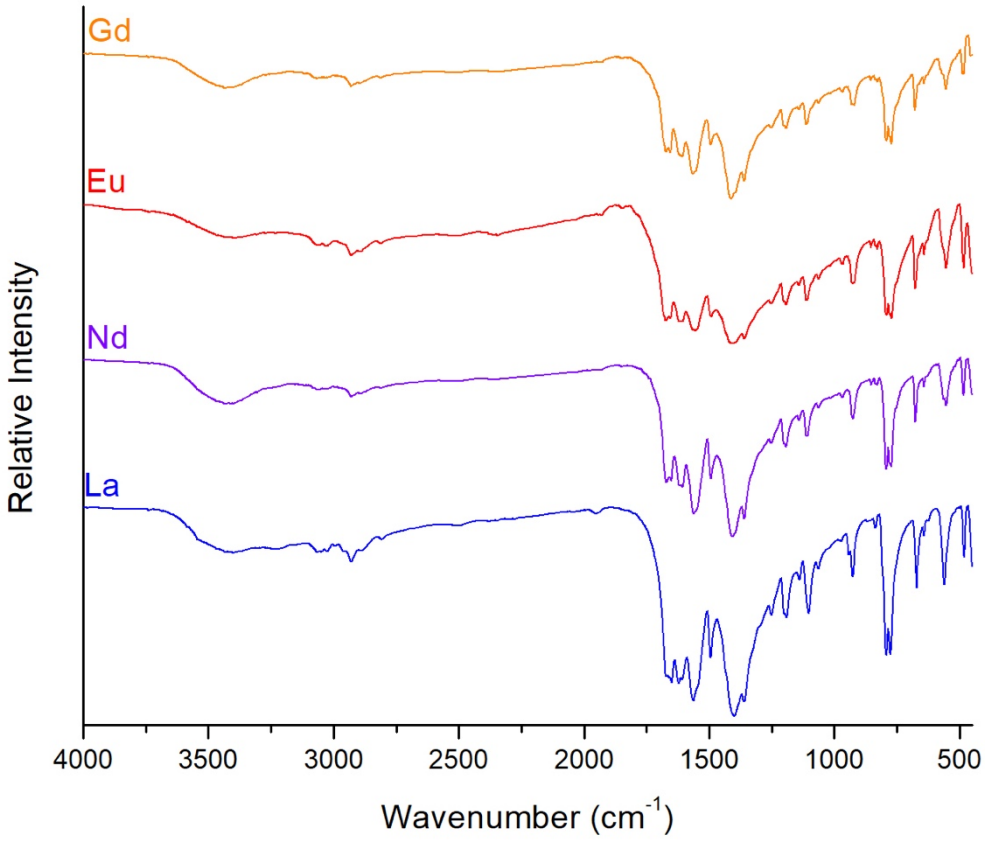

Figure 3.2.15. FTIR spectra of SLUG-49 through -52.

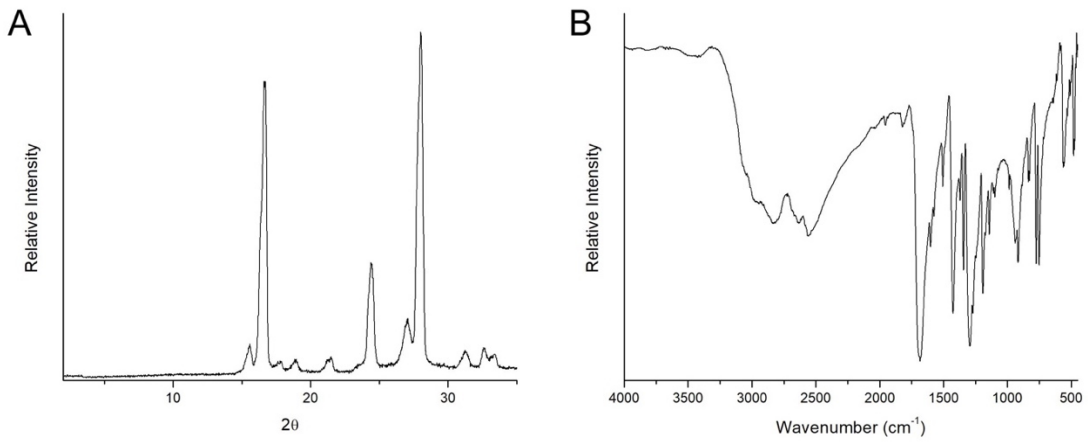

Figure 3.2.16. Characterizations of the free ligand 2,6-H_2NDC: A) PXRD pattern of H_2NDC; B) FTIR spectrum of H_2NDC.

3.2.4. Photoluminescence Spectroscopy

The Eu(III)-based MOF, SLUG-51, exhibits intense luminescence in the visible red-orange region (Figure 3.2.17). These emission bands are due to $^5D_0 \rightarrow {}^7F_J$ (J = 1, 2, 4) electronic transitions. The $^5D_0 \rightarrow {}^7F_3$ transition is weakly observed at 660 nm. These electronic transitions are known to be the most notable for Eu(III) complexes.[4] SLUG-51 displays a quantum efficiency of 3.56%. This fluorescence is due to a ligand to metal charge transfer process that is well-characterized in europium-based compounds. As expected, none of the SLUG-49 (La), SLUG-50 (Nd), or SLUG-52 (Gd) materials were fluorescent. The photoluminescence of SLUG-51 is quenched after the material is heated to 500 °C (Figure 3.2.18). As the organic is evolved, the LMCT process is likely disrupted and as a result, Eu(III) no longer emits light.

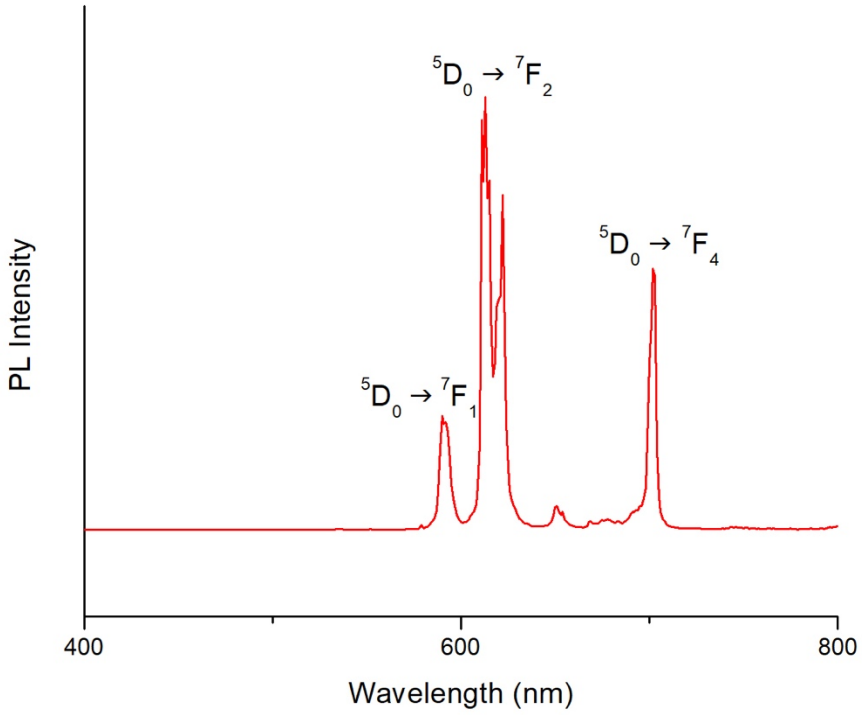

Figure 3.2.17. Solid state fluorescence emission spectrum of SLUG-51 (Eu), excited at 362 nm.

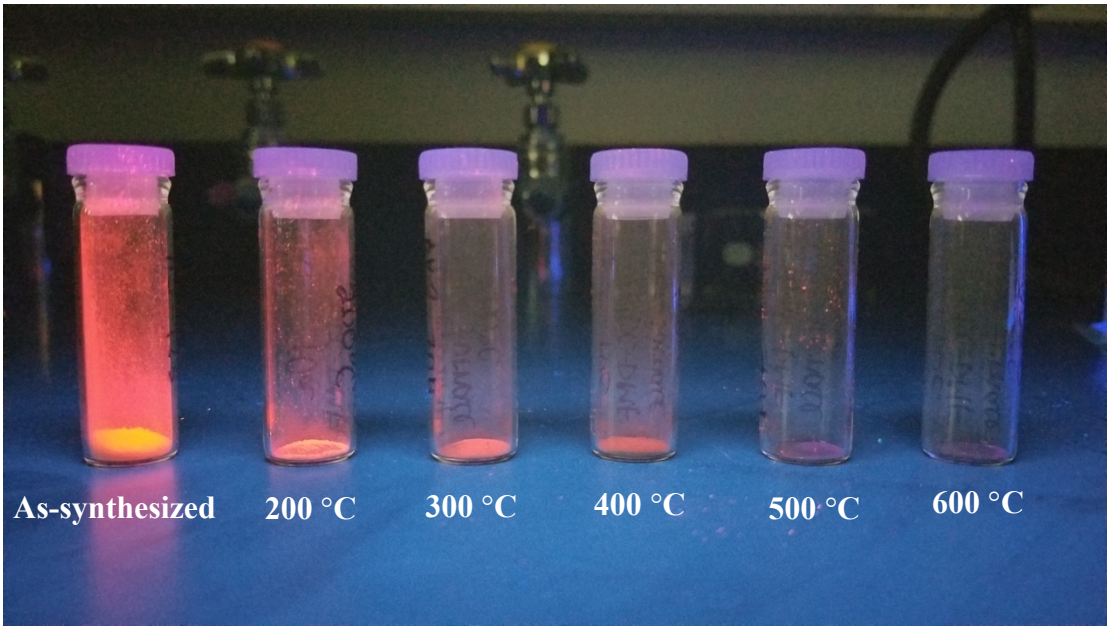

Figure 3.2.18. Optical image of SLUG-46 (Eu) and post-heating samples, illuminated under 254 nm light. The photoluminescence is quenched after heating to 500 °C, signifying a disruption of the LMCT process.

3.2.5. Other Investigations

A variety of synthesis conditions and ion exchanges were attempted with the Ln-NDC materials. These investigations are presented in the Appendix (Table A2, A5), and include exchanges with ammonium bicarbonate (NH_4HCO_3), ammonium nitrate (NH_4NO_3), sodium nitrate ($NaNO_3$), tetramethylammonium bromide [$(CH_3)_4NBr$], lead(II) nitrate [$Pb(NO_3)_2$], sodium perchlorate ($NaClO_4$), perfluorooctanoic acid (PFOA, $HO_2C_8F_{15}$), malonic acid [$CH_2(CO_2H)_2$], succinic acid [$(CH_2)_2(CO_2H)_2$], glutaric acid [$(CH_2)_3(CO_2H)_2$], suberic acid [$(CH_2)_6(CO_2H)_2$], and sebacic acid [$(CH_2)_8(CO_2H)_2$].

3.3. Nd-ADS LREHs (SLUG-28–30)

3.3.1. Structures

SLUG-28, -29 and -30 were all synthesized hydrothermally in high yields [80 to 86% based on Nd(III)]. The single crystal structure of SLUG-28 was obtained and solved (Figure 3.3.1) and the crystal data for this structure is summarized in Table 3.3.1. SCXRD reveals that SLUG-28 crystallizes in the triclinic space group *P*-1. SLUG-28 is composed of layers of nine-coordinate neodymium polyhedra linked by six μ_3-OH groups and two μ_2-OH_2 groups. One sulfonate oxygen from the organosulfonate completes the neodymium coordination sphere and covalently connects the inorganic layers together (Figure 3.3.1A). The PXRD patterns of SLUG-28, -29, and -30 demonstrate a clear decrease in low angle (001) peak as the carbon chain length of the organosulfonate increases (Figure 3.3.2). The structures of SLUG-29 and -30 are isostructural to those of a lanthanum-based material that was solved by Rietveld refinement of PXRD data.[5]

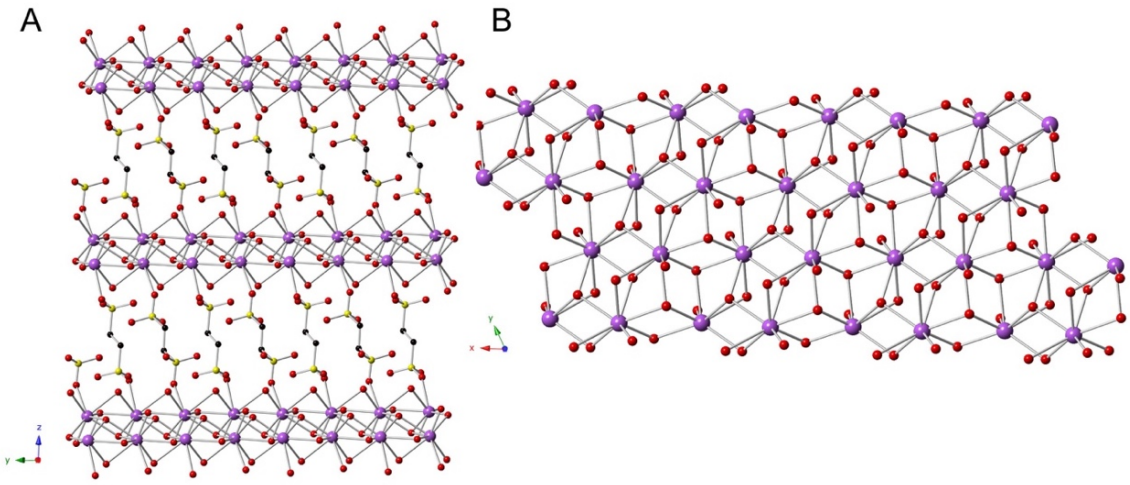

Figure 3.3.1. Crystallographic projections of SLUG-28: A) View along the *a*-axis, showing the cationic inorganic layers connected by ethanedisulfonate ligands (Nd – purple; O – red; C – black; S – yellow; H omitted for clarity); B) View along the *c*-axis, showing a top-down view of one inorganic layer.

Table 3.3.1. Crystallographic Data and Structure Refinement for SLUG-28

Material	SLUG-28
Empirical Formula	$Nd_2C_2H_{12}O_{12}S_2$
Formula Weight (g mol^{-1})	580.72
Temperature (K)	120(2)
Crystal system	Triclinic
Space group	*P*-1
a, b, c (Å)	7.396(3), 7.403(3), 12.251(5)
α, β, γ (°)	86.666(5), 76.969(5), 63.435(5)
Volume ($Å^3$)	583.8(4)
Z	2
ρ_{calc} ($g \cdot cm^{-3}$)	2.712
μ (mm^{-1})	9.142
F (000)	544
Crystal dimensions (mm)	0.134 × 0.078 × 0.022
Index ranges	$-9 \le h \le 9$ $-9 \le k \le 9$ $-16 \le l \le 16$
Reflections Collected	2903
Unique Data	2177 [R_{int} = 0.0228]
Data / restraints / parameters	2903 / 18 / 228
Goodness of fit on F^2	1.021
Final R factors [I > 2σ (I)]	R_1 = 0.0195 wR_2 = 0.0355
Largest Residual Peak/Hole ($e \cdot Å^{-3}$)	0.802 / -0.780

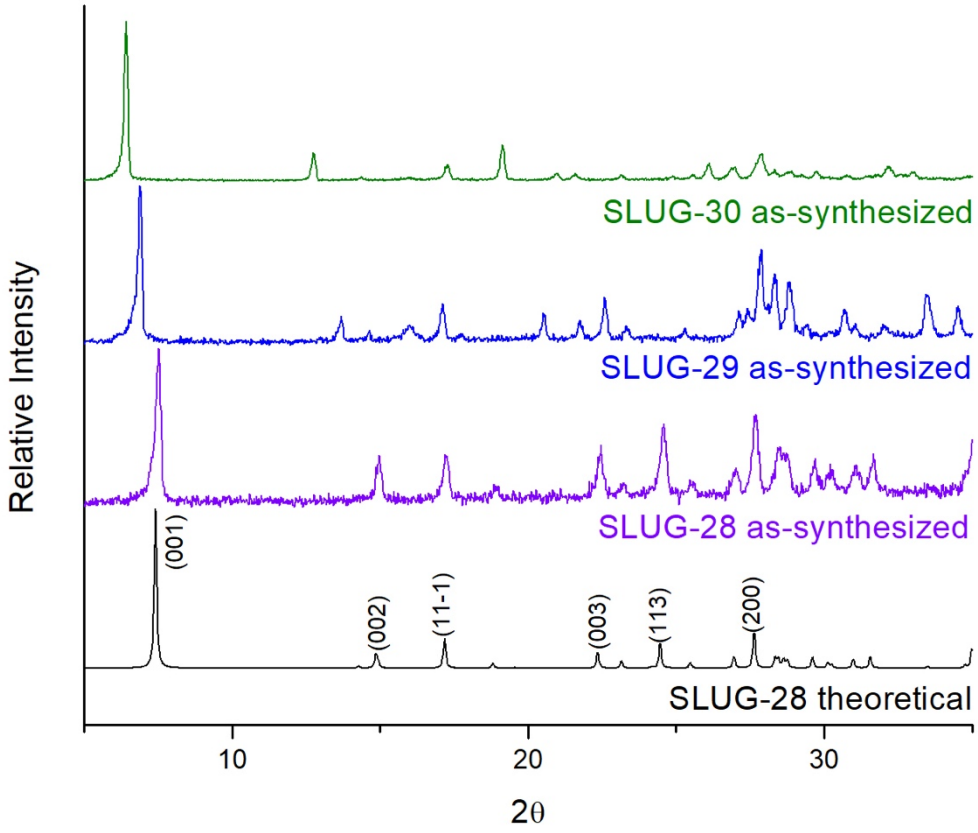

Figure 3.3.2. PXRD patterns of SLUG-28 to 30, with the theoretical pattern for SLUG-28 and main Miller indices shown at the bottom.

3.3.2. Thermal Characterization

Thermogravimetric analysis of SLUG-28 displayed three decomposition events (Figure 3.3.3A). The first decomposition was at approximately 175 °C, which likely corresponds to the loss of the μ_2-OH_2 groups (Table 3.3.2). It can be inferred from the VT-PXRD that the loss of water results in a free sulfonate oxygen atom filling the empty coordination site, decreasing the spacing between the inorganic layers (Figure 3.3.3B, 200 °C at which ~ 80% of the material has transformed at this temperature

based on the area of first peaks). The second mass loss event at ~ 250 °C is attributed to the loss of two μ_3-OH groups; the theoretical mass loss of 5.86% matches nicely with the observed loss of 5.80% (Table 3.3.2). The last decomposition around 375 °C corresponds to the loss of the organic component and one of the sulfonates, resulting in the formation of $Nd_2O_2SO_4$ (PDF 00-048-1829). SLUG-29 and SLUG-30 (Figures 3.3.4A, 3.3.5A respectively) exhibit similar thermal profiles compared to SLUG-28. SLUG-29 maintains the same three decomposition events as SLUG-28 but at slightly higher temperatures, likely due to the greater amount of van der Waals interaction by the longer chains. It also loses an additional 4.53% mass after the loss of the organic. This extra mass loss matches nicely with the theoretical loss of the additional carbon. Likewise, the decomposition events of SLUG-30 occur at higher temperatures than those of SLUG-28 and -29. Additionally, SLUG-30 loses the hydrocarbons of the butanedisulfonate abruptly at ~ 450 °C but the sulfonates remain a part of the $Nd_2O_2SO_4$ layers.[6] The observed weight losses reasonably match the theoretical mass losses in all cases, except for the loss of the sulfonate in SLUG-30 (Table 3.3.2).

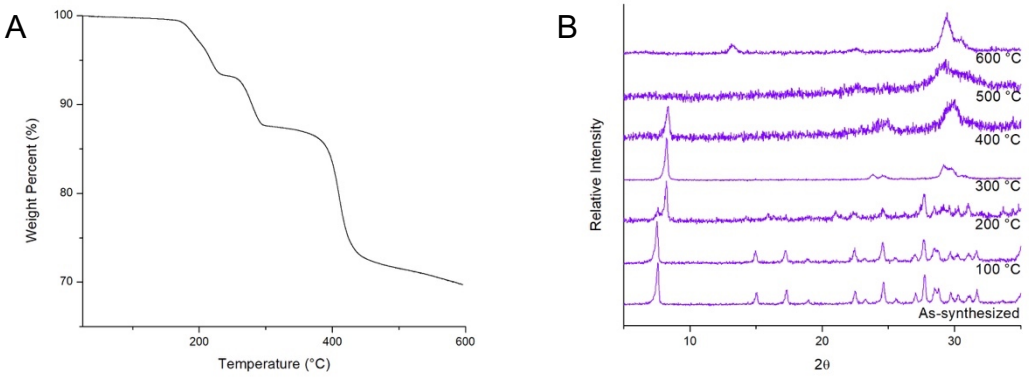

Figure 3.3.3. A) Thermogravimetric trace of SLUG-28 (Nd-EDS); B) *Ex situ* VT-PXRD of SLUG-28 (Nd-EDS).

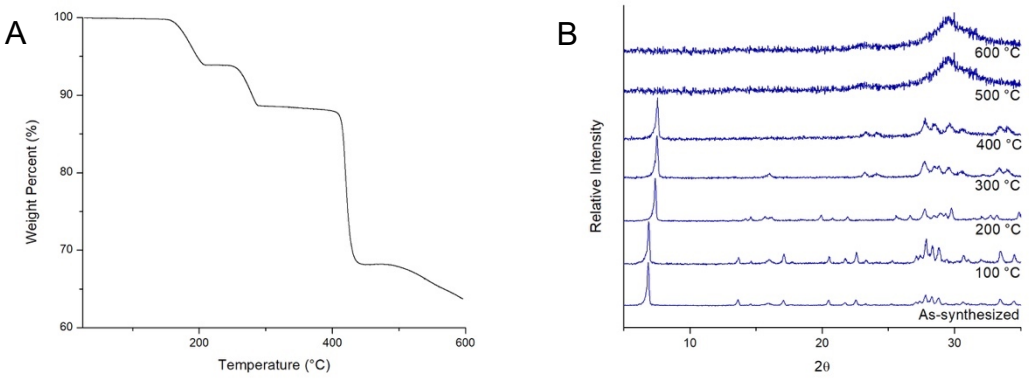

Figure 3.3.4. A) Thermogravimetric trace of SLUG-29 (Nd-PDS); B) *Ex situ* VT-PXRD of SLUG-29 (Nd-PDS).

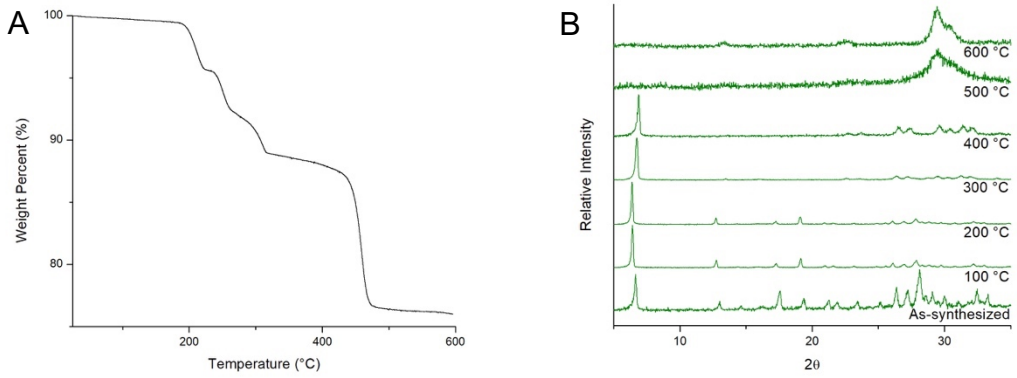

Figure 3.3.5. A) Thermogravimetric trace of SLUG-30 (Nd-BDS); B) *Ex situ* VT-PXRD of SLUG-30 (Nd-BDS).

Table 3.3.2. Observed and Theoretical Mass Losses of Major Decomposition Events

Material	SLUG-28		SLUG-29		SLUG-30	
	Observed	Theoretical	Observed	Theoretical	Observed	Theoretical
Loss of two H_2O	6.56%	6.20%	6.07%	6.06%	4.36%	5.92%
Loss of two OH	5.80%	5.86%	5.29%	5.72%	6.70%	5.59%
Loss of $(CH_2)_nSO_3^-$	17.93%	18.62%	20.38%	20.57%	12.92%	22.37%

3.3.3. Anion Exchange

The anion exchange capability of these materials was investigated using α,ω-dicarboxylates of varying chain length as well as several oxyanions. All three materials showed exchange capabilities for adipate [$^-O_2C(CH_2)_4CO_2^-$]. As expected, the PXRD of the three exchanged materials have similar powder patterns (Figure 3.3.6). Attempts to intercalate other α,ω-alkanedicarboxylates such as succinate

[$^{-}O_2C(CH_2)_2CO_2^{-}$], suberate [$^{-}O_2C(CH_2)_6CO_2^{-}$], sebacate [$^{-}O_2C(CH_2)_8CO_2^{-}$], and terephthalate [$^{-}O_2C(C_6H_4)CO_2^{-}$] as well as oxyanions such as perchlorate (ClO_4^{-}), chromate (CrO_4^{2-}), and permanganate (MnO_4^{-}) have been unsuccessful. It is likely that the solubility of these anions plays a role in facilitating anion exchange between the alkanedisulfonates and adipate (Table 3.3.3). As the chain length of the aforementioned α,ω-alkanedicarboxylates increases, their solubility in water decreases. We speculate that the solubility of adipic acid, which is between that of succinate and suberate, allows for partial dissolution which promotes solvent-mediated ion exchange (Table 3.3.3). The solubility of succinate is so great that the material may be too unstable to form. The carbon chain length of adipate is preferred over succinate perhaps due to its ability to intercalate the [$Nd_2(OH)_4(OH_2)_2^{2+}$] layers.

Table 3.3.3. Solubility Values of various α,ω-Alkanedicarboxylates[7]

Alkanedicarboxylate	Solubility (g / kg H_2O)	Temperature (°C)
Succinate	83.5	25
Adipate	15	15
Suberate	2.43	25
Sebacate	1	20
Terephthalate	0.065	25

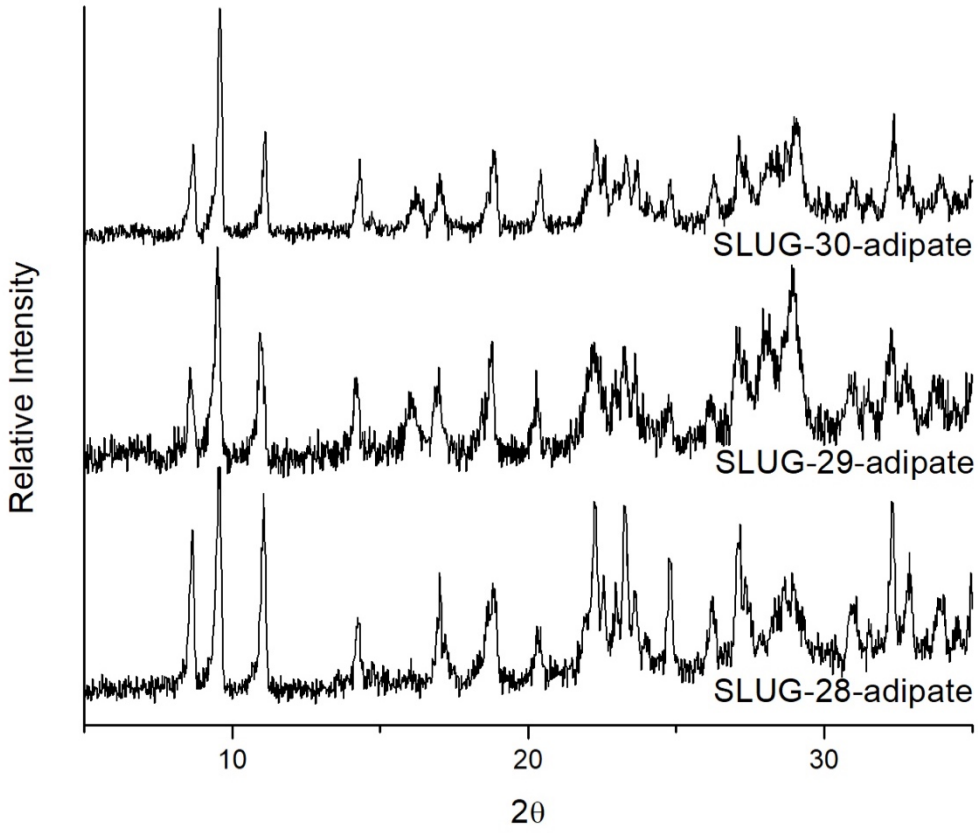

Figure 3.3.6. PXRD patterns of SLUG-28, -29 and -30 exchanged with adipate.

3.3.4. Vibrational Spectroscopy

The FTIR spectra of SLUG-28 through 30 are similar owing to their similar components. The FTIR spectra of SLUG-28 and SLUG-28-adipate highlight the sulfonate stretch (1200 cm^{-1}) and carboxylate stretch (1700 cm^{-1}), respectively, supporting that exchange has occurred (Figure 3.3.7).

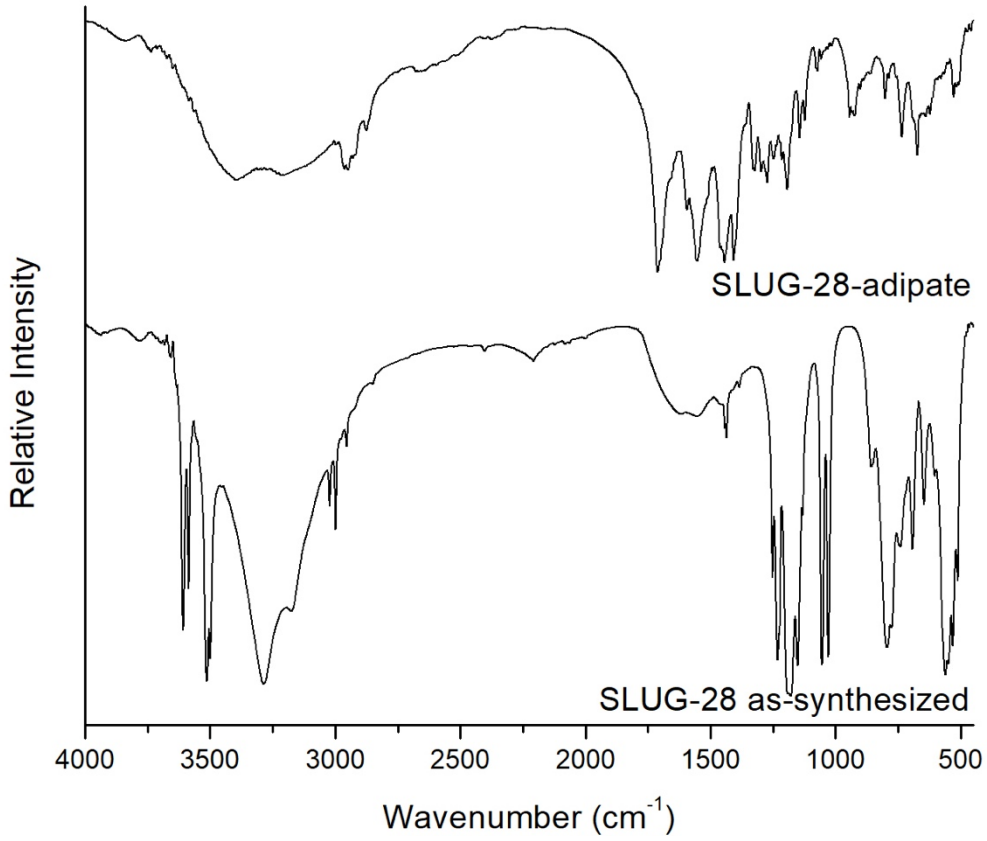

Figure 3.3.7. FTIR of SLUG-28 as-synthesized (bottom) and after exchange with adipate (top).

3.3.5. Other Investigations

A variety of synthesis conditions and ion exchanges were attempted with the Nd-ADS materials. These investigations are presented in the Appendix (Table A3, A5), and include exchanges with malonic acid [$CH_2(CO_2H)_2$], succinic acid [$(CH_2)_2(CO_2H)_2$], glutaric acid [$(CH_2)_3(CO_2H)_2$], adipic acid [$(CH_2)_4(CO_2H)_2$], suberic acid [$(CH_2)_6(CO_2H)_2$], sebacic acid [$(CH_2)_8(CO_2H)_2$], terephthalic acid [$C_6H_4(CO_2H)_2$], sodium nitrate ($NaNO_3$), sodium chloride (NaCl), sodium chlorate ($NaClO_3$),

potassium chromate (K_2CrO_4), potassium permanganate ($KMnO_4$), and perfluorooctanoic acid (PFOA, $HO_2C_8F_{15}$).

3.4. References

(1) Sienkiewicz-Gromiuk, J.; Rzączyńska, Z. Structural, Thermal, and Spectral Investigations of the Lanthanide(III) Biphenyl-4,4′-Dicarboxylates. *J. Therm. Anal. Calorim.* **2013**, *112* (2), 877–884. https://doi.org/10.1007/s10973-012-2590-1.

(2) Silverstein, R. M.; Webster, F. X.; Kiemle, D. J. *Spectrometric Identification of Organic Compounds*, 7th ed.; John Wiley & Sons, Inc., 2005.

(3) Crystallographic Evidence for Decomposition of Dimethylformamide in the Presence of Ruthenium(III) Chloride. *Inorganica Chim. Acta* **2003**, *355*, 420–423. https://doi.org/10.1016/S0020-1693(03)00312-8.

(4) Binnemans, K. Interpretation of Europium(III) Spectra. *Coord. Chem. Rev.* **2015**, *295*, 1–45. https://doi.org/10.1016/j.ccr.2015.02.015.

(5) Liang, J.; Ma, R.; Ebina, Y.; Geng, F.; Sasaki, T. New Family of Lanthanide-Based Inorganic–Organic Hybrid Frameworks: Ln2(OH)4[O3S(CH2)NSO3]·2H2O (Ln = La, Ce, Pr, Nd, Sm; n = 3, 4) and Their Derivatives. *Inorg. Chem.* **2013**, *52* (4), 1755–1761. https://doi.org/10.1021/ic301294j.

(6) Golovnev, N. N.; Molokeev, M. S.; Vereshchagin, S. N.; Atuchin, V. V. Synthesis and Thermal Transformation of a Neodymium(III) Complex [Nd(HTBA)2(C2H3O2)(H2O)2]·2H2O to Non-Centrosymmetric Oxosulfate

Nd2O2SO4. *J. Coord. Chem.* **2015**, *68* (11), 1865–1877. https://doi.org/10.1080/00958972.2015.1031119.

(7) Haynes, W. M., Ed. *CRC Handbook of Chemistry & Physics*, 92nd ed.; CRC Press, 2011.

Chapter 4

Insights on 3-Dimensional and Layered Lanthanide Metal-Organic Structures

Abstract

In comparing the three projects of this thesis [SLUG-43 through 48 (Ln-BPDC), SLUG-49 through 52 (Ln-NDC), and SLUG-28 through 30 (Nd-ADS)], two main questions arise: 1) what conditions contribute to forming three-dimensional MOFs versus two-dimensional LREHs? and 2) why are the NDC-based materials not isomorphous like those of Ln-BPDC? In this chapter, the factors contributing toward the dimensionality of lanthanide-based materials will be discussed. A reason for the lack of isomorphous nature of the NDC-based series is also proposed.

4.1. 2-D and 3-D Lanthanide-based Materials

In this work, we have seen three-dimensional lanthanide-MOF structures and two-dimensional LREH structures (Figure 4.1.1). As mentioned in chapter 1.2.1, the lanthanides are hard acids and prefer to react with hard bases such as oxygen.[1] Additionally, the high coordination number of the lanthanides favors the coordination sphere to be filled with small molecules such as hydroxide or water.[2] With this information in hand, it allows us to identify factors that contribute toward the

dimensionality of Ln-MOFs versus LREHs. The general formula of LREHs $\{[RE_4(OH)_{10}(H_2O)_4]_nA_n\}$ demonstrates the propensity of hydroxide ions and water molecules to fill the coordination sphere of the lanthanide ions. The process of hydroxide molecules reacting with lanthanide ions is solution is known as alkalization. Methods of homogenous alkalization, in which a reagent undergoes hydrolysis to slowly produce hydroxide ions, are well documented in LREH syntheses by the Sasaki group.[3–7] Another synthetic strategy to produce LREHs is the hydrothermal treatment of rare earth reagents to transform them to the hydroxide forms. In either case, hydroxide ions and water molecules surround the rare earth ion to produce a positively charged layer; these layers are charge-balanced by interlamellar anions. These anions have been demonstrated to be small molecules such as halides, nitrate, and sulfate, and longer organic chains with terminal disulfonate functionalities.[8]

In our syntheses of SLUG-28 through 30, we employed a slightly different synthesis technique: solid NaOH pellets were added to a reagent solution of water, $Nd(NO_3)_3 \cdot 6 H_2O$, and disodium α,ω-alkanedisulfonate to raise the pH from ~ 4 to ~ 7. The addition of NaOH produced a gel-like solution, and the solution was transferred to an autoclave, where it was heated hydrothermally. This synthesis procedure is similar to that of the sol-gel method. In a general sol-gel process, a metal ion can form a variety of different oxyhydroxyl species depending on the pH.[9] A metal ion that is soluble in an acidic aqueous environment can form an insoluble polymeric and cationic species coordinated to hydroxide ions and water molecules as the pH is increased. Sol-gel

methods are typically used in zeolite and ceramic syntheses. In our syntheses, the addition of NaOH provides a rich hydroxide source for the layered $[Nd_2(OH)_4(OH_2)_2^{2+}][^{-}O_3S(CH_2)_nSO_3^{-}]$ (n = 2 – 4) materials to form. Thus, the dimensionality of MOFs versus LREHs can be dictated by controlling the pH of the solution. The starting solutions of Ln-BPDC and Ln-NDC are approximately at pH ~ 4 in DMF as the solvent. This acidic and solvothermal environment keeps hydroxide ions and water molecules in low concentrations. Under these conditions, the ligands can coordinate to the metal ions and form three-dimensional MOF structures.

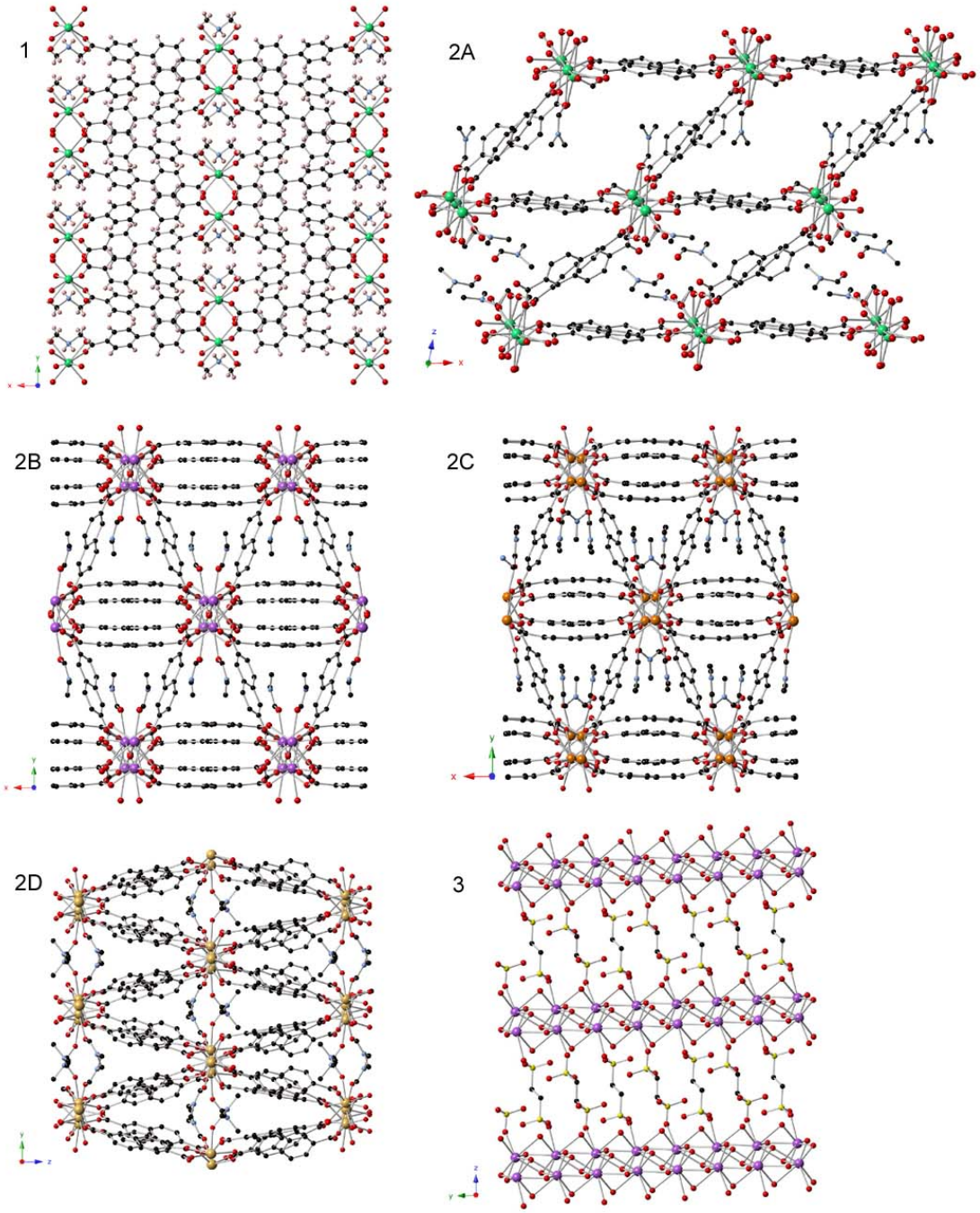

Figure 4.1.1. Representative crystallographic images of the three different projects presented in this work: 1) Ln-BPDC**;** 2A) La-NDC, 2B) Nd-NDC, 2C) Eu-NDC, 2D) Gd-NDC; 3) Nd-EDS

4.2. Conditions contributing toward Isomorphism

The second question that arises when comparing these projects concerns the difference between the Ln-BPDC and Ln-NDC structures. The Ln-BPDC series is isomorphous, meaning that the structures crystallize in the same space group and the only difference between the structures is the replacement of lanthanide ions.[10] In the case of the Ln-NDC materials, each structure crystallizes in a different space group, and the lanthanide ions are surrounded by different coordination numbers and binding modes of the organic linker and solvent.

One apparent difference in these structures is the extraframework ion/molecule. In the case of Ln-BPDC, the anionic framework is charge-balanced by a dimethylammonium cation [$NH_2(CH_3)_2^+$]. In the Ln-NDC series, the neutral frameworks contain coordinated and floating dimethylformamide molecules [DMF, $OCHN(CH_3)_2$]. Both of these sets of materials were synthesized solvothermally in DMF. An explanation for this difference is the reaction temperature. The Ln-BPDC materials were synthesized at temperatures between 140 and 150 °C, while the Ln-NDC materials were synthesized at temperatures between 110 and 125 °C. The boiling point of DMF is approximately 153 °C.[11] DMF is known to decompose to dimethylammonium and formic acid through a hydrolysis reaction.[12,13] The higher temperatures of the Ln-BPDC syntheses likely promotes the decomposition of DMF to the dimethylammonium cation, which charge-balances the anionic frameworks. At the lower synthesis temperatures of Ln-NDC, DMF is not decomposed, and thus acts as a coordinating or floating solvent molecule in the structures. At lower synthesis

temperatures for the Ln-BPDC series, no crystalline product formed. At higher synthesis temperatures for the Ln-NDC series, a different crystal phase which could not be isolated was formed.

Another argument that can be made to explain the differences in structures is due to the rigidity of the organic linker. BPDC has a freedom of rotation between the two aromatic phenyl rings. This allows for twisting of the BPDC ligand to coordinate to two different metal centers on one carboxylate end, and bidentate coordination to another lanthanide metal on the other carboxylate end (Figure 4.2.1, 1). This freedom of rotation between phenyl rings is evidenced in the single crystal data of the Ln-BPDC series. Slight variations in the torsion angles between the rings ranging from 29 to 32 degrees are observed. The fused rings of NDC, by contrast, are rigid and multiple coordination modes are observed (Figure 4.2.1, 2A-B). The rigidity of the NDC ligand is likely responsible for the different structures that form. When a lanthanide ion is first coordinated to a carboxyl group from the ligand, the lack of rotation of NDC hinders the possibilities of other lanthanides coordinating on the other end. Thus, DMF solvent molecules can compete with NDC to fill the lanthanide coordination sphere. DMF has been shown to have a greater coordinating ability toward lanthanides than toward transition metals.[14] This possibly explains the various coordination numbers and binding modes of the lanthanides observed in the Ln-NDC series.

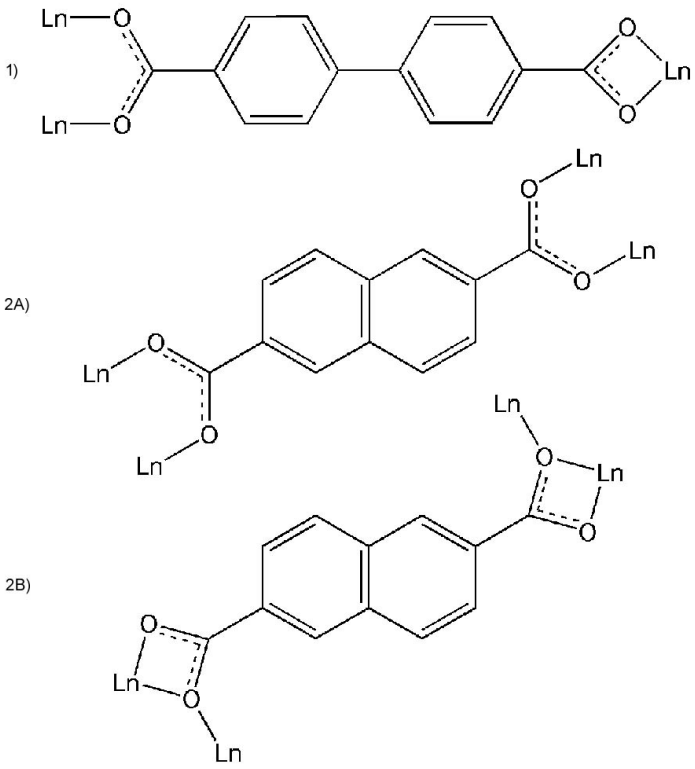

Figure 4.2.1. Comparison of the coordination modes and rigidity of 1) BPDC and 2A-B) NDC ligands.

The NDC ligands are observed to undergo π-π stacking. This is most evident in the Nd-NDC and Eu-NDC structures (Figure 4.1.1, 2B-C). These intermolecular forces likely play a role in establishing the long-range order among these structures and stabilizing various lanthanide coordination spheres. So as NDC ligands and DMF molecules compete for coordination with the lanthanides, the π stacking of the NDC ligands stabilizes these structures and allow for different structures to form in the Ln-NDC series.

4.3. Conclusions

In this section, the three projects of this thesis were compared, and various factors identified to explain the differences in dimensionality and structure among the projects. The main factor identified in controlling the dimensionality of Ln-MOFs versus LREHs is pH. Lanthanides are hard acids with large coordination numbers. When hydroxide ions and water molecules are readily available in solution (at an intermediate pH), they will fill the lanthanide coordination sphere and form layered, two-dimensional materials. Factors of reaction temperature, ligand rigidity, and ligand π stacking are possibly responsible for the disparity between the Ln-BPDC and Ln-NDC series. The decomposition of DMF into dimethylammonium is dependent on the reaction temperature. At lower temperatures, DMF is more likely to act as a coordinating solvent. The increased rigidity of the NDC ligand in comparison with BPDC perhaps explains the different lanthanide coordination numbers and binding modes in the Ln-NDC series. Effects of the π stacking of the ligands likely contribute toward stabilizing the structures.

4.4. References

(1) Cotton, S. *Lanthanides and Actinides*; Macmillan Physical Science Series; Macmillan Education LTD: London, 1991.

(2) Soni, P. L.; Soni, V. *Coordination Chemistry: Metal Complexes Transition Metal Chemistry with Lanthanides and Actinides*; CRC Press: Boca Raton, FL, 2013.

(3) Liang, J.; Ma, R.; Sasaki, T. Layered Rare Earth Hydroxides: Structural Aspects and Photoluminescence Properties. In *Photofunctional Layered Materials*; Yan, D., Wei, M., Eds.; Structure and Bonding; Springer International Publishing: Cham, 2015; pp 69–103. https://doi.org/10.1007/978-3-319-16991-0_2.

(4) Ma, R.; Liu, Z.; Li, L.; Iyi, N.; Sasaki, T. Exfoliating Layered Double Hydroxides in Formamide: A Method to Obtain Positively Charged Nanosheets. *J. Mater. Chem.* **2006**, *16* (39), 3809–3813. https://doi.org/10.1039/B605422F.

(5) Ma, R.; Sasaki, T. Nanosheets of Oxides and Hydroxides: Ultimate 2D Charge-Bearing Functional Crystallites. *Adv. Mater.* **2010**, *22* (45), 5082–5104. https://doi.org/10.1002/adma.201001722.

(6) Liu, Z.; Ma, R.; Osada, M.; Takada, K.; Sasaki, T. Selective and Controlled Synthesis of α- and β-Cobalt Hydroxides in Highly Developed Hexagonal Platelets. *J. Am. Chem. Soc.* **2005**, *127* (40), 13869–13874. https://doi.org/10.1021/ja0523338.

(7) Ma, R.; Liu, Z.; Takada, K.; Iyi, N.; Bando, Y.; Sasaki, T. Synthesis and Exfoliation of Co2+−Fe3+ Layered Double Hydroxides: An Innovative Topochemical Approach. *J. Am. Chem. Soc.* **2007**, *129* (16), 5257–5263. https://doi.org/10.1021/ja0693035.

(8) Liang, J.; Ma, R.; Sasaki, T. Layered Rare Earth Hydroxides (LREHs): Synthesis and Structure Characterization towards Multifunctionality. *Dalton Trans.* **2014**, *43* (27), 10355–10364. https://doi.org/10.1039/C4DT00425F.

(9) West, A. R. *Solid State Chemistry and Its Applications*, Second Edition.; Wiley, 2014.

(10) Isomorphous crystals - Online Dictionary of Crystallography http://reference.iucr.org/dictionary/Isomorphous_crystals (accessed Feb 19, 2019).

(11) Haynes, W. M., Ed. *CRC Handbook of Chemistry & Physics*, 92nd ed.; CRC Press, 2011.

(12) Murphy, C. A.; Cameron, T. S.; Cooke, M. W.; Aquino, M. A. S. Synthesis and Structure of Trans-Dimethylammonium Bis(Oxalato)Diaquaruthenate(III) Tetrahydrate. *Inorganica Chim. Acta* **2000**, *305* (2), 225–229. https://doi.org/10.1016/S0020-1693(00)00137-7.

(13) Kahrovic, E.; Orioli, P.; Bruni, B.; Di Vaira, M.; Messori, L. Crystallographic Evidence for Decomposition of Dimethylformamide in the Presence of Ruthenium(III) Chloride. *Inorganica Chim. Acta* **2003**, *355*, 420–423. https://doi.org/10.1016/S0020-1693(03)00312-8.

(14) Díaz-Torres, R.; Alvarez, S. Coordinating Ability of Anions and Solvents towards Transition Metals and Lanthanides. *Dalton Trans.* **2011**, *40* (40), 10742–10750. https://doi.org/10.1039/C1DT11000D.

Chapter 5

Summary and Future Work

5.1. Summary

Three projects have been presented in this thesis: 1) an anionic, isomorphous series of six lanthanide MOFs based on the linker 4,4'-biphenyldicarboxylate, 2) a neutral series of four lanthanide MOFs based on the linker 2,6-naphthalenedicarboxylate which crystallize in distinct space groups, and 3) a series of three cationic, Nd-based LREHs with increasing chain length α,ω-alkanedisulfonates with a potential application in anion exchange. All structures were characterized via XRD, TGA, and IR. The solid state luminescence and quantum efficiency of the Eu(III)-based materials were additionally characterized.

5.2. Future Work

There is future work that can be proposed for each of the three projects presented in this thesis. Generally, it would be possible for all three projects to be expanded to include the remaining lanthanide ion series. The lanthanides La, Ce, Nd, Eu, Gd, and Er were chosen because they were readily available in the Oliver lab chemical inventory.

5.2.1. Ln-BPDC and Ln-NDC Projects

The projects containing Ln-BPDC and Ln-NDC currently do not have applications. The Ln-BPDC framework is anionic in charge, which would make it a possible candidate for cation exchange. Based on the previously reported Tb-BPDC material, the Ln-BPDC series would be a candidate for UO_2^{2+} ion exchange in exchange for $NH_2(CH_3)_2^+$.[1] With post-synthetic modification, the neutral Ln-NDC series could potentially be transformed into an ionic framework.[2,3] Otherwise, there would be the possibility of exchanging floating DMF molecules in the Ln-NDC series with other neutral, small molecules.

In this work, four crystal structures of Ln-BPDC (Ln = La, Ce, Eu, Gd) and four crystal structures of Ln-NDC (Ln = La, Nd, Eu, Gd) were presented. Crystals of Nd-BPDC, Er-BPDC, Ce-NDC, and Er-NDC large enough for SCXRD were unable to be successfully grown. Conditions for growing these crystal structures can be improved so that the series may be completed. Longer synthesis times and temperature cycling in the respective optimal temperature ranges would be suggested.

Due to their luminescent properties, the materials Eu-BPDC (SLUG-46) and Eu-NDC (SLUG-51) have potential applications as sensors. It would be of interest to attempt to synthesize a more cost-effective sensor. Europium is a particularly costly element, typically $400 per 25 grams. By contrast, cerium is the most earth-abundant lanthanoid, and the 26th most abundant element (roughly $18 per 25 grams).[4] Given the disparity of these abundances and prices, it would be of financial interest to

synthesize a heterobimetallic Ln-MOF. This would be especially plausible for the isomorphous Ln-BPDC series, but more challenging for the Ln-NDC series, since the latter does not crystallize in the same space group for each structure. Additionally, it would be worthwhile to explore preparing films of Eu-BPDC and Eu-NDC, respectively. To be employed as a sensor, it would be useful to have a MOF anchored to a solid support that could be immersed in solution and easily retrieved.[5] MOF thin films have been grown by multiple methods.[6] Perhaps the most straightforward and promising technique would be via *in-situ* crystallization from a mother solution. A substrate is added to a MOF reagent mixture, and the mixture is heated as a whole as usually required. The substrate(s) should be inserted face down or vertically into the solution to avoid sedimentation. This technique has been successfully used to grow a variety of MOF films. The chosen substrate must be compatible with the growing MOF, thus there are reports of metal oxides, metal slices, textiles, and glass slides used as substrates.

5.2.2. Nd-ADS Project

The crystal structure of SLUG-28 (Nd-EDS) was solved via SCXRD. We were able to make claims about SLUG-29 (Nd-PDS) and SLUG-30 (Nd-BDS) based on the change in d-spacing in comparing the three PXRD patterns. It would be useful to grow crystals of Nd-PDS and Nd-BDS in order to complete this series and be able to further compare the details of the structures. Crystals of SLUG-28 were obtained from a synthesis which used 4,4'-bipyridine as a pH modifier (chapter 2.3). Similar syntheses with SLUG-29 and -30 reagents did not produce crystals of the intended

materials. Therefore, other homogenous alkalization strategies should be explored for their potential to yield single crystals.

Attempts to synthesize LREHs with lanthanides other than Nd were attempted, but no structures were formed. Therefore, reaction conditions can be optimized to synthesize Ln-EDS, -PDS, and -BDS structures. The hydroxide source used for the synthesis of Nd-EDS was NaOH. Other, perhaps less harsh bases can be explored in these syntheses.

The three structures SLUG-28 through 30 were shown to exchange their α,ω-alkanedisulfonates for adipic acid. This exchange was characterized qualitatively through XRD and IR, but it would be of interest to characterize this exchange quantitatively to report an uptake value in mg g^{-1}. A possible technique to do this would be with GC-MS.

5.3 References

(1) Ye, J.; Bogale, R. F.; Shi, Y.; Chen, Y.; Liu, X.; Zhang, S.; Yang, Y.; Zhao, J.; Ning, G. A Water-Stable Dual-Channel Luminescence Sensor for UO22+ Ions Based on an Anionic Terbium(III) Metal–Organic Framework. *Chem. – Eur. J.* **2017**, *23* (32), 7657–7662. https://doi.org/10.1002/chem.201700713.

(2) Karmakar, A.; Desai, A. V.; Ghosh, S. K. Ionic Metal-Organic Frameworks (IMOFs): Design Principles and Applications. *Coord. Chem. Rev.* **2016**, *307*, 313–341. https://doi.org/10.1016/j.ccr.2015.08.007.

(3) Postsynthetic Covalent Modification of a Neutral Metal−Organic Framework. *J. Am. Chem. Soc.* **2007**, *129* (41), 12368–12369. https://doi.org/10.1021/ja074366o.

(4) Voncken, J. H. L. Applications of the Rare Earths. In *The Rare Earth Elements: An Introduction*; Voncken, J. H. L., Ed.; SpringerBriefs in Earth Sciences; Springer International Publishing: Cham, 2016; pp 89–106. https://doi.org/10.1007/978-3-319-26809-5_5.

(5) Kreno, L. E.; Leong, K.; Farha, O. K.; Allendorf, M.; Van Duyne, R. P.; Hupp, J. T. Metal–Organic Framework Materials as Chemical Sensors. *Chem. Rev.* **2012**, *112* (2), 1105–1125. https://doi.org/10.1021/cr200324t.

(6) Bétard, A.; Fischer, R. A. Metal–Organic Framework Thin Films: From Fundamentals to Applications. *Chem. Rev.* **2012**, *112* (2), 1055–1083. https://doi.org/10.1021/cr200167v.

Appendix

Tables of Synthesis Conditions and Exchanges

List of abbreviations:

Adipic acid = hexanedioic acid
ADS = α,ω-alkanedisulfonate
BDS = butane-1,4-disulfonate, disodium salt
BPDC = biphenyl-4,4'-dicarboxylic acid
BTC = 1,3,5-benzenetricarboxylic acid
CPB = 4-(4-carboxy)phenyl benzoic acid (BPDC)
CTAB = cetyl trimethylammonium bromide
EDS = ethane-1,2-disulfonate, disodium salt
EDSA = 1,2-ethanedisulfonic acid dihydrate
Glutaric acid = pentanedioic acid
Malonic acid = propanedioic acid
NDC = 2,6-naphthalenedicarboxylic acid
PDS = propane-1,3-disulfonate, disodium salt
PFOA = perfluorooctanoic acid
RT = room temperature
Sebacic acid = decanedioic acid
Suberic acid = octanedioic acid
Succinic acid = butanedioic acid
Terephthalic acid = benzene-1,4-dicarboxylic acid

Table A1. SLUG-43 through 48 (Ln-BPDC) Syntheses

Sample ID	Reagents	Weight/Volume Used	Temperature (°C)	Time (days)
AK2_05a	$Nd(NO_3)_3 \cdot 6\ H_2O$ CPB H_2O	0.2021 g 0.1115 g 10 mL	150	3
AK2_05c	$Er(NO_3)_3 \cdot x\ H_2O$ CPB H_2O	0.2041 g 0.1099 g 10 mL	150	3
AK2_05e	$La(NO_3)_3 \cdot 6\ H_2O$ CPB H_2O	0.2004 g 0.1129 g 10 mL	150	3
AK2_28d	$La(NO_3)_3 \cdot 6\ H_2O$ CPB DMF	0.2021 g 0.2247 g 10 mL	140	3
AK2_28e	$Nd(NO_3)_3 \cdot 6\ H_2O$ CPB DMF	0.2003 g 0.2262 g 10 mL	140	3
AK2_28f	$Gd(NO_3)_3 \cdot 6\ H_2O$ CPB DMF	0.2029 g 0.2260 g 10 mL	140	3
AK2_28g	$Er(NO_3)_3 \cdot x\ H_2O$ CPB DMF	0.2015 0.2247 g 10 mL	140	3
AK2_35a	$Ce(NO_3)_3 \cdot 6\ H_2O$ CPB DMF	0.1998 g 0.2264 g 10 mL	140	4
AK2_35b	$Nd(NO_3)_3 \cdot 6\ H_2O$ CPB DMF	0.2007 g 0.2266 g 10 mL	140	4
AK2_35c	$Gd(NO_3)_3 \cdot 6\ H_2O$ CPB DMF	0.2034 g 0.2262 g 10 mL	140	4
AK2_35d	$Er(NO_3)_3 \cdot x\ H_2O$ CPB DMF	0.2008 g 0.2255 g 10 mL	140	4
AK2_37a	$Eu(NO_3)_3 \cdot 6\ H_2O$ CPB DMF	0.2018 g 0.2262 g 10 mL	142	3
AK2_37b	$Gd(NO_3)_3 \cdot 6\ H_2O$ CPB DMF	0.2030 g 0.2262 g 10 mL	142	3

AK2_37c	$Er(NO_3)_3 \cdot 5\ H_2O$ CPB DMF	0.2013 g 0.2269 g 10 mL	142	3
AK2_37d	$Nd(NO_3)_3 \cdot 6\ H_2O$ CPB DMF	0.2006 g 0.2250 g 10 mL	142	3
AK2_38a	$Eu(NO_3)_3 \cdot 6\ H_2O$ CPB DMF	0.2010 g 0.2266 g 10 mL	142	6
AK2_38b	$Gd(NO_3)_3 \cdot 6\ H_2O$ CPB DMF	0.2009 g 0.2264 g 10 mL	142	6
AK2_38c	$Er(NO_3)_3 \cdot 5\ H_2O$ CPB DMF	0.2019 g 0.2264 g 10 mL	142	6
AK2_38d	$Nd(NO_3)_3 \cdot 6\ H_2O$ CPB DMF	0.2015 g 0.2269 g 10 mL	142	6
AK2_42a	$Nd(NO_3)_3 \cdot 6\ H_2O$ CPB DMF	0.2006 g 0.2247 g 10 mL	140 – 150	6
AK2_42b	$Er(NO_3)_3 \cdot 5\ H_2O$ CPB DMF	0.2006 g 0.2254 g 10 mL	140 – 150	6
AK2_45a	$Eu(NO_3)_3 \cdot 6\ H_2O$ CPB DMF	0.2005 g 0.2281 g 10 mL	145	7
AK2_45b	$Eu(NO_3)_3 \cdot 6\ H_2O$ CPB DMF	0.2009 g 0.2265 g 10 mL	145	7
AK2_52a	$La(NO_3)_3 \cdot 6\ H_2O$ CPB DMF	0.2001 g 0.2265 g 10 mL	146	19
AK2_52b	$Ce(NO_3)_3 \cdot 6\ H_2O$ CPB DMF	0.2008 g 0.2265 g 10 mL	146	19
AK2_52c	$Nd(NO_3)_3 \cdot 6\ H_2O$ CPB DMF	0.2007 g 0.2266 g 10 mL	146	19
AK2_52d	$Eu(NO_3)_3 \cdot 6\ H_2O$ CPB DMF	0.2008 g 0.2265 g 10 mL	146	19

AK2_52e	$Gd(NO_3)_3 \cdot 6\ H_2O$ CPB DMF	0.2001 g 0.2265 g 10 mL	146	19
AK2_52f	$Er(NO_3)_3 \cdot 5\ H_2O$ CPB DMF	0.2002 g 0.2267 g 10 mL	146	19
AK2_54a	$La(NO_3)_3 \cdot 6\ H_2O$ CPB DMF	0.2006 g 0.2263 g 10 mL	200	
AK2_54b	$Ce(NO_3)_3 \cdot 6\ H_2O$ CPB DMF	0.2008 g 0.2263 g 10 mL	200	
LW1_10a	$La(NO_3)_3 \cdot 6\ H_2O$ CPB DMF	0.2001 g 0.1128 g 10 mL	175	3
LW1_10c	$Nd(NO_3)_3 \cdot 6\ H_2O$ CPB DMF	0.2000 g 0.115 g 10 mL	175	3
LW1_10e	$Er(NO_3)_3 \cdot 5\ H_2O$ CPB DMF	0.2006 g 0.1103 g 10 mL	175	3
LW1_22a	$La(NO_3)_3 \cdot 6\ H_2O$ CPB DMF	0.2025 g 0.0567 g 10 mL	150	3
LW1_22b	$Nd(NO_3)_3 \cdot 6\ H_2O$ CPB DMF	0.2019 g 0.0541 g 10 mL	150	3
LW1_22c	$Er(NO_3)_3 \cdot 5\ H_2O$ CPB DMF	0.2036 g 0.0553 g 10 mL	150	3
LW1_25a	$La(NO_3)_3 \cdot 6\ H_2O$ CPB DMF	0.2022 g 0.1145 g 10 mL	125	3
LW1_25c	$Nd(NO_3)_3 \cdot 6\ H_2O$ CPB DMF	0.2037 g 0.1131 g 10 mL	125	3
LW1_25e	$Er(NO_3)_3 \cdot 5\ H_2O$ CPB DMF	0.2016 g 0.1111 g 10 mL	125	3
LW1_30c	$Gd(NO_3)_3 \cdot 6\ H_2O$ CPB DMF	0.204 g 0.106 g 10 mL	55	3

LW1_31b	$Gd(NO_3)_3 \cdot 6\ H_2O$ CPB DMF	0.2019 g 0.1069 g 10 mL	150	3
LW1_32a	$Gd(NO_3)_3 \cdot 6\ H_2O$ CPB DMF	0.203 g 0.104 g 10 mL	125	3
LW1_32b	$Gd(NO_3)_3 \cdot 6\ H_2O$ CPB DMF	0.202 g 0.105 g 10 mL	100	3
LW1_32d	$Er(NO_3)_3 \cdot 5\ H_2O$ CPB DMF	0.214 g 0.103 g 10 mL	100	3
LW1_43a	$La(NO_3)_3 \cdot 6\ H_2O$ CPB DMF	0.2008 g 0.1181 g 10 mL	125	3
LW1_43b	$Nd(NO_3)_3 \cdot 6\ H_2O$ CPB DMF	0.2016 g 0.1124 g 10 mL	125	3
LW1_43c	$Er(NO_3)_3 \cdot 5\ H_2O$ CPB DMF	0.2035 g 0.1112 g 10 mL	125	3
LW1_47a	$La(NO_3)_3 \cdot 6\ H_2O$ CPB DMF	0.2020 g 0.1139 g 10 mL	150	3
LW1_47b	$La(NO_3)_3 \cdot 6\ H_2O$ CPB DMF	0.2008 g 0.2210 g 10 mL	150	3
LW1_47c	$Nd(NO_3)_3 \cdot 6\ H_2O$ CPB DMF	0.2042 g 0.1113 g 10 mL	150	3
LW1_47d	$Nd(NO_3)_3 \cdot 6\ H_2O$ CPB DMF	0.2002 g 0.2270 g 10 mL	150	3
LW1_47e	$Gd(NO_3)_3 \cdot 6\ H_2O$ CPB DMF	0.2018 g 0.1135 g 10 mL	150	3
LW1_58e	$La(NO_3)_3 \cdot 6\ H_2O$ CPB DMF	0.2002 g 0.1158 g 10 mL	125	3
LW1_58f	$La(NO_3)_3 \cdot 6\ H_2O$ CPB DMF	0.2006 g 0.2282 g 10 mL	125	3

LW1_58g	$Nd(NO_3)_3 \cdot 6\ H_2O$ CPB DMF	0.2009 g 0.1155 g 10 mL	125	3
LW1_58h	$Nd(NO_3)_3 \cdot 6\ H_2O$ CPB DMF	0.2002 g 0.2279 g 10 mL	125	3
LW1_63d	$La(NO_3)_3 \cdot 6\ H_2O$ CPB DMF	0.2033 g 0.2254 g 10 mL	150	3
LW1_63e	$Nd(NO_3)_3 \cdot 6\ H_2O$ CPB DMF	0.2039 g 0.2262 g 10 mL	150	3
LW1_63f	$Gd(NO_3)_3 \cdot 6\ H_2O$ CPB DMF	0.2026 g 0.2276 g 10 mL	150	3
LW1_63g	$Er(NO_3)_3 \cdot 5\ H_2O$ CPB DMF	0.2005 g 0.2267 g 10 mL	150	3
LW1_67d	$La(NO_3)_3 \cdot 6\ H_2O$ CPB DMF	0.2041 g 0.2225 g 10 mL	145	3
LW1_67e	$Ce(NO_3)_3 \cdot 6\ H_2O$ CPB DMF	0.2015 g 0.2289 g 10 mL	145	3
LW1_67f	$Nd(NO_3)_3 \cdot 6\ H_2O$ CPB DMF	0.2014 g 0.2259 g 10 mL	145	3
LW1_67g	$Gd(NO_3)_3 \cdot 6\ H_2O$ CPB DMF	0.2007 g 0.2268 g 10 mL	145	3
LW1_67h	$Er(NO_3)_3 \cdot 5\ H_2O$ CPB DMF	0.2041 g 0.2271 g 10 mL	145	3
LW1_71a	$La(NO_3)_3 \cdot 6\ H_2O$ CPB DMF	0.2004 g 0.2239 g 10 mL	150	3
LW1_71c	$Ce(NO_3)_3 \cdot 6\ H_2O$ CPB DMF	0.2006 g 0.2268 g 10 mL	150	3
LW1_71e	$Gd(NO_3)_3 \cdot 6\ H_2O$ CPB DMF	0.2010 g 0.2275 g 10 mL	150	3

LW1_71g	$Er(NO_3)_3 \cdot 5\ H_2O$ CPB DMF	0.2005 g 0.2265 g 10 mL	150	3
LW1_75d	$La(NO_3)_3 \cdot 6\ H_2O$ CPB DMF	0.2014 g 0.2229 g 10 mL	115	3
LW1_75e	$Ce(NO_3)_3 \cdot 6\ H_2O$ CPB DMF	0.2007 g 0.2231 g 10 mL	115	3
LW1_75f	$Gd(NO_3)_3 \cdot 6\ H_2O$ CPB DMF	0.2011 g 0.2247 g 10 mL	115	3
LW1_75g	$Er(NO_3)_3 \cdot 5\ H_2O$ CPB DMF	0.2004 g 0.2241 g 10 mL	115	3
LW1_76d	$Er(NO_3)_3 \cdot 5\ H_2O$ CPB DMF	0.2003 g 0.2286 g 10 mL	155	3
LW1_76f	$Gd(NO_3)_3 \cdot 6\ H_2O$ CPB DMF	0.2021 g 0.2252 g 10 mL	145	3
LW1_78d	$Er(NO_3)_3 \cdot 5\ H_2O$ CPB DMF	0.2016 g 0.2283 g 10 mL	160	3
LW1_87a	$Eu(NO_3)_3 \cdot 6\ H_2O$ CPB DMF	0.2049 g 0.2249 g 10 mL	144	6
LW1_87b	$Eu(NO_3)_3 \cdot 6\ H_2O$ CPB DMF	0.2006 g 0.2221 g 10 mL	144	6
LW1_92c	$Nd(NO_3)_3 \cdot 6\ H_2O$ CPB DMF	0.2006 g 0.2330 g 10 mL	135 – 155	5
JM1_05a	$Eu(NO_3)_3 \cdot 6\ H_2O$ CPB DMF	0.2008 g 0.2259 g 10 mL	135 – 155	6
JM1_05b	$Gd(NO_3)_3 \cdot 6\ H_2O$ CPB DMF	0.1995 g 0.2258 g 10 mL	135 – 155	6
JM1_09a	$Nd(NO_3)_3 \cdot 6\ H_2O$ CPB DMF	0.1996 g 0.2249 g 10 mL	125 – 135	6

JM1_09b	$Er(NO_3)_3 \cdot 6\ H_2O$ CPB DMF	0.1995 g 0.2255 g 10 mL	125 – 135	6
JM1_11a	$Nd(NO_3)_3 \cdot 6\ H_2O$ CPB DMF	0.1997 g 0.2249 g 10 mL	115 – 125	7
JM1_11b	$Er(NO_3)_3 \cdot 6\ H_2O$ CPB DMF	0.1999 g 0.2254 g 10 mL	115 – 125	7
JM1_23c	$Er(NO_3)_3 \cdot 6\ H_2O$ CPB DMF	0.1996 g 0.2255 g 10 mL	145	5
JM1_25a	$Er(NO_3)_3 \cdot 6\ H_2O$ CPB DMF	0.2000 g 0.2250 g 10 mL	175	5
JM1_30b	$Er(NO_3)_3 \cdot 6\ H_2O$ CPB DMF	0.2005 g 0.2250 g 10 mL	145 – 155	5
JM1_31	$Nd(NO_3)_3 \cdot 6\ H_2O$ CPB DMF	0.2003 g 0.2256 g 10 mL	145 – 155	4
JM1_77a	$La(NO_3)_3 \cdot 6\ H_2O$ CPB DMF	0.2009 g 0.2243 g 10 mL	130	5
JM1_77b	$La(NO_3)_3 \cdot 6\ H_2O$ CPB DMF	0.1996 g 0.2246 g 10 mL	130	5
SW1_07a	$Eu(NO_3)_3 \cdot 6\ H_2O$ CPB DMF	0.2015 g 0.2268 g 10 mL	132	6
SW1_12d	$Nd(NO_3)_3 \cdot 6\ H_2O$ CPB DMF	0.2016 g 0.2262 g 10 mL	135 – 155	6
SW1_12e	$Er(NO_3)_3 \cdot 5\ H_2O$ CPB DMF	0.2014 g 0.2267 g 10 mL	135 – 155	6
SW1_14a	$Nd(NO_3)_3 \cdot 6\ H_2O$ CPB DMF	0.2017 g 0.2268 g 10 mL	140 – 150	6
SW1_14b	$Er(NO_3)_3 \cdot 5\ H_2O$ CPB DMF	0.2015 g 0.2267 g 10 mL	140 – 150	6

SW1_32a	$Ce(NO_3)_3 \cdot 6\ H_2O$ CPB DMF	0.2015 g 0.2269 g 10 mL	150	3
SW1_32b	$Er(NO_3)_3 \cdot 5\ H_2O$ CPB DMF	0.2017 g 0.2269 g 10 mL	150	3

Table A2. SLUG-49 through 52 (Ln-NDC) Syntheses

Sample ID	Reagents	Weight/Volume Used	Temperature (°C)	Time (days)
AK2_05b	$Nd(NO_3)_3 \cdot 6\ H_2O$ NDC H_2O	0.2033 g 0.0986 g 10 mL	150	3
AK2_05d	$Er(NO_3)_3 \cdot x\ H_2O$ NDC H_2O	0.2027 g 0.0981 g 10 mL	150	3
AK2_05f	$La(NO_3)_3 \cdot 6\ H_2O$ NDC H_2O	0.2008 g 0.0999 g 10 mL	150	3
AK2_19a	$La(NO_3)_3 \cdot 6\ H_2O$ NDC CTAB DMF	0.2014 g 0.1008 g 0.0478 g 10 mL	125	3
AK2_19b	$La(NO_3)_3 \cdot 6\ H_2O$ NDC PFOA DMF	0.2001 g 0.1002 g 0.0501 g 10 mL	125	3
AK2_22a	$La(NO_3)_3 \cdot 6\ H_2O$ NDC PFOA H_2O	0.202 g 0.108 g 0.195 g 10 mL	150	3
AK2_22b	$La(NO_3)_3 \cdot 6\ H_2O$ NDC PFOA H_2O	0.202 g 0.104 g 0.383 g 10 mL	150	3
AK2_22c	$La(NO_3)_3 \cdot 6\ H_2O$ NDC PFOA DMF	0.207 g 0.101 g 0.190 g 10 mL	150	3
AK2_22d	$La(NO_3)_3 \cdot 6\ H_2O$ NDC PFOA DMF	0.207 g 0.107 g 0.382 g 10 mL	150	3
AK2_28a	$Nd(NO_3)_3 \cdot 6\ H_2O$ NDC DMF	0.2021 g 0.2044 g 10 mL	140	3
AK2_28b	$Gd(NO_3)_3 \cdot 6\ H_2O$ NDC DMF	0.2032 g 0.2044 g 10 mL	140	3

AK2_28c	$Er(NO_3)_3 \cdot 5\ H_2O$ NDC DMF	0.2022 g 0.2056 g 10 mL	140	3
LW1_10b	$La(NO_3)_3 \cdot 6\ H_2O$ NDC DMF	0.2009 g 0.0990 g 10 mL	175	3
LW1_10d	$Nd(NO_3)_3 \cdot 6\ H_2O$ NDC DMF	0.2004 g 0.1000 g 10 mL	175	3
LW1_10f	$Er(NO_3)_3 \cdot 5\ H_2O$ NDC DMF	0.2014 g 0.0985 g 10 mL	175	3
LW1_20b	$Er(NO_3)_3 \cdot 5\ H_2O$ NDC DMF	0.2052 g 0.0987 g 10 mL	150	3
LW1_20c	$Er(NO_3)_3 \cdot 5\ H_2O$ NDC DMF	0.2054 g 0.0489 g 10 mL	150	3
LW1_24b	$La(NO_3)_3 \cdot 6\ H_2O$ NDC DMF	0.2046 g 0.0504 g 10 mL	140 – 160	3
LW1_24c	$Nd(NO_3)_3 \cdot 6\ H_2O$ NDC DMF	0.2084 g 0.0509 g 10 mL	140 – 160	3
LW1_25b	$La(NO_3)_3 \cdot 6\ H_2O$ NDC DMF	0.2078 g 0.1145 g 10 mL	125	3
LW1_25d	$Nd(NO_3)_3 \cdot 6\ H_2O$ NDC DMF	0.2013 g 0.1027 g 10 mL	125	3
LW1_26b	$Er(NO_3)_3 \cdot 5\ H_2O$ NDC DMF	0.2058 g 0.1076 g 10 mL	125	3
LW1_30d	$Gd(NO_3)_3 \cdot 6\ H_2O$ NDC DMF	0.209 g 0.112 g 10 mL	150	3
LW1_32c	$La(NO_3)_3 \cdot 6\ H_2O$ NDC DMF	0.208 g 0.114 g 10 mL	125	3
LW1_35a	$La(NO_3)_3 \cdot 6\ H_2O$ NDC DMF	0.2041 g 0.0511 g 10 mL	125	5

LW1_35b	$La(NO_3)_3 \cdot 6\ H_2O$ NDC DMF	0.2041 g 0.0759 g 10 mL	125	5
LW1_40a	$La(NO_3)_3 \cdot 6\ H_2O$ NDC Triethylamine HNO_3 DMF H_2O	0.6655 g 0.2774 g 60 µL 30 µL 8 mL 1.6 mL	110	< 1
LW1_42a	$La(NO_3)_3 \cdot 6\ H_2O$ NDC DMF	0.2013 g 0.1102 g 10 mL	125	3
LW1_42b	$La(NO_3)_3 \cdot 6\ H_2O$ NDC DMF	0.2004 g 0.1102 g 10 mL	125	3
LW1_42c	$La(NO_3)_3 \cdot 6\ H_2O$ NDC DMF	0.2018 g 0.1113 g 10 mL	125	3
LW1_42d	$La(NO_3)_3 \cdot 6\ H_2O$ NDC Triethylamine HNO_3 DMF	0.2012 g 0.1104 g 64 µL 32 µL 10 mL	125	3
LW1_42e	$La(NO_3)_3 \cdot 6\ H_2O$ NDC DMF	0.2010 g 0.2256 g 10 mL	125	3
LW1_47f	$Nd(NO_3)_3 \cdot 6\ H_2O$ NDC DMF	0.2074 g 0.1018 g 10 mL	150	3
LW1_47g	$Nd(NO_3)_3 \cdot 6\ H_2O$ NDC DMF	0.2044 g 0.2050 g 10 mL	150	3
LW1_47h	$Er(NO_3)_3 \cdot 5\ H_2O$ NDC DMF	0.2007 g 0.1039 g 10 mL	150	3
LW1_51a	$La(NO_3)_3 \cdot 6\ H_2O$ NDC DMF	0.2011 g 0.2030 g 10 mL	125	3
LW1_51b	$Nd(NO_3)_3 \cdot 6\ H_2O$ NDC DMF	0.2000 g 0.2029 g 10 mL	125	3

LW1_51c	$Er(NO_3)_3 \cdot 5\ H_2O$ NDC DMF	0.1999 g 0.2028 g 10 mL	125	3
LW1_58a	$La(NO_3)_3 \cdot 6\ H_2O$ NDC DMF	0.2011 g 0.2036 g 10 mL	125	3
LW1_58b	$Nd(NO_3)_3 \cdot 6\ H_2O$ NDC DMF	0.2000 g 0.2049 g 10 mL	125	3
LW1_58c	$Er(NO_3)_3 \cdot 5\ H_2O$ NDC DMF	0.2004 g 0.2059 g 10 mL	125	3
LW1_58d	$Gd(NO_3)_3 \cdot 6\ H_2O$ NDC DMF	0.2025 g 0.2049 g 10 mL	125	3
LW1_63a	$Nd(NO_3)_3 \cdot 6\ H_2O$ NDC DMF	0.2039 g 0.2119 g 10 mL	150	3
LW1_63b	$Gd(NO_3)_3 \cdot 6\ H_2O$ NDC DMF	0.2035 g 0.2115 g 10 mL	150	3
LW1_63c	$Er(NO_3)_3 \cdot 5\ H_2O$ NDC DMF	0.2044 g 0.2120 g 10 mL	150	3
LW1_67a	$Nd(NO_3)_3 \cdot 6\ H_2O$ NDC DMF	0.2026 g 0.2125 g 10 mL	145	3
LW1_67b	$Gd(NO_3)_3 \cdot 6\ H_2O$ NDC DMF	0.2005 g 0.2169 g 10 mL	145	3
LW1_67c	$Er(NO_3)_3 \cdot 5\ H_2O$ NDC DMF	0.2009 g 0.2142 g 10 mL	145	3
LW1_71b	$Ce(NO_3)_3 \cdot 6\ H_2O$ NDC DMF	0.2006 g 0.2182 g 10 mL	150	3
LW1_71d	$Gd(NO_3)_3 \cdot 6\ H_2O$ NDC DMF	0.2013 g 0.2173 g 10 mL	150	3
LW1_71f	$Er(NO_3)_3 \cdot 5\ H_2O$ NDC DMF	0.2013 g 0.2192 g 10 mL	150	3

LW1_75a	$Ce(NO_3)_3 \cdot 6\ H_2O$ NDC DMF	0.2008 g 0.2221 g 10 mL	115	3
LW1_75b	$Gd(NO_3)_3 \cdot 6\ H_2O$ NDC DMF	0.2009 g 0.2228 g 10 mL	115	3
LW1_75c	$Er(NO_3)_3 \cdot 5\ H_2O$ NDC DMF	0.2015 g 0.2228 g 10 mL	115	3
LW1_76a	$Ce(NO_3)_3 \cdot 6\ H_2O$ NDC DMF	0.2009 g 0.2153 g 10 mL	155	3
LW1_76b	$Gd(NO_3)_3 \cdot 6\ H_2O$ NDC DMF	0.2007 g 0.2169 g 10 mL	155	3
LW1_76c	$Er(NO_3)_3 \cdot 5\ H_2O$ NDC DMF	0.2006 g 0.2187 g 10 mL	155	3
LW1_76e	$Gd(NO_3)_3 \cdot 6\ H_2O$ NDC DMF	0.2016 g 0.2162 g 10 mL	145	3
LW1_78a	$Ce(NO_3)_3 \cdot 6\ H_2O$ NDC DMF	0.2010 g 0.2121 g 10 mL	160	3
LW1_78b	$Gd(NO_3)_3 \cdot 6\ H_2O$ NDC DMF	0.2012 g 0.2136 g 10 mL	160	3
LW1_78c	$Er(NO_3)_3 \cdot 5\ H_2O$ NDC DMF	0.2008 g 0.2169 g 10 mL	160	3
LW1_84a	$Ce(NO_3)_3 \cdot 6\ H_2O$ NDC DMF	0.2014 g 0.2205 g 10 mL	130	3
LW1_84b	$Eu(NO_3)_3 \cdot 6\ H_2O$ NDC DMF	0.2014 g 0.2206 g 10 mL	130	3
LW1_84c	$Gd(NO_3)_3 \cdot 6\ H_2O$ NDC DMF	0.2010 g 0.2210 g 10 mL	130	3
LW1_84d	$Er(NO_3)_3 \cdot 5\ H_2O$ NDC DMF	0.2003 g 0.2214 g 10 mL	130	3

LW1_87c	$Eu(NO_3)_3 \cdot 6\ H_2O$ NDC DMF	0.2013 g 0.2147 g 10 mL	144	6
LW1_87d	$Eu(NO_3)_3 \cdot 6\ H_2O$ NDC DMF	0.2013 g 0.2152 g 10 mL	144	6
LW1_88a	$Eu(NO_3)_3 \cdot 6\ H_2O$ NDC DMF	0.2023 g 0.2138 g 10 mL	150	3
LW1_88b	$Eu(NO_3)_3 \cdot 6\ H_2O$ NDC DMF	0.2013 g 0.2153 g 10 mL	150	3
LW1_88c	$Ce(NO_3)_3 \cdot 6\ H_2O$ NDC DMF	0.2005 g 0.2157 g 10 mL	150	3
LW1_92a	$Ce(NO_3)_3 \cdot 6\ H_2O$ NDC DMF	0.2015 g 0.2174 g 10 mL	135 – 155	5
LW1_92b	$Eu(NO_3)_3 \cdot 6\ H_2O$ NDC DMF	0.2019 g 0.2175 g 10 mL	135 – 155	5
JM1_15a	$Ce(NO_3)_3 \cdot 6\ H_2O$ NDC DMF	0.2001 g 0.2169 g 10 mL	147	7
JM1_15b	$Gd(NO_3)_3 \cdot 6\ H_2O$ NDC DMF	0.2001 g 0.2032 g 10 mL	147	7
JM1_15c	$Er(NO_3)_3 \cdot 6\ H_2O$ NDC DMF	0.2003 g 0.2025 g 10 mL	147	7
JM1_16a	$Ce(NO_3)_3 \cdot 6\ H_2O$ NDC DMF	0.1994 g 0.2185 g 10 mL	110	7
JM1_16b	$Gd(NO_3)_3 \cdot 6\ H_2O$ NDC DMF	0.2007 g 0.2038 g 10 mL	110	7
JM1_16c	$Er(NO_3)_3 \cdot 6\ H_2O$ NDC DMF	0.2004 g 0.2029 g 10 mL	110	7
JM1_18a	$Ce(NO_3)_3 \cdot 6\ H_2O$ NDC DMF	0.2007 g 0.2044 g 10 mL	168	7

JM1_18b	$Gd(NO_3)_3 \cdot 6\ H_2O$ NDC DMF	0.2007 g 0.2037 g 10 mL	168	7
JM1_18c	$Er(NO_3)_3 \cdot 6\ H_2O$ NDC DMF	0.1994 g 0.2023 g 10 mL	168	7
JM1_19a	$Ce(NO_3)_3 \cdot 6\ H_2O$ NDC DMF	0.2003 g 0.218 g 10 mL	127	7
JM1_19b	$Gd(NO_3)_3 \cdot 6\ H_2O$ NDC DMF	0.2006 g 0.2039 g 10 mL	127	7
JM1_19c	$Er(NO_3)_3 \cdot 6\ H_2O$ NDC DMF	0.1999 g 0.2025 g 10 mL	127	7
JM1_23a	$Ce(NO_3)_3 \cdot 6\ H_2O$ NDC DMF	0.2008 g 0.2178 g 10 mL	145	7
JM1_23b	$Er(NO_3)_3 \cdot 6\ H_2O$ NDC DMF	0.2010 g 0.2024 g 10 mL	145	7
JM1_30a	$Er(NO_3)_3 \cdot 6\ H_2O$ NDC DMF	0.1994 g 0.2020 g 10 mL	145 – 155	5
JM1_38a	$Ce(NO_3)_3 \cdot 6\ H_2O$ NDC DMF	0.2005 g 0.202 g 10 mL	110 – 125	6
JM1_38b	$Ce(NO_3)_3 \cdot 6\ H_2O$ NDC DMF	0.1998 g 0.201 g 10 mL	110 – 125	6
JM1_38c	$Eu(NO_3)_3 \cdot 6\ H_2O$ NDC DMF	0.1997 g 0.201 g 10 mL	110 – 125	6
JM1_38d	$Eu(NO_3)_3 \cdot 6\ H_2O$ NDC DMF	0.2007 g 0.201 g 10 mL	110 – 125	6
JM1_39a	$Er(NO_3)_3 \cdot 6\ H_2O$ NDC DMF	0.2005 g 0.202 g 10 mL	110 – 125	6
JM1_39b	$Er(NO_3)_3 \cdot 6\ H_2O$ NDC DMF	0.2008 g 0.2009 g 10 mL	110 – 125	6
JM1_43a	$Nd(NO_3)_3 \cdot 6\ H_2O$ NDC DMF	0.201 g 0.205 g 10 mL	110 – 125	5

JM1_43b	$Nd(NO_3)_3 \cdot 6\ H_2O$ NDC DMF	0.199 g 0.205 g 10 mL	110 – 125	5
JM1_43c	$La(NO_3)_3 \cdot 6\ H_2O$ NDC DMF	0.119 g 0.203 g 10 mL	110 – 125	5
JM1_43d	$La(NO_3)_3 \cdot 6\ H_2O$ NDC DMF	0.200 g 0.204 g 10 mL	110 – 125	5
JM1_43e	$Gd(NO_3)_3 \cdot 6\ H_2O$ NDC DMF	0.201 g 0.205 g 10 mL	110 – 125	5
JM1_43f	$Gd(NO_3)_3 \cdot 6\ H_2O$ NDC DMF	0.200 g 0.205 g 10 mL	110 – 125	5
JM1_44a	$Er(NO_3)_3 \cdot 6\ H_2O$ NDC DMF	0.2003 g 0.2021 g 10 mL	110 – 125	4
JM1_44b	$Er(NO_3)_3 \cdot 6\ H_2O$ NDC DMF	0.1999 g 0.2027 g 10 mL	110 – 125	4
JM1_44c	$Ce(NO_3)_3 \cdot 6\ H_2O$ NDC DMF	0.2001 g 0.2046 g 10 mL	110 – 125	4
JM1_44d	$Ce(NO_3)_3 \cdot 6\ H_2O$ NDC DMF	0.2006 g 0.2044 g 10 mL	110 – 125	4
JM1_49a	$La(NO_3)_3 \cdot 6\ H_2O$ NDC DMF	0.2008 g 0.2039 g 10 mL	110 – 125	9
JM1_49b	$Ce(NO_3)_3 \cdot 6\ H_2O$ NDC DMF	0.2007 g 0.2048 g 10 mL	110 – 125	9
JM1_49c	$Nd(NO_3)_3 \cdot 6\ H_2O$ NDC DMF	0.2007 g 0.2048 g 10 mL	110 – 125	9
JM1_49d	$Eu(NO_3)_3 \cdot 6\ H_2O$ NDC DMF	0.2018 g 0.2010 g 10 mL	110 – 125	9
JM1_49e	$Gd(NO_3)_3 \cdot 6\ H_2O$ NDC DMF	0.2009 g 0.2040 g 10 mL	110 – 125	9
JM1_52a	$La(NO_3)_3 \cdot 6\ H_2O$ NDC DMF	0.200 g 0.204 g 10 mL	110 – 125	11

JM1_52b	$Ce(NO_3)_3 \cdot 6\ H_2O$ NDC DMF	0.201 g 0.202 g 10 mL	110 – 125	11
JM1_52c	$Nd(NO_3)_3 \cdot 6\ H_2O$ NDC DMF	0.200 g 0.205 g 10 mL	110 – 125	11
JM1_52d	$Eu(NO_3)_3 \cdot 6\ H_2O$ NDC DMF	0.201 g 0.201 g 10 mL	110 – 125	11
JM1_52e	$Gd(NO_3)_3 \cdot 6\ H_2O$ NDC DMF	0.200 g 0.204 g 10 mL	110 – 125	11
JM1_75a	$Eu(NO_3)_3 \cdot 6\ H_2O$ NDC DMF	0.196 g 0.200 g 10 mL	110 – 125	7
JM1_75b	$Eu(NO_3)_3 \cdot 6\ H_2O$ NDC DMF	0.201 g 0.201 g 10 mL	110 – 125	7
JM1_78a	$La(NO_3)_3 \cdot 6\ H_2O$ NDC DMF	0.1999 g 0.1991 g 10 mL	130	5
JM1_78b	$La(NO_3)_3 \cdot 6\ H_2O$ NDC DMF	0.1999 g 0.1991 g 10 mL	130	5
SW1_03a	$Ce(NO_3)_3 \cdot 6\ H_2O$ NDC DMF	0.2007 g 0.2012 g 10 mL	143	6
SW1_03b	$Eu(NO_3)_3 \cdot 6\ H_2O$ NDC DMF	0.2002 g 0.2018 g 10 mL	143	6
SW1_03c	$Er(NO_3)_3 \cdot 5\ H_2O$ NDC DMF	0.2006 g 0.2015 g 10 mL	143	6
SW1_05a	$Ce(NO_3)_3 \cdot 6\ H_2O$ NDC DMF	0.2008 g 0.2014 g 10 mL	132	6
SW1_05b	$Ce(NO_3)_3 \cdot 6\ H_2O$ NDC DMF	0.2001 g 0.2018 g 10 mL	132	6
SW1_05c	$Eu(NO_3)_3 \cdot 6\ H_2O$ NDC DMF	0.2003 g 0.2017 g 10 mL	132	6

SW1_05d	$Eu(NO_3)_3 \cdot 6\ H_2O$ NDC DMF	0.2004 g 0.2019 g 10 mL	132	6
SW1_07b	$Eu(NO_3)_3 \cdot 6\ H_2O$ NDC DMF	0.2002 g 0.2014 g 10 mL	132	6
SW1_12a	$Ce(NO_3)_3 \cdot 6\ H_2O$ NDC DMF	0.2001 g 0.2017 g 10 mL	135 – 155	6
SW1_12b	$Eu(NO_3)_3 \cdot 6\ H_2O$ NDC DMF	0.2003 g 0.2015 g 10 mL	135 – 155	6
SW1_12c	$Er(NO_3)_3 \cdot 5\ H_2O$ NDC DMF	0.2005 g 0.2016 g 10 mL	135 – 155	6
SW1_18a	$Ce(NO_3)_3 \cdot 6\ H_2O$ NDC DMF	0.2003 g 0.2018 g 10 mL	125 – 140	6
SW1_18b	$Eu(NO_3)_3 \cdot 6\ H_2O$ NDC DMF	0.2002 g 0.2018 g 10 mL	125 – 140	6
SW1_18c	$Er(NO_3)_3 \cdot 5\ H_2O$ NDC DMF	0.2007 g 0.2019 g 10 mL	125 – 140	6
SW1_29a	$Ce(NO_3)_3 \cdot 6\ H_2O$ NDC DMF	0.2008 g 0.2015 g 10 mL	175	6
SW1_29b	$Er(NO_3)_3 \cdot 5\ H_2O$ NDC DMF	0.2004 g 0.2016 g 10 mL	175	6
SW1_31a	$Ce(NO_3)_3 \cdot 6\ H_2O$ NDC DMF	0.2003 g 0.2017 g 10 mL	110 – 125	6
SW1_31b	$Ce(NO_3)_3 \cdot 6\ H_2O$ NDC DMF	0.2003 g 0.2016 g 10 mL	110 – 125	6
SW1_31c	$Eu(NO_3)_3 \cdot 6\ H_2O$ NDC DMF	0.2000 g 0.2015 g 10 mL	110 – 125	6
SW1_31d	$Eu(NO_3)_3 \cdot 6\ H_2O$ NDC DMF	0.2003 g 0.2019 g 10 mL	110 – 125	6

SW1_31e	$Er(NO_3)_3 \cdot 5\ H_2O$ NDC DMF	0.2008 g 0.2019 g 10 mL	110 – 125	6
SW1_31f	$Er(NO_3)_3 \cdot 5\ H_2O$ NDC DMF	0.2001 g 0.2019 g 10 mL	110 – 125	6

Table A3. SLUG-28 through 30 (Ln-ADS) Syntheses

Sample ID	Reagents	Weight/Volume Used	Temperature (°C)	Time (days)
AK1_65a	$Nd(NO_3)_3 \cdot 6\ H_2O$ EDS 4,4'-bipyridine H_2O	0.1257 g 0.0677 g 0.0252 g 8 mL	175	3
AK1_65b	$Nd(NO_3)_3 \cdot 6\ H_2O$ PDS 4,4'-bipyridine H_2O	0.1198 g 0.0678 g 0.0241 g 8 mL	175	6
AK1_66a	$Nd(NO_3)_3 \cdot 6\ H_2O$ EDS 4,4'-bipyridine H_2O	2.4256 g 1.3014 g 0.6504 g 10 mL	175	6
AK1_69a	$Nd(NO_3)_3 \cdot 6\ H_2O$ EDS 4,4'-bipyridine H_2O	2.4328 g 1.2996 g 0.6501 g 10 mL	175	3
AK1_69b	$Nd(NO_3)_3 \cdot 6\ H_2O$ PDS 4,4'-bipyridine H_2O	2.4328 g 1.3775 g 0.6501 g 10 mL	175	11
AK1_71a	$Nd(NO_3)_3 \cdot 6\ H_2O$ EDS Urea H_2O	2.4371 g 1.2997 g 13.9943 g 10 mL	175	4
AK1_71b	$Nd(NO_3)_3 \cdot 6\ H_2O$ EDS 4,4'-bipyridine H_2O	3.1931 g 1.3014 g 0.6499 g 10mL	175	4
AK1_73a	$Nd(NO_3)_3 \cdot 6\ H_2O$ EDS 4,4'-bipyridine H_2O	2.4603 g 1.3354 g 0.6773 g 10 mL	175	3
AK1_73b	$Nd(NO_3)_3 \cdot 6\ H_2O$ PDS 4,4'-bipyridine H_2O	2.4335 g 1.3793 g 0.8630 g 10 mL	175	3
AK1_77a	$Nd(NO_3)_3 \cdot 6\ H_2O$ EDS Urea H_2O	2.4367 g 1.3090 g 0.9256 g 10 mL	175	4

AK1_83a	$Nd(NO_3)_3 \cdot 6\ H_2O$ EDS Urea H_2O	2.5600 g 1.3037 g 1.0052 g 10 mL	175	2
AK1_83b	$Nd(NO_3)_3 \cdot 6\ H_2O$ EDS Urea H_2O	2.4328 g 1.3023 g 1.0094 g 10 mL	150	2
AK1_85a	$Nd(NO_3)_3 \cdot 6\ H_2O$ EDS Urea H_2O	2.4543 g 1.3010 g 0.2929 g 10 mL	175	3
AK1_85b	$Nd(NO_3)_3 \cdot 6\ H_2O$ EDS Urea H_2O	2.4588 g 1.3023 g 0.2384 g 10 mL	150	3
AK1_92a	$Nd(NO_3)_3 \cdot 6\ H_2O$ EDS Urea H_2O	2.433 g 1.292 g 0.501 g 10 mL	175	3
AK1_97a	$Nd(NO_3)_3 \cdot 6\ H_2O$ EDS 4,4’-bipyridine H_2O	2.4319 g 1.3014 g 0.6514 g 10 mL	175	3
AK1_99a	$Nd(NO_3)_3 \cdot 6\ H_2O$ EDS NaOH H_2O	2.433 g 1.300 g 1 pellet 10 mL	175	3
AK1_99b	$Nd(NO_3)_3 \cdot 6\ H_2O$ EDS NaOH H_2O	2.432 g 1.300 g 2 pellets 10 mL	175	3
AK1_104a	$Nd(NO_3)_3 \cdot 6\ H_2O$ EDS NaOH H_2O	2.4318 g 1.3011 g 0.0559 g 10 mL	175	3
AK1_104b	$Nd(NO_3)_3 \cdot 6\ H_2O$ EDS NaOH H_2O	1.2044 g 0.6933 g 0.0664 g 10 mL	175	3
AK1_108a	$Nd(NO_3)_3 \cdot 6\ H_2O$ EDS NaOH H_2O	2.4300 g 1.3000 g 0.1141 g 10 mL	150	3

AK1_108b	$Nd(NO_3)_3 \cdot 6\ H_2O$ EDS NaOH H_2O	2.4330 g 1.3007 g 0.1312 g 10 mL	200	3
AK1_111a	$Nd(NO_3)_3 \cdot 6\ H_2O$ EDS NaOH H_2O	2.4300 g 1.3002 g 0.2228 g 10 mL	150	2
AK1_111b	$Nd(NO_3)_3 \cdot 6\ H_2O$ EDS NaOH H_2O	2.4303 g 1.3003 g 0.2547 g 10 mL	175	2
AK1_115a	$Nd(NO_3)_3 \cdot 6\ H_2O$ EDS NaOH H_2O	2.4300 g 1.3001 g 0.2921 g 10 mL	150	3
AK1_115b	$Nd(NO_3)_3 \cdot 6\ H_2O$ EDS NaOH H_2O	2.4301 g 1.3000 g 0.3416 g 10 mL	175	3
AK1_117a	$Nd(NO_3)_3 \cdot 6\ H_2O$ EDS NaOH H_2O	2.4296 g 1.2991 g 0.4446 g 10 mL	150	3
AK1_117b	$Nd(NO_3)_3 \cdot 6\ H_2O$ EDS NaOH H_2O	2.4297 g 1.2994 g 0.4303 g 10 mL	175	3
AK1_121a	$Nd(NO_3)_3 \cdot 6\ H_2O$ EDS NaOH H_2O	2.4300 g 1.3004 g 0.3910 g 10 mL	130	3
AK1_121b	$Nd(NO_3)_3 \cdot 6\ H_2O$ PDS NaOH H_2O	2.4303 g 1.3772 g 0.3825 g 10 mL	175	3
AK1_122a	$Nd(NO_3)_3 \cdot 6\ H_2O$ PDS NaOH H_2O	2.4320 g 1.3770 g 0.2504 10 mL	175	3
AK1_122b	$Nd(NO_3)_3 \cdot 6\ H_2O$ PDS NaOH H_2O	2.4331 g 1.2709 g 0.2890 g 10 mL	175	3

AK1_125a	$Nd(NO_3)_3 \cdot 6\ H_2O$ EDS NaOH H_2O	2.4328 g 1.3006 g 0.4435 g 10 mL	150	3
AK1_125b	$Nd(NO_3)_3 \cdot 6\ H_2O$ PDS NaOH H_2O	2.4310 g 1.3776 g 0.4277 g 10 mL	175	3
AK1_129a	$Nd(NO_3)_3 \cdot 6\ H_2O$ PDS NaOH H_2O	2.4326 g 1.3779 g 0.5014 g 10 mL	150	3
AK1_129b	$Nd(NO_3)_3 \cdot 6\ H_2O$ PDS NaOH H_2O	2.4323 g 1.3778 g 0.5772 g 10 mL	150	3
AK1_131a	$Nd(NO_3)_3 \cdot 6\ H_2O$ EDS NaOH H_2O	2.4333 g 1.3006 g 0.4491 g 10 mL	150	3
AK1_135a	$Nd(NO_3)_3 \cdot 6\ H_2O$ BDS NaOH H_2O	2.4346 g 1.4525 g 0.5207 g 10 mL	150	3
AK1_137a	$Nd(NO_3)_3 \cdot 6\ H_2O$ PDS NaOH H_2O	2.4331 g 1.3744 g 0.4999 g 10 mL	175	4
AK1_137b	$Nd(NO_3)_3 \cdot 6\ H_2O$ BDS NaOH H_2O	2.4354 g 1.4514 g 0.4798 g 10 mL	175	4
AK1_147a	$Nd(NO_3)_3 \cdot 6\ H_2O$ PDS 4,4’-bipyridine H_2O	2.4327 g 1.3777 g 0.6501 g 10 mL	175	3
AK1_147b	$Nd(NO_3)_3 \cdot 6\ H_2O$ PDS 4,4’-bipyridine H_2O	2.4327 g 1.3776 g 0.6494 g 10 mL	175	3
AK1_151a	$Nd(NO_3)_3 \cdot 6\ H_2O$ BDS 4,4’-bipyridine H_2O	2.4379 g 1.4457 g 0.6479 g 10 mL	175	3

AK1_152a	$Nd(NO_3)_3 \cdot 6\ H_2O$ BDS 4,4'-bipyridine H_2O	2.4300 g 1.4515 g 0.6488 g 10 mL	175	3
AK1_152b	$Nd(NO_3)_3 \cdot 6\ H_2O$ EDS 4,4'-bipyridine H_2O	2.4352 g 1.3040 g 0.6496 g 10 mL	175	3
AK1_153a	$Nd(NO_3)_3 \cdot 6\ H_2O$ EDS 4,4'-bipyridine H_2O	2.4375 g 1.3075 g 0.6461 g 10 mL	175	3
AK1_153b	$Nd(NO_3)_3 \cdot 6\ H_2O$ EDS 4,4'-bipyridine H_2O	2.4353 g 1.3055 g 0.6497 g 10 mL	175	3
AK2_05g	$Nd(NO_3)_3 \cdot 6\ H_2O$ BDS 4,4'-bipyridine H_2O	2.433 g 1.455 g 0.650 g 10 mL	175	3
AK2_09c	$Nd(NO_3)_3 \cdot 6\ H_2O$ EDS NaOH H_2O	2.4333 g 1.3000 g 0.4524 g 10 mL	150	3
AK2_09d	$Nd(NO_3)_3 \cdot 6\ H_2O$ EDS 4,4'-bipyridine H_2O	2.4334 g 1.3001 g 0.6503 g 10 mL	175	3
AK2_09e	$Nd(NO_3)_3 \cdot 6\ H_2O$ EDS 4,4'-bipyridine H_2O	2.4332 g 1.3008 g 0.6500 g 10 mL	175	3
AK2_18a	$Nd(NO_3)_3 \cdot 6\ H_2O$ EDS 4,4'-bipyridine H_2O	2.4337 g 1.3000 g 0.6501 g 10 mL	175	3
AK2_18b	$Nd(NO_3)_3 \cdot 6\ H_2O$ EDS 4,4'-bipyridine H_2O	2.4335 g 1.2999 g 0.6501 g 10 mL	175	3
AK2_23a	$Nd(NO_3)_3 \cdot 6\ H_2O$ EDS 4,4'-bipyridine H_2O	2.4339 g 1.3004 0.6500 g 10 mL	175	3

AK2_23b	$Nd(NO_3)_3 \cdot 6\ H_2O$ EDS 4,4'-bipyridine H_2O	2.4345 g 1.3003 g 0.6495 g 10 mL	175	3
AK2_23c	$Nd(NO_3)_3 \cdot 6\ H_2O$ EDSA 4,4'-bipyridine H_2O	2.4330 g 1.3000 g 0.6494 g 10 mL	175	3
AK2_23d	$Nd(NO_3)_3 \cdot 6\ H_2O$ EDSA 4,4'-bipyridine H_2O	2.4341 g 1.30000 g 0.6522 g 10 mL	175	3
AK2_25a	$Nd(NO_3)_3 \cdot 6\ H_2O$ EDS 4,4'-bipyridine H_2O	2.4335 g 1.2996 g 0.6548 g 10 mL	175	3
LW1_50a	$Nd(NO_3)_3 \cdot 6\ H_2O$ EDS 4,4'-bipyridine H_2O	2.4342 g 1.2996 g 0.6505 g 10 mL	175	3
LW1_50b	$Nd(NO_3)_3 \cdot 6\ H_2O$ EDS 4,4'-bipyridine H_2O	2.4341 g 1.3001 g 0.6504 g 10 mL	175	3
LW1_50c	$Nd(NO_3)_3 \cdot 6\ H_2O$ EDS 4,4'-bipyridine H_2O	2.4345 g 1.3003 g 0.5601 g 10 mL	175	3
LW1_50d	$Nd(NO_3)_3 \cdot 6\ H_2O$ EDS 4,4'-bipyridine H_2O	1.9459 g 1.0402 g 0.5208 g 8 mL	175	3
LW1_50e	$Nd(NO_3)_3 \cdot 6\ H_2O$ EDS 4,4'-bipyridine H_2O	1.9468 g 1.0408 g 0.5202 g 8 mL	175	3
JM1_55a	$Nd(NO_3)_3 \cdot 6\ H_2O$ EDS H_2O	2.423 g 1.304 g 10 mL	150	4
JM1_55b	$Nd(NO_3)_3 \cdot 6\ H_2O$ PDS H_2O	2.436 g 1.365 g 10 mL	150	4

JM1_55c	$Nd(NO_3)_3 \cdot 6\ H_2O$ BDS H_2O	2.439 g 0.680 g 10 mL	150	4
JM1_59a	$Nd(NO_3)_3 \cdot 6\ H_2O$ EDS H_2O NaOH	2.4261 g 1.2982 g 10.0 mL 0.3610 g	150	4
JM1_59b	$La(NO_3)_3 \cdot 6\ H_2O$ EDS H_2O NaOH	2.4314 g 1.2999 g 10 mL 0.3793 g	150	4
JM1_60a	$Nd(NO_3)_3 \cdot 6\ H_2O$ EDS H_2O NaOH	2.4305 g 1.3013 g 10 mL 0.3475 g	150	7
JM1_60b	$Gd(NO_3)_3 \cdot 6\ H_2O$ EDS H_2O NaOH	2.4297 g 1.3001 g 10 mL 0.3627 g	150	7
JM1_67a	$Nd(NO_3)_3 \cdot 6\ H_2O$ EDS H_2O NaOH	2.400 g 1.308 g 10 mL 0.361 g	150	5
JM1_67a	$Nd(NO_3)_3 \cdot 6\ H_2O$ EDS H_2O NaOH	2.413 g 1.291 g 10 mL 0.341 g	150	5
JM1_69a	$Ce(NO_3)_3 \cdot 6\ H_2O$ EDS H_2O NaOH	2.4296 g 1.3010 g 10 mL 0.3745 g	155	4
JM1_69b	$Ce(NO_3)_3 \cdot 6\ H_2O$ EDS H_2O NaOH	2.4297 g 1.3014 g 10 mL 0.3705 g	155	4
JM1_71a	$Nd(NO_3)_3 \cdot 6\ H_2O$ EDS H_2O NaOH	0.1996 g 0.2004 g 10 mL 0.0967 g	150	4
JM1_71b	$Nd(NO_3)_3 \cdot 6\ H_2O$ EDS H_2O NaOH	0.2010 g 0.2006 g 10 mL 0.1010 g	150	4

JM1_73a	$Nd(NO_3)_3 \cdot 6\ H_2O$ EDS H_2O NaOH	2.000 g 1.001 g 10 mL 5 drops, 1.0 M	150	5
JM1_73b	$Nd(NO_3)_3 \cdot 6\ H_2O$ EDS H_2O NaOH	2.001g 1.001g 10mL 5 drops, 1.0 M	150	5

Table A4. Exploratory Ln Syntheses

Sample ID	Reagents	Weight/Volume Used	Temperature (°C)	Time (days)
AK1_140a	$Nd(NO_3)_3 \cdot 6\ H_2O$ Adipic acid NaOH H_2O	2.4375 g 0.8111 g 0.4483 g 10 mL	150	3
AK1_141a	$Nd(NO_3)_3 \cdot 6\ H_2O$ Adipic acid NaOH H_2O	2.4370 g 0.8217 g 0.4480 g 10 mL	RT	4
AK1_141b	$Nd(NO_3)_3 \cdot 6\ H_2O$ Adipic acid NaOH H_2O	2.4312 g 0.8232 g 0.5221 g 10 mL	150	3
AK1_141c	$Nd(NO_3)_3 \cdot 6\ H_2O$ Adipic acid NaOH H_2O	2.4363 g 0.8165 g 0.4350 g 10 mL	175	3
AK1_145a	$Nd(NO_3)_3 \cdot 6\ H_2O$ Adipic acid NaOH H_2O	1.2169 g 2.7372 g 0.2394 g 10 mL	RT	3
AK1_149a	$Nd(NO_3)_3 \cdot 6\ H_2O$ 4,4'-bipyridine NaOH H_2O	0.7299 g 0.1348 g 0.0932 g 10 mL	150	4
AK1_149b	$Nd(NO_3)_3 \cdot 6\ H_2O$ 4,4'-bipyridine NaOH H_2O	1.3240 g 0.1977 g 0.3224 g 10 mL	150	4
AK1_154a	$Nd(NO_3)_3 \cdot 6\ H_2O$ 4,4'-bipyridine H_2O	0.2017 g 0.0736 g 10 mL	150	4
AK1_154b	$Nd(NO_3)_3 \cdot 6\ H_2O$ BTC H_2O	0.2023 g 0.0960 g 10 mL	150	4
AK1_154c	$La(NO_3)_3 \cdot 6\ H_2O$ 4,4'-bipyridine H_2O	0.2069 g 0.0740 g 10 mL	150	4
AK1_154d	$La(NO_3)_3 \cdot 6\ H_2O$ BTC H_2O	0.2069 g 0.0981 10 mL	150	4

AK1_154e	$Er(NO_3)_3 \cdot x\ H_2O$ 4,4'-bipyridine H_2O	0.2035 g 0.0720 g 10 mL	150	4
AK1_154f	$Er(NO_3)_3 \cdot x\ H_2O$ BTC H_2O	0.2030 g 0.0975 g 10 mL	150	4
AK2_05h	$Nd(NO_3)_3 \cdot 6\ H_2O$ BTC H_2O	0.2011 g 0.0960 g 10 mL	RT	1
AK2_05i	$Er(NO_3)_3 \cdot x\ H_2O$ BTC H_2O	0.2009 g 0.0988 g 10 mL	RT	1
AK2_05j	$La(NO_3)_3 \cdot 6\ H_2O$ BTC H_2O	0.2005 g 0.0973 g 10 mL	RT	1
AK2_08a	$La(NO_3)_3 \cdot 6\ H_2O$ 4,4'-bipyridine DMF	0.2527 g 0.1033 g 10 mL	150	3
AK2_08b	$La(NO_3)_3 \cdot 6\ H_2O$ BTC DMF	0.2607 g 0.1439 g 10 mL	150	3
AK2_08c	$Nd(NO_3)_3 \cdot 6\ H_2O$ 4,4'-bipyridine DMF	0.2548 g 0.1031 g 10 mL	150	3
AK2_08d	$Nd(NO_3)_3 \cdot 6\ H_2O$ BTC DMF	0.2416 g 0.1603 g 10 mL	150	3
AK2_08e	$Er(NO_3)_3 \cdot x\ H_2O$ 4,4'-bipyridine DMF	0.2185 g 0.1109 g 10 mL	150	3
AK2_08f	$Er(NO_3)_3 \cdot x\ H_2O$ BTC DMF	0.2579 g 0.1616 g 10 mL	150	3
AK2_16a	$Er(NO_3)_3 \cdot x\ H_2O$ BTC DMF	0.2035 g 0.1011 g 10 mL	140 – 160	4
AK2_20a	$La(NO_3)_3 \cdot 6\ H_2O$ Benzene-1,3-disulfonic acid DMF	0.2000 g 0.1304 g 10 mL	150	3
AK2_20b	$Nd(NO_3)_3 \cdot 6\ H_2O$ Benzene-1,3-disulfonic acid DMF	0.1999 g 0.1287 g 10 mL	150	3

AK2_20c	$Gd(NO_3)_3 \cdot 6\ H_2O$ Benzene-1,3-disulfonic acid DMF	0.2009 g 0.1250 g 10 mL	150	3
AK2_20d	$Er(NO_3)_3 \cdot x\ H_2O$ Benzene-1,3-disulfonic acid DMF	0.2002 g 0.1276 g 10 mL	150	3
AK2_55a	$Gd(NO_3)_3$ $Fe(NO_3)_3$ $Cr(NO_3)_3$ NaOH	7.5 mL, 0.4 M 1.25 mL, 0.4 M 1.25 mL, 0.4 M 0.3993 g	240	2
AK2_55b	$Gd(NO_3)_3$ $Fe(NO_3)_3$ $Cr(NO_3)_3$ NaOH	7.5 mL, 0.4 M 1.25 mL, 0.4 M 1.25 mL, 0.4 M 0.4005 g	240	2
AK2_58a	$Gd(NO_3)_3$ $Fe(NO_3)_3$ $Cr(NO_3)_3$ NaOH	7.5 mL, 0.4 M 1.25 mL, 0.4 M 1.25 mL, 0.4 M 0.3646 g	220	2
AK2_58b	$Gd(NO_3)_3$ $Fe(NO_3)_3$ $Cr(NO_3)_3$ NaOH	7.5 mL, 0.4 M 1.25 mL, 0.4 M 1.25 mL, 0.4 M 0.4111 g	220	2
AK2_58c	$Gd(NO_3)_3$ $Fe(NO_3)_3$ $Cr(NO_3)_3$ NaOH	7.5 mL, 0.4 M 1.25 mL, 0.4 M 1.25 mL, 0.4 M 0.3744 g	220	2
AK2_58d	$Gd(NO_3)_3$ $Fe(NO_3)_3$ $Cr(NO_3)_3$ NaOH	7.5 mL, 0.4 M 1.25 mL, 0.4 M 1.25 mL, 0.4 M 0.3869 g	220	2
AK2_65a	$Gd(NO_3)_3$ $AlCl_3$ $MgCl_2$ KOH	8.5 mL, 0.4 M 1.25 mL, 0.4 M 1.25 mL, 0.4 M 0.5636 g	230	2
AK2_65b	$Gd(NO_3)_3$ $AlCl_3$ $MgCl_2$ KOH	8.5 mL, 0.4 M 1.25 mL, 0.4 M 1.25 mL, 0.4 M 0.5607 g	230	2
AK2_65c	$Gd(NO_3)_3$ $AlCl_3$ $MgCl_2$ KOH	8.5 mL, 0.4 M 1.25 mL, 0.4 M 1.25 mL, 0.4 M 0.5610 g	230	2

AK2_65d	$Gd(NO_3)_3$ $AlCl_3$ $MgCl_2$ KOH	4.5 mL, 0.4 M 1.25 mL, 0.4 M 1.25 mL, 0.4 M 0.5582 g	230	2
LW1_03a	$Nd(NO_3)_3 \cdot 6\ H_2O$ 4,4'-bipyridine H_2O	0.2085 g 0.0728 g 10 mL	RT	3
LW1_03b	$Er(NO_3)_3 \cdot 5\ H_2O$ 4,4'-bipyridine H_2O	0.2043 g 0.0715 g 10 mL	RT	3
LW1_03c	$La(NO_3)_3 \cdot 6\ H_2O$ 4,4'-bipyridine H_2O	0.2018 g 0.0727 g 10 mL	RT	3
LW1_04a	$Nd(NO_3)_3 \cdot 6\ H_2O$ 4,4'-bipyridine Methanol	0.2010 g 0.0724 g 10 mL	RT	2
LW1_04b	$Er(NO_3)_3 \cdot 5\ H_2O$ 4,4'-bipyridine Methanol	0.2030 g 0.0715 g 10 mL	RT	2
LW1_04c	$La(NO_3)_3 \cdot 6\ H_2O$ 4,4'-bipyridine Methanol	0.2001 g 0.0738 g 10 mL	RT	2
LW1_06a	$Nd(NO_3)_3 \cdot 6\ H_2O$ BTC H_2O	0.2011 g 0.0960 g 10 mL	RT	2
LW1_06b	$Er(NO_3)_3 \cdot x\ H_2O$ BTC H_2O	0.2009 g 0.0988 g 10 mL	RT	2
LW1_06c	$La(NO_3)_3 \cdot 6\ H_2O$ BTC H_2O	0.2005 g 0.0973 g 10 mL	RT	2
LW1_14a	$Er(NO_3)_3 \cdot x\ H_2O$ BTC DMF	0.2036 g 0.0991 g 10 mL	150	3
LW1_14c	$Er(NO_3)_3 \cdot x\ H_2O$ BTC DMF	0.2047 g 0.0997 g 10 mL	175	3
LW1_14d	$Er(NO_3)_3 \cdot x\ H_2O$ BTC DMF	0.2009 g 0.0505 g 10 mL	150	3
LW1_14e	$Er(NO_3)_3 \cdot x\ H_2O$ BTC DMF	0.2005 g 0.0496 g 10 mL	175	3

LW1_16a	$La(NO_3)_3 \cdot 6\ H_2O$ 4,4'-bipyridine Methanol	0.2046 g 0.0750 10 mL	RT	3
LW1_16b	$La(NO_3)_3 \cdot 6\ H_2O$ BTC DMF	0.2003 g 0.0990 g 10 mL	175	3
LW1_16c	$La(NO_3)_3 \cdot 6\ H_2O$ BTC DMF	0.2006 g 0.0497 g 10 mL	150	3
LW1_16d	$La(NO_3)_3 \cdot 6\ H_2O$ BTC DMF	0.2008 g 0.0500 g 10 mL	175	3
LW1_19a	$Nd(NO_3)_3 \cdot 6\ H_2O$ BTC DMF	0.204 g 0.098 g 10 mL	175	3
LW1_19b	$Nd(NO_3)_3 \cdot 6\ H_2O$ BTC DMF	0.200 g 0.051 g 10 mL	150	3
LW1_19c	$Nd(NO_3)_3 \cdot 6\ H_2O$ BTC DMF	0.202 g 0.049 g 10 mL	175	3
LW1_19d	$Er(NO_3)_3 \cdot 5\ H_2O$ 4,4'-bipyridine DMF	0.208 g 0.074 g 10 mL	175	3
LW1_19e	$Er(NO_3)_3 \cdot 5\ H_2O$ 4,4'-bipyridine DMF	0.201 g 0.036 g 10 mL	150	3
LW1_19f	$Er(NO_3)_3 \cdot 5\ H_2O$ 4,4'-bipyridine DMF	0.208 g 0.039 g 10 mL	175	3
LW1_22d	$Er(NO_3)_3 \cdot 5\ H_2O$ BTC DMF	0.2012 g 0.0993 g 10 mL	125	3
LW1_24a	$Er(NO_3)_3 \cdot 5\ H_2O$ BTC DMF	0.2082 g 0.1016 g 10 mL	RT	5
LW1_26a	$Er(NO_3)_3 \cdot 5\ H_2O$ BTC DMF	0.2082 g 0.1016 g 10 mL	100	3
LW1_26c	$Er(NO_3)_3 \cdot 5\ H_2O$ BTC DMF Ethanol	0.2017 g 0.1052 g 10 mL 2 mL	55	5

LW1_27a	$Er(NO_3)_3 \cdot 5\ H_2O$ BTC DMF	0.2039 g 0.1004 g 10 mL	150	2
LW1_30a	$Gd(NO_3)_3 \cdot 6\ H_2O$ 4,4'-bipyridine DMF	0.203 g 0.078 g 10 mL	55	3
LW1_30b	$Gd(NO_3)_3 \cdot 6\ H_2O$ BTC DMF	0.205 g 0.101 g 10 mL	150	3
LW1_31a	$Gd(NO_3)_3 \cdot 6\ H_2O$ 4,4'-bipyridine DMF	0.2015 g 0.0289 g 10 mL	150	3
LW1_35c	$Er(NO_3)_3 \cdot 5\ H_2O$ BTC 4,4'-bipyridine DMF	0.2036 g 0.0454 g 0.0792 g 10 mL	150	5
LW1_36a	$La(NO_3)_3 \cdot 6\ H_2O$ BTC 4,4'-bipyridine DMF	0.2086 g 0.0476 g 0.799 g 10 mL	150	4
LW1_36b	$Nd(NO_3)_3 \cdot 6\ H_2O$ BTC 4,4'-bipyridine DMF	0.2104 g 0.0450 g 0.0798 g 10 mL	150	4
LW1_36c	$Gd(NO_3)_3 \cdot 6\ H_2O$ BTC 4,4'-bipyridine DMF	0.2022 g 0.0343 g 0.0809 g 10 mL	150	4
LW1_64a	$La(NO_3)_3 \cdot 6\ H_2O$ PFOA H_2O	0.2029 g 0.1247 g 10 mL	150	3
JM1_45a	$Gd(NO_3)_3$ NaOH $AlCl_3$ $MgCl_2$	7.5 mL, 0.4 M 0.4191 g 1.25 mL, 0.4 M 1.25 mL, 0.4 M	220	5
JM1_45b	$Gd(NO_3)_3$ NaOH $AlCl_3$ $MgCl_2$	7.5 mL, 0.4 M 0.3860 g 1.25 mL, 0.4 M 1.25 mL, 0.4 M	220	5
JM1_45c	$Gd(NO_3)_3$ NaOH $AlCl_3$ $MgCl_2$	7.5 mL, 0.4 M 0.4206 g 1.25 mL, 0.4 M 1.25 mL, 0.4 M	220	5

JM1_45d	$Gd(NO_3)_3$ NaOH $AlCl_3$ $MgCl_2$	7.5 mL, 0.4 M 0.4203 g 1.25 mL, 0.4 M 1.25 mL, 0.4 M	220	5
JM1_53a	$Fe(NO_3)_3$ $Cr(NO_3)_3$ NaOH 0.4M $Dy(NO_3)_3$	1.25 mL, 0.4 M 1.25 mL, 0.4 M 0.4245 g 7.5 mL, 0.4 M	230	2
JM1_53b	$Fe(NO_3)_3$ $Cr(NO_3)_3$ NaOH $Dy(NO_3)_3$	1.25 mL, 0.4 M 1.25 mL, 0.4 M 0.4245 g 7.5 mL, 0.4 M	230	2
SW1_26a	$Ce(NO_3)_3 \cdot 6\ H_2O$ CPB NDC DMF	0.2005 g 0.1187 g 0.0999 g 10 mL	140 – 150	5
SW1_26b	$Nd(NO_3)_3 \cdot 6\ H_2O$ CPB NDC DMF	0.2008 g 0.1175 g 0.0983 g 10 mL	140 – 150	5
SW1_26c	$La(NO_3)_3 \cdot 6\ H_2O$ CPB NDC DMF	0.2006 g 0.1191 g 0.0997 g 10 mL	140 – 150	5
SW1_27a	$Ce(NO_3)_3 \cdot 6\ H_2O$ CPB NDC DMF	0.200 g 0.119 g 0.099 g 10 mL	135 – 155	6
SW1_27b	$Nd(NO_3)_3 \cdot 6\ H_2O$ CPB NDC DMF	0.200 g 0.118 g 0.098 g 10 mL	135 – 155	6
SW1_27c	$La(NO_3)_3 \cdot 6\ H_2O$ CPB NDC DMF	0.201 g 0.119 g 0.099 g 10 mL	135 – 155	6

Table A5. Attempted Ion Exchanges with Ln-Materials

Sample ID	Reagents	Weight/Volume Used	Temperature	Time (days)
AK1_118a	Nd-EDS Succinic acid H_2O	0.1010 g 1.0220 g 50 mL	RT	< 1
AK1_118b	Nd-EDS Succinic acid H_2O	0.1010 g 1.0222 g 50 mL	RT	< 1
AK1_118c	Nd-EDS Succinic acid H_2O	0.1013 g 1.0218 g 50 mL	RT	1
AK1_119a	Nd-EDS Succinic acid Methanol	0.096 g 1.000 g 10 mL	RT	< 1
AK1_123a	Nd-EDS Succinic acid H_2O	0.0542 g 0.3547 g 10 mL	RT	1
AK1_123b	Nd-EDS Adipic acid H_2O	0.0606 g 0.4598 g 10 mL	RT	1
AK1_125c	Nd-EDS Adipic acid H_2O	0.1020 g 0.2511 g 10 mL	RT	< 1
AK1_125d	Nd-EDS Adipic acid H_2O	0.1010 g 0.5034 g 10 mL	RT	< 1
AK1_125e	Nd-EDS Adipic acid H_2O	0.1038 g 0.2515 g 10 mL	RT	< 1
AK1_125f	Nd-EDS Adipic acid H_2O	0.1015 g 0.5030 g 10 mL	RT	< 1
AK1_125g	Nd-EDS Sebacic acid H_2O	0.1011 g 1.0446 g 10 mL	RT	1
AK1_127a	Nd-PDS Adipic acid H_2O	0.1019 g 0.2455 g 10 mL	RT	< 1
AK1_127b	Nd-PDS Adipic acid H_2O	0.1029 g 0.0250 g 10 mL	RT	< 1

AK1_127c	Nd-EDS Adipic acid H_2O	0.1009 g 0.0254 g 10 mL	RT	< 1
AK1_127d	Nd-PDS Sebacic acid H_2O	0.1029 g 1.2407 g 10 mL	RT	1
AK1_128a	Nd-EDS Glutaric acid H_2O	0.1006 g 0.9090 g 10 mL	RT	1
AK1_128b	Nd-PDS Glutaric acid H_2O	0.1001 g 0.8887 g 10 mL	RT	1
AK1_130a	Nd-EDS Adipic acid H_2O	0.4032 g 1.0065 g 10 mL	RT	< 1
AK1_130b	Nd-EDS Glutaric acid H_2O	0.2013 g 0.5919 g 10 mL	RT	< 1
AK1_131b	Nd-EDS Terephthalic acid, disodium salt H_2O	0.5056 g 1.8018 g 10 mL	RT	< 1
AK1_131c	Nd-EDS $NaNO_3$ H_2O	0.3009 g 0.4407 g 10 mL	RT	< 1
AK1_131d	Nd-EDS K_2CrO_4 H_2O	0.3009 g 1.0046 g 10 mL	RT	< 1
AK1_131e	Nd-EDS $KMnO_4$ H_2O	0.3062 g 0.8268 g 10 mL	RT	< 1
AK1_131f	Nd-EDS $NaClO_3 \cdot H_2O$ H_2O	0.3076 g 0.7406 g 10 mL	RT	< 1
AK1_132a	Nd-EDS Terephthalic acid, disodium salt H_2O	0.1998 g 0.7148 g 10 mL	RT	1
AK1_132b	Nd-EDS $NaNO_3$ H_2O	0.2000 g 0.2888 g 10 mL	RT	1
AK1_132c	Nd-EDS $NaClO_3 \cdot H_2O$ H_2O	0.2001 g 0.4806 g 10 mL	RT	1

AK1_132d	Nd-EDS K_2CrO_4 H_2O	0.2001 g 0.6606 g 10 mL	RT	1
AK1_132e	Nd-EDS $KMnO_4$ H_2O	0.2001 g 0.5364 g 10 mL	RT	1
AK1_133a	Nd-EDS Suberic acid H_2O	0.0994 g 0.2994 g 10 mL	RT	1
AK1_133b	Nd-EDS Terephthalic acid, disodium salt Methanol	0.1062 g 0.3955 g 10 mL	RT	1
AK1_133c	Nd-EDS $KMnO_4$ Methanol	0.1006 g 0.2742 g 10 mL	RT	1
AK1_133d	Nd-EDS K_2CrO_4 Methanol	0.1062 g 0.3447 g 10 mL	RT	1
AK1_134a	Nd-EDS Terephthalic acid, disodium salt Acetonitrile	0.1001 g 0.3685 g 10 mL	RT	1
AK1_134b	Nd-EDS K_2CrO_4 Acetonitrile	0.1023 g 0.3294 g 10 mL	RT	1
AK1_134c	Nd-EDS $KMnO_4$ Acetonitrile	1.004 g 0.2796 g 10 mL	RT	1
AK1_137c	Nd-EDS Adipic acid H_2O	0.1002 g 0.1270 g 10 mL	RT	1
AK1_137d	Nd-PDS Adipic acid H_2O	0.1004 g 0.1231 g 10 mL	RT	1
AK1_137e	Nd-BDS Adipic acid H_2O	0.1003 g 0.1215 g 10 mL	RT	1
AK1_138a	Nd-EDS Adipic acid H_2O	0.1512 g 0.3025 g 10 mL	RT	1
AK1_138b	Nd-PDS Adipic acid H_2O	0.1517 g 0.2950 g 10 mL	RT	1

AK1_138c	Nd-BDS Adipic acid H_2O	0.1547 g 0.2880 g 10 mL	RT	1
AK2_10c	Nd-EDS PFOA H_2O	0.0545 g 0.3556 g 30 mL	RT	1
AK2_48a	Er-CPB NH_4HCO_3 H_2O	0.0400 g 0.2251 g 50 mL	RT	1
AK2_48b	Er-CPB NH_4HCO_3 DMF	0.0402 g 0.2252 g 50 mL	RT	1
AK2_49a	Er-NDC $Pb(NO_3)_2$	0.0250 g 50 mL, 100 ppm	RT	1
AK2_71a	Nd-EDS Adipic acid H_2O	0.0304 g 0.0100 g 50 mL	RT	1
AK2_71b	Nd-PDS Adipic acid H_2O	0.0308 g 0.0100 g 50 mL	RT	1
AK2_71c	Nd-BDS Adipic acid H_2O	0.0309 g 0.0101 g 50 mL	RT	1
LW1_11c	Nd-EDS PFOA H_2O	0.100 g 0.071 g 50 mL	RT	< 1
LW1_27b	Er-BTC $NaClO_4$ H_2O	0.0254 g 0.1997 g 50 mL	RT	1
LW1_27c	Er-BTC PFOA H_2O	0.0255 g 0.2083 g 50 mL	RT	1
LW1_27d	Er-BTC Adipic acid H_2O	0.0259 g 0.2074 g 50 mL	RT	1
LW1_32e	La-NDC $NaClO_4$ H_2O	0.0319 g 0.1242 g 50 mL	RT	< 1
LW1_32f	La-NDC Adipic acid H_2O	0.0301 g 0.1253 g 50 mL	RT	< 1
LW1_32g	La-NDC PFOA H_2O	0.0319 g 0.1283 g 50 mL	RT	< 1

LW1_34a	La-NDC Malonate, disodium salt H_2O	0.0405 g 0.1036 g 50 mL	RT	1
LW1_34b	La-NDC Succinate, disodium salt H_2O	0.0413 g 0.1006 g 50 mL	RT	1
LW1_34c	La-NDC Glutaric acid, disodium salt H_2O	0.0401 g 0.1009 g 50 mL	RT	1
LW1_34d	La-NDC Sebatic acid, disodium salt H_2O	0.401 g 0.1020 g 50 mL	RT	1
LW1_40b	La-NDC PFOA H_2O	0.0312 g 0.1288 g 50 mL	RT	1
LW1_40c	La-NDC PFOA H_2O	0.0323 g 0.1274 g 50 mL	RT	1
LW1_45a	La-NDC PFOA H_2O	0.0303 g 0.1171 g 50 mL	RT	1
LW1_45b	La-NDC PFOA H_2O	0.0335 g 0.1162 g 50 mL	RT	1
LW1_45c	La-NDC PFOA H_2O	0.0328 g 0.1156 g 50 mL	RT	1
LW1_48a	La-NDC PFOA H_2O	0.0297 g 0.1001 g 50 mL	RT	2
LW1_48b	La-NDC PFOA H_2O	0.0308 g 0.0506 g 50 mL	RT	2
LW1_48c	La-NDC PFOA H_2O	0.0305 g 0.0299 g 50 mL	RT	2
LW1_49a	Nd-NDC PFOA H_2O	0.0302 g 0.1256 g 50 mL	RT	1

LW1_49b	Er-NDC PFOA H_2O	0.0308 g 0.1256 g 50 mL	RT	1
LW1_55a	La-NDC PFOA H_2O	0.0305 g 0.0054 g 50 mL	RT	2
LW1_55b	Nd-NDC PFOA H_2O	0.0299 g 0.0053 g 50 mL	RT	2
LW1_55c	Er-NDC PFOA H_2O	0.0306 g 0.0051 g 50 mL	RT	2
LW1_55d	La-NDC PFOA H_2O	0.0306 g 0.1251 g 30 mL	40	1
LW1_56a	La-NDC NH_4NO_3 H_2O	0.0259 g 0.1076 g 50 mL	RT	2
LW1_56b	La-NDC NH_4NO_3 H_2O	0.0259 g 0.0582 g 50 mL	RT	2
LW1_56c	La-NDC $NaNO_3$ H_2O	0.0249 g 0.1021 g 50 mL	RT	2
LW1_56d	La-NDC $NaNO_3$ H_2O	0.0262 g 0.0517 g 50 mL	RT	2
LW1_60a	La-CPB $NaClO_4$ H_2O	0.0321 g 0.1036 g 50 mL	RT	1
LW1_60b	Nd-CPB $NaClO_4$ H_2O	0.0302 g 0.1064 g 50 mL	RT	1
LW1_60c	Gd-CPB $NaClO_4$ H_2O	0.0316 g 0.1061 g 50 mL	RT	1
LW1_60d	Er-CPB $NaClO_4$ H_2O	0.0314 g 0.1015 g 50 mL	RT	1
LW1_60e	La-CPB PFOA H_2O	0.0318 g 0.1038 g 50 mL	RT	1
LW1_60f	Nd-CPB PFOA H_2O	0.0313 g 0.1015 g 50 mL	RT	1

LW1_60g	Gd-CPB PFOA H_2O	0.309 g 0.1031 g 50 mL	RT	1
LW1_60h	Er-CPB PFOA H_2O	0.0304 g 0.1016 g 50 mL	RT	1
LW1_62a	La-NDC PFOA H_2O	0.0303 g 0.1261 g 50 mL	33	4
LW1_62b	$La(NO_3)_3 \cdot 6\ H_2O$ PFOA H_2O	0.0317 g 0.1267 g 50 mL	RT	1
LW1_62c	Gd-NDC PFOA H_2O	0.0313 g 0.1027 g 50 mL	RT	2
LW1_69a	La-CPB $KMnO_4$ H_2O	0.0305 g 0.1048 g 50 mL	RT	1
LW1_69b	Nd-CPB $KMnO_4$ H_2O	0.0310 g 0.1012 g 50 mL	RT	1
LW1_69c	Gd-CPB $KMnO_4$ H_2O	0.0312 g 0.1009 g 50 mL	RT	1
LW1_69d	Er-CPB $KMnO_4$ H_2O	0.0311 g 0.1021 g 50 mL	RT	1
LW1_74a	Ce-NDC PFOA H_2O	0.0303 g 0.1008 g 50 mL	RT	1
LW1_74b	Ce-CPB PFOA H_2O	0.0308 g 0.1008 g 50 mL	RT	1
LW1_74c	Ce-CPB PFOA H_2O	0.304 g 0.1002 g 50 mL	RT	1
LW1_77a	Ce-CPB PFOA H_2O	0.0304 g 0.1012 g 50 mL	RT	6
LW1_77b	Nd-NDC PFOA H_2O	0.0302 g 0.1001 g 50 mL	RT	6
LW1_77c	Er-NDC PFOA H_2O	0.0303 g 0.1002 g 50 mL	RT	6

LW1_77d	Ce-NDC PFOA H_2O	0.0305 g 0.1009 g 50 mL	RT	6
LW1_77e	Nd-CPB PFOA H_2O	0.0308 g 0.1008 g 50 mL	RT	6
LW1_77f	Er-CPB PFOA H_2O	0.0301 g 0.1001 g 50 mL	RT	6
LW1_80e	La-NDC Suberic acid H_2O	0.0316 g 0.1262 g 50 mL	RT	1
LW1_80f	Nd-NDC Suberic acid H_2O	0.0316 g 0.1249 g 50 mL	RT	1
LW1_80g	Gd-NDC Suberic acid H_2O	0.0303 g 0.1279 g 50 mL	RT	1
LW1_80h	La-CPB Suberic acid H_2O	0.0321 g 0.1255 g 50 mL	RT	1
LW1_80i	Nd-CPB Suberic acid H_2O	0.0322 g 0.1271 g 50 mL	RT	1
LW1_82a	La-NDC PFOA H_2O	0.0302 g 0.1261 g 50 mL	RT	1
LW1_82b	La-NDC PFOA H_2O	0.0312 g 0.1332 g 50 mL	RT	1
LW1_85a	Eu-CPB PFOA H_2O	0.0301 g 0.1252 g 50 mL	RT	1
JM1_24a	Er-CPB NH_4HCO_3 H_2O	0.070 g 0.227 g 50 mL	RT	1
JM1_31a	Ce-NDC $Pb(NO_3)_2$ H_2O	0.0401 g 0.5009 g 50 mL	RT	1
JM1_31b	Ce-NDC NH_4HCO_3 H_2O	0.0399 g 0.5007 g 50 mL	RT	1
JM1_31c	Eu-NDC $Pb(NO_3)_2$ H_2O	0.0393 g 0.5016 g 50 mL	RT	1

JM1_31d	Eu-NDC NH_4HCO_3 H_2O	0.0402 g 0.5002 g 50 mL	RT	1
JM1_32a	Er-NDC $Pb(NO_3)_2$ H_2O	0.0396 g 0.5000 g 50 mL	RT	1
JM1_32b	Er-NDC NH_4HCO_3 H_2O	0.0404 g 0.5000 g 50 mL	RT	1
JM1_33	Er-CPB NH_4HCO_3 H_2O	0.0402 g 0.2283 g 50 mL	RT	1
JM1_37a	Ce-NDC $Pb(NO_3)_2$	0.0250 g 50 mL, 100 ppm	RT	1
JM1_37b	Eu-NDC $Pb(NO_3)_2$	0.0245 g 50 mL, 100 ppm	RT	1
JM1_37c	Er-NDC $Pb(NO_3)_2$	0.0248 g 50 mL, 100 ppm	RT	1
JM1_42b	Ce-NDC $Pb(NO_3)_2$	0.0249 g 50 mL, 50 ppm	RT	1
JM1_42d	Eu-NDC $Pb(NO_3)_2$	0.0253 g 50 mL, 50 ppm	RT	1
JM1_42f	Er-NDC $Pb(NO_3)_2$	0.0250 g 50 mL, 50 ppm	RT	1
JM1_57a	Nd-EDS Adipic Acid H_2O	0.0298 g 0.0499 g 50 mL	RT	1
JM1_57b	Nd-EDS Adipic Acid H_2O NaCl	0.0304 g 0.0506 g 10 mL 0.0505 g	RT	1
JM1_65a	Nd-EDS Adipic acid H_2O	0.3995 g 0.7003 g 50 mL	RT	1
JM1_65b	Nd-EDS Succinic acid H_2O	0.6507 g 0.3997 g 50 mL	RT	1
SW1_06a	Eu-NDC PFOA H_2O	0.0301 g 0.1253 g 50 mL	RT	1
SW1_06b	Eu-CPB PFOA H_2O	0.0307 g 0.1253 g 50 mL	RT	1
SW1_10a	Nd-NDC PFOA	0.0025 g 50 mL, 1 ppm	RT	1

SW1_10b	Nd-NDC PFOA	0.0026 g 50 mL, 1 ppm	RT	1
SW1_10c	La-NDC PFOA	0.0025 g 50 mL, 1 ppm	RT	1
SW1_10d	La-NDC PFOA	0.0027 g 50 mL, 1 ppm	RT	1
SW1_10e	Eu-CPB PFOA	0.0026 g 50 mL, 1 ppm	RT	1
SW1_10f	Eu-CPB PFOA	0.0026 g 50 mL, 1 ppm	RT	1
SW1_15a	Ce-NDC PFOA	0.0505 g 50 mL, 1 ppm	RT	1
SW1_15b	Eu-NDC PFOA	0.0501 g 50 mL, 1 ppm	RT	1
SW1_15c	Er-NDC PFOA	0.0508 g 50 mL, 1 ppm	RT	1
SW1_15d	Nd-CPB PFOA	0.0511 g 50 mL, 1 ppm	RT	1
SW1_20a	Eu-CPB $Pb(NO_3)_2$ H_2O	0.0502 g 0.2444 g 50 mL	RT	1
SW1_20b	Eu-CPB $(CH_3)_4NBr$ H_2O	0.0506 g 0.1138 g 50 mL	RT	1
SW1_24a	Eu-CPB $Pb(NO_3)_2$ H_2O	0.0504 g 1.2204 g 50 mL	70	1
SW1_24b	Eu-CPB $(CH_3)_4NBr$ H_2O	0.0508 g 0.5675 g 50 mL	70	1